Biomolecules in Microthermal Fields

Philipp Baaske

Dissertation

München, Dezember 2009

Biomolecules in Microthermal Fields

Philipp Baaske

Dissertation
an der Fakultät für Physik
der Ludwig-Maximilians-Universität München

vorgelegt von
Philipp Ewald Baaske
aus
Kulmbach

München, Dezember 2009

Erstgutachter: Prof. Dr. Dieter Braun

Zweitgutachter: Prof. Dr. Joachim Rädler

Tag der mündlichen Prüfung: 03. Februar 2010

Table of Contents

I. Zusammenfassung

In dieser Arbeit wird das Verhalten von gelösten Biomolekülen in mikroskopischen, zeitlich und räumlich veränderlichen Temperaturfeldern untersucht. Die räumliche Ausdehnung der Temperaturdifferenzen hat dabei eine Ausdehnung, die mit der Diffusionslänge gelöster Biomoleküle vergleichbar ist. In diesen optisch erzeugten Temperaturfeldern können die Gleichgewichtskonstanten biochemischer Reaktionen quantifiziert und Biomoleküle exponentiell akkumuliert und vervielfältigt werden.

Im ersten Teil wird eine rein optische Messmethode für die Analyse frei diffundierender Biomoleküle in wässrigen Lösungen beschrieben. Mit einem IR-Laser werden in wässrigen Lösungen mikroskopisch kleine, räumliche Temperaturverteilungen erzeugt, die je nach Laserleistung alle Temperaturen zwischen 20°C und 100°C gleichzeitig enthalten können. Diese optisch erzeugten räumlichen Temperaturverteilungen haben zwei verschiedene Wirkungen auf Biomoleküle. Zum einen reagieren die Biomoleküle, entsprechend ihrer thermischen Stabilität, nahezu unmittelbar auf eine Änderung der absoluten Temperatur an ihrem jeweiligen Aufenthaltsort. Zum anderen zeigen die gelösten Moleküle eine gerichtete Bewegung entlang der Temperaturgradienten, ein Effekt der als Thermophorese bezeichnet wird. Diese beiden Effekte werden ausgenutzt, um Punktmutationen im Erbgut zu detektieren und um die Affinität von biochemischen Reaktionen im Blutserum zu quantifizieren.

Im zweiten Teil dieser Arbeit wird gezeigt, dass Temperaturdifferenzen in den weit verzweigten Porensystemen hydrothermaler Quellen einen Mechanismus antreiben, der Biomoleküle exponentiell akkumulieren kann. Dieser Mechanismus basiert auf einer Kombination aus Thermophorese und thermischer Konvektion. Anhand von Simulationen, die auf Thermophorese-Messungen von Nukleotiden beruhen, wird gezeigt, dass selbst einzelne Nukleotide mehr als millionenfach akkumuliert werden können. Diese starke Akkumulation ermöglicht es, die hohen Molekül-Konzentrationen zu erreichen, die für das Funktionieren der RNA-Welt-Hypothese vorausgesetzt werden. In diesen Porensystemen werden die Moleküle nicht nur akkumuliert, sondern durch die thermische Konvektion auch zyklisch durch Bereiche unterschiedlicher Temperatur transportiert. Es wird hier ein Reaktions-Schema vorgeschlagen, mit dem kurze RNA-Sequenzen auch ohne Enzyme exponentiell vervielfältigt werden können. Das Schema beruht dabei alleine auf den zyklischen Temperaturvariationen und auf einer kreuzkatalytischen Hybridisierungs-Reaktion zwischen vier verschiedenen RNA-Hairpin-Strukturen.

II. Summary

The mean topic of this thesis is the study of the characteristics of biomolecules exposed to microscopic small temperature fields, which vary in space and time. The spatial dimensions of these temperature fields are comparable to the diffusion length of dissolved biomolecules and can be used to quantify the equilibrium constants of biochemical reactions and also to exponentially accumulate and replicate biomolecules.

The first part of this thesis describes an all-optical method to analyze freely diffusing molecules in close to physiological conditions. An IR-laser, whose radiation is strongly absorbed by water molecules, is used to create spatial temperature distributions. These temperature distributions contain, depending on the laser power, all temperatures between 20°C and 100°C at once within an area of 200µm diameter. In these temperature distributions two distinct responses of biomolecules are observed. Firstly, the molecules react, according to their thermal stability, nearly instantaneously to the local increase of the absolute temperature at their respective position. Secondly, a directed movement of molecules along the temperature gradients, an effect termed thermophoresis, can be observed. It is shown, that these molecular responses to the generated temperature distributions can be used to detect single point mutations in DNA and to quantify the equilibrium constants of biomoleculare reactions even in human blood serum.

In the second part, simulations of the molecular transport in elongated hydrothermal pore systems influenced by a thermal gradient are described. Driven by the thermal gradient across the pores the fluid is shuttled by thermal convection along the pore and additionally molecules drift across the pore, driven by thermophoresis. The simulations show, that this combination of thermal convection and thermophoresis is able to exponentially accumulate even single nucleotides in a wide variety of plugged pores. This mechanism is able to provide highly concentrated single nucleotides, suitable for operations of an RNA world at the origin of life.

The microscale thermal convection found in the poresystems is a natural setting for temperature oscillations. Here, a reaction scheme of a protein-free exponential replication mechanism, solely driven by the temperature oscillations and the hybridization of hairpins is presented. The energy to drive the system is kinetically trapped in metastable RNA hairpins and is released in a template initiated crosscatalytic hybridization reaction between four different hairpins. During the temperature oscillation the hybridization takes place at the lower temperatures, whereas the formed products efficiently dissociate from the template at the elevated temperatures, allowing for an exponential replication of the template sequence.

III. Overview

Melting Curve Analysis in a Snapshot

The thermal denaturation of molecules is an essential method in biochemistry and diagnostics such as the measurement of single nucleotide polymorphisms (SNP) and the binding analysis of proteins. Here a novel method for the all-optical high speed measurement of high resolution melting curves with a very low material consumption (2nl detection volume, below 100nM concentration) is presented. A thin sheet of water is locally heated with an infrared laser to obtain a spatial temperature distribution between 20°C and 100°C. Using microscope fluorescence imaging an entire melting curve is recorded within 50ms. This is about 10000-times faster than state of the art fluorometry and yields the same results for the validation example of a DNA hairpin. As shown, such fast high resolution melting curves can be used for the detection of single nucleotide polymorphisms (SNPs) even in mixtures. The approach can also be extended to the thermal stability analysis of proteins. For example it can be used to detect the binding of small molecules to enzymes as these binding events induce a shift in the thermal stability of the enzymes.

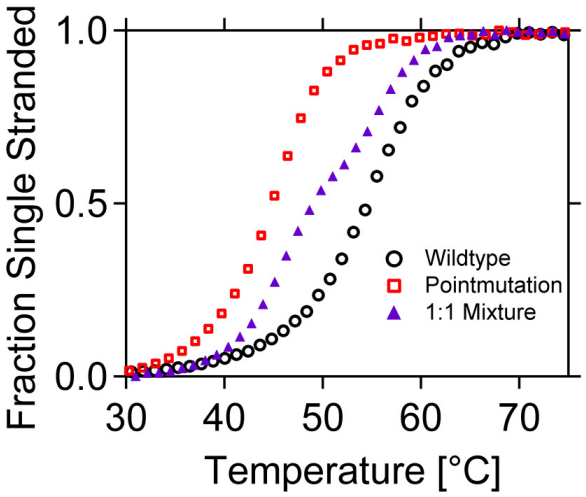

Figure 1. ***Point mutation detection within a 50ms snapshot.*** *The 22 base oligonucleotide hybridized to its fully complementary strand (wildtype, black circles) can be well discriminated from the oligonucleotid hybridized to a strand containing one point mutation (pointmutation, red squares). Even a mixture of wildtype and pointmutation (1:1 mixture, blue triangles), as it is found in PCR-products, can be well discriminated from the wildtype.*

Quantification of Aptamer-Target Binding with Thermophoresis

Aptamers are nucleic acid ligands selected in vitro for their ability to bind to specific molecular targets. They are promising candidates for medical and diagnostic applications because of their antibody comparable specificity and sensitivity. In this thesis a novel approach for the quantification of aptamer-target interactions in buffers and biological liquids is described. The approach is based on the directed movement of molecules in temperature gradients, an effect termed "Thermophoresis". Thermophoresis depends on the interface between molecule and solvent and probes the size, charge and solvation energy of the molecules. The thermophoresis of an aptamer differs significantly from the thermophoresis of an aptamer-target complex due to size, charge and solvation energy differences. This difference in the molecule's thermophoresis is used to quantify aptamer-target binding in titration experiments. The approach can be used equally well in buffers and biological liquids like blood serum without loosing sensitivity and specificity like it is the case for chip-based technologies such as Surface Plasmon Resonance (SPR). As result, the approach enables to determine the efficacy of aptamer based drug candidates, for example "Spiegelmers", in close to physiological conditions. The method is also applicable to the screen for new aptamers since the binding of unlabelled aptamers to a labelled target can also be quantified with thermophoresis.

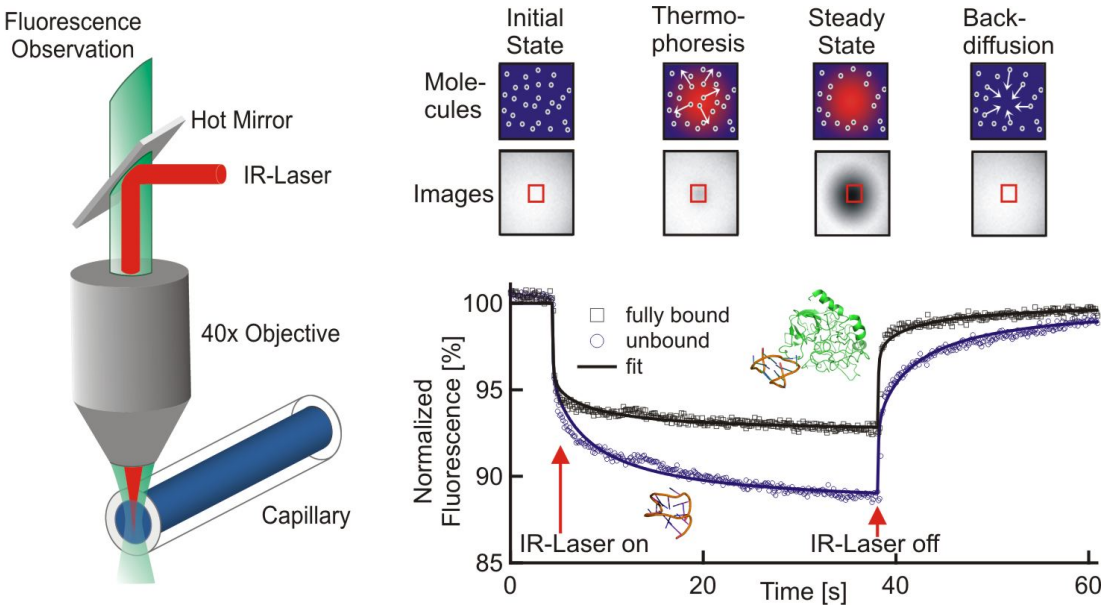

Figure 2. ***Thermophoresis assay.*** *The blood serum solution inside the capillary is locally heated with a focussed IR-laser, which is coupled into an epifluorescence microscope using a hot mirror. The fluorescence inside the capillary is imaged with a CCD-camera and the normalized fluorescence in the heated spot is plotted against time. The IR-laser is switched on at t=5s and the fluorescence decreases as the temperature increases and the labelled Aptamers move away from the heated spot due to thermophoresis. As the IR-laser is switched off the molecules diffuse back.*

Hydrothermal Accumulation of Biomolecules

All approaches to the molecular origin of life require fairly high concentrations of small protobiotic molecules, whereas geochemical extrapolations indicate a highly dilute prebiotic ocean with too low concentrations of molecules. This discrepancy has been termed the concentration problem of the origin of life. The simulations of the molecular transport in elongated hydrothermal pore systems influenced by a thermal gradient showed an extreme accumulation of molecules in a wide variety of plugged pores. The mechanism is able to provide highly concentrated single nucleotides, suitable for operations of an RNA world at the origin of life. It is driven solely by the thermal gradient across a pore. On the one hand the fluid is shuttled by thermal convection along the pore, whereas on the other hand, the molecules drift across the pore, driven by thermophoresis. As a result, millimeter-sized pores accumulate even single nucleotides more than 10^8-fold into micrometer-sized regions. While thin pores can concentrate only long polynucleotides, thicker pores accumulate short and long polynucleotides equally well and allow various molecular compositions. This setting also provides a temperature oscillation, in which DNA can be exponentially replicated in the protein-assisted Polymerase Chain Reaction (PCR).This interlinked mineral pores in a thermal gradient are providing a compelling high-concentration starting point for the molecular evolution of life.

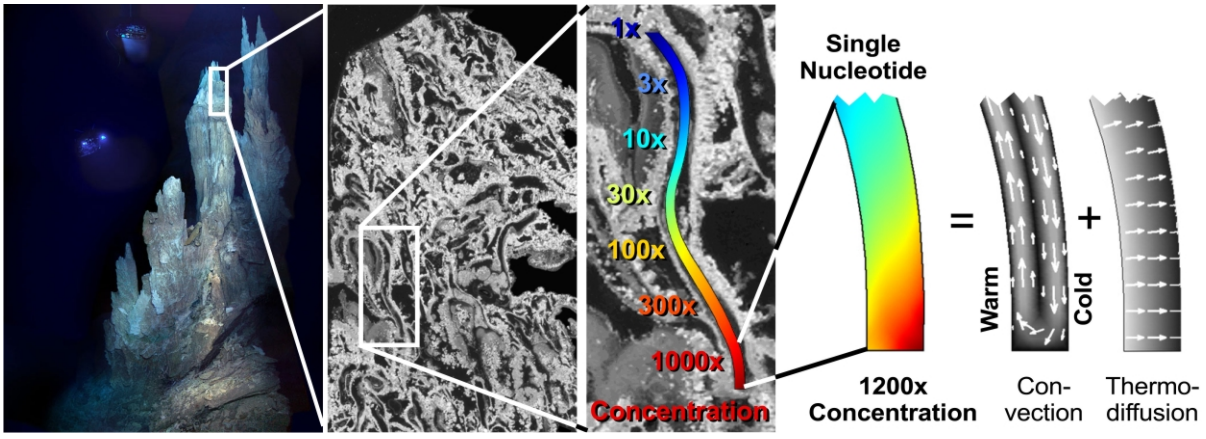

Figure 3. ***Temperature driven molecular accumulation in hydrothermal pores.*** *Section through aragonite ($CaCO_3$) from the submarine hydrothermal vent field at Lost City. Simulations of a part of the pore system show a 1200 fold accumulation of single nucleotides. The mechanism of accumulation is driven by heat in a twofold way. Thermal convection shuttles the molecules vertically up and down and thermophoresis pushes the molecules horizontally to the right. The result is a strong molecular accumulation from the top to the bottom.*

Hairpin Replicators: Protein-Free Replication by Hybridization?

In this chapter a protein-free exponential replication mechanism, solely driven by a temperature oscillation and the hybridization of hairpins is presented. Microscale thermal convection is a natural setting for the temperature oscillation and is found in submarine hydrothermal vents. In a cross-catalytic chain reaction, initiated by a template, metastable RNA hairpins form multimers and replicate a succession of short sequence snippets of the template. The energy to drive the system is kinetically trapped in metastable RNA hairpins and is released by the template catalyzed hybridization of hairpins towards more stable multimers. During the temperature oscillation the hybridization takes place at lower temperatures whereas the formed products efficiently dissociate from the template at the elevated temperatures. Thus the temperature oscillation prevents product inhibition and allows an exponential replication. By combining two hairpins, a succession of templates is replicated. This double hairpin strongly resembles the cloverleaf structure of tRNA. The scheme suggests that tRNA evolved from a primitive replication mechanism driven by microscale thermal convection.

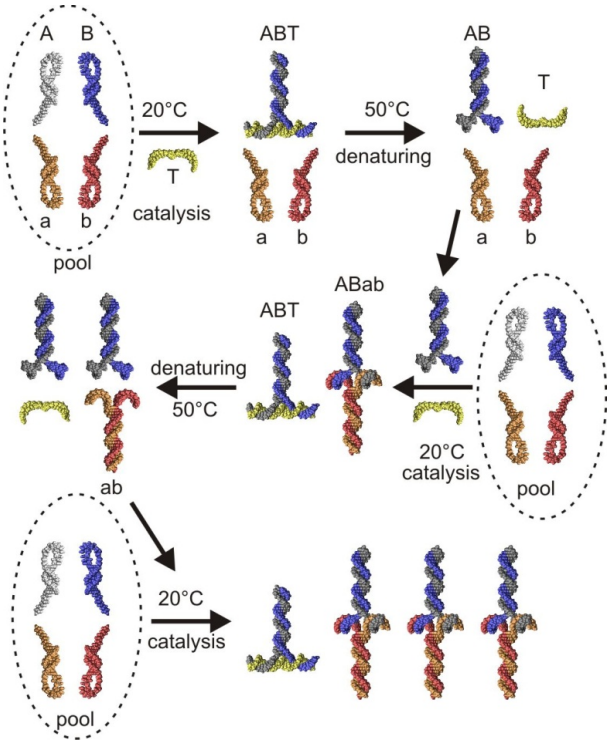

Figure 4. ***Exponential hairpin amplification by thermal cycling.*** *(a) Starting point is a pool of highly concentrated hairpins **A**, **B**, **a**, **b**. The addition of the template **T** catalyses the formation of the Triplex **ABT** at 20°C. At 50°C the template strand **T** dissociates from **ABT**, while the duplex **AB** is stable due to its long common sequence. (b) The duplex **AB** catalyzes the formation of the duplex **ab** into a quadruplex **ABab**. At 20°C the products **ABab** and **ABT** form. At 50°C the triplex and quadruplex dissociate into **AB**, **ab** and **T**. (c) Again at 20°C the duplexes **AB** and **ab** catalyze the reactions of **a** with **b** and **A** with **B**, respectively. The information of the template **T** is exponentially amplified into the quadruplex complexes by temperature cycling.*

IV. Optothermal Biotechnology

Melting Curve Analysis in a Snapshot

Measuring the stability of biomolecules and especially of DNA is of great importance in the field of biology, medical diagnostics and biotechnology. It is often inferred from thermal denaturation experiments [1] and directly provides information about the DNA sequence or the biomolecular structure. In most cases, the temperature dependent conformation of the molecules is recorded by fluorescence and plotted against temperature, yielding a so called melting curve [2]. Traditionally, a small sample volume inside a comparably large cuvette or multi-well plate is heated by thermal contact. The big thermal mass of the setup results in long equilibration times and slow heating rates. Measurement times on the order of 6-70 minutes are typical [3].

With the developed all optical method presented here the thermal stability of biomolecules is determined in less than 50 milliseconds. The temporal scan of temperatures is replaced by the application of a spatial temperature distribution, generated by heating a 20 µm thin fluid film with an infrared laser. In the experiments, a spatial temperature distribution with all temperatures between ambient temperature and 100°C was achieved with a temperature resolution of <1°C. Such high resolution melting curves can be used for the detection of single nucleotide polymorphisms (SNP), genetic screening and biomolecule binding assays [4-6].

Setup

The broad spatial temperature distribution is generated by focussing an infrared laser into a 20 µm thin sheet of aqueous solution. The wavelength of 1455 nm of the IR-laser is strongly absorbed by water with an attenuation length of 305 µm. In the 2µl aqueous solution, sandwiched between two 170 µm thick glass coverslips (Figure 5), temperatures between 20°C and 100°C are created within several milliseconds in a field of view of 200x200 μm^2. Imaging is provided with a fluorescence microscope with a 40 x oil immersion objective and a CCD camera. The measurement volume is 2 nl and concentrations in the 100 nM regime and below are accessible due to sensitive fluorescence imaging with high numerical aperture optics. Typically, a fluorescence dye reports the conformation of molecules in a melting curve. In the experiments shown here, a DNA hairpin is measured, which was labelled with a fluorophore-quencher pair, a configuration termed molecular beacon [7, 8].

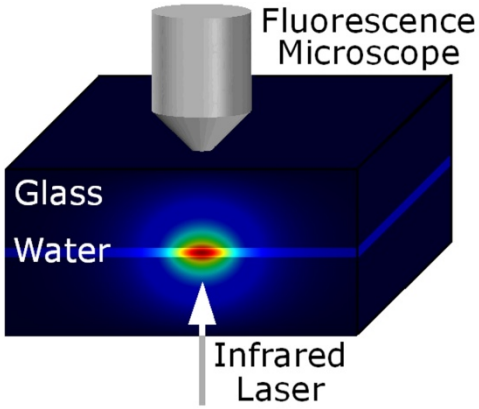

Figure 5. ***Setup.*** *Fluorescence from molecules in a 20 µm thin sheet of water is imaged from the top while it is heated with a focussed infrared laser from below. Plotting the fluorescence image versus the temperature yields a high speed measurement of a melting curve at low molecule concentration. The simulated temperature field is color coded.*

The spatial temperature distribution T(x,y) inside the chamber is measured with the temperature dependent dye tetramethylrhodamine (TAMRA,). For calibration, the temperature dependent fluorescence signal $F_{TAMRA}(T)$ of TAMRA is measured with a thermally controlled fluorometer. From the temperature dependent fluorescence $F_{TAMRA}(T)$ the $T(F_{TAMRA})$ is inferred as shown in Figure 6a. With this calibration one can calculate the temperature T(x,y) of each point of the measurement-chamber which was imaged onto a pixel of the CCD camera.

Timescales

For the measurement of melting curves a precise timing of events is necessary to prevent artefacts from thermophoresis (Figure 6b). To ensure this, numerical simulations [9, 10] of the heat conduction and the temperature dependent movement of the molecules were done. The temperature relaxes with a time scale which is essentially given by the heat diffusion relaxation time:

$$\tau = \frac{d^2}{\pi^2}\frac{C\rho}{k}$$

A relaxation time of $\tau = 0.32$ ms was found for a thickness of the chamber of $d = 20$ µm, the heat capacity of water $C = 4200$ J/(kg*K), the thermal conductivity of water $k = 0.54$ W/(K*m) and the density of water $\rho = 1000$ kg/m^3. The glass chamber walls conduct the heat comparably to water with $k \approx 0.8$ W/(K*m). This results in an effective increase of the thermal thickness d, which changes the thermal relaxation time to 2.2 ms, seen in the numerical simulation (Figure 6b, solid line). The time of 40 ms between the two images I_0 and I_1 therefore ensures steady state temperature distribution. Due to the low conducting glass walls the temperature distribution along the z-direction follows a flat parabolic profile [10].

The most important condition is that the molecule concentration within a pixel of the chamber has to remain constant between the two images I_0 and I_1. But due to thermophoresis [9-11], molecules drift along a temperature gradient and alter the concentration distribution. Therefore, the measurements have to be conducted on a time scale at which thermophoresis can still be neglected.

Thermophoresis is parameterized with a thermophoretic mobility D_T relating the molecule velocity with the thermal gradient ∇T according to $v = -D_T \nabla T$. In the steady state, the molecule concentration at a given temperature difference ΔT is given by $c/c_0 = e^{-S_T \Delta T}$ [12] with the Soret coefficient defined as $S_T = D_T / D$. For the simulation of the hairpin system, the measured parameters D_T=1.15µm^2/(s*K), D=115µm^2/s [9, 13] were used. This simulation showed, that the temperature gradients along the chamber result only in a <1% drop of the central concentration within 50ms (Figure 6b, dashed line). A similar simulation shows, that the thermophoresis of the temperature dye TAMRA does not affect the temperature measurement due to the fast experimental timing. The simulation of convection in the chamber including the laser light pressure results in a maximum speed of convection of 1.4µm/s. Within the short measurement time of 50ms this slow convection does not affect the measurement.

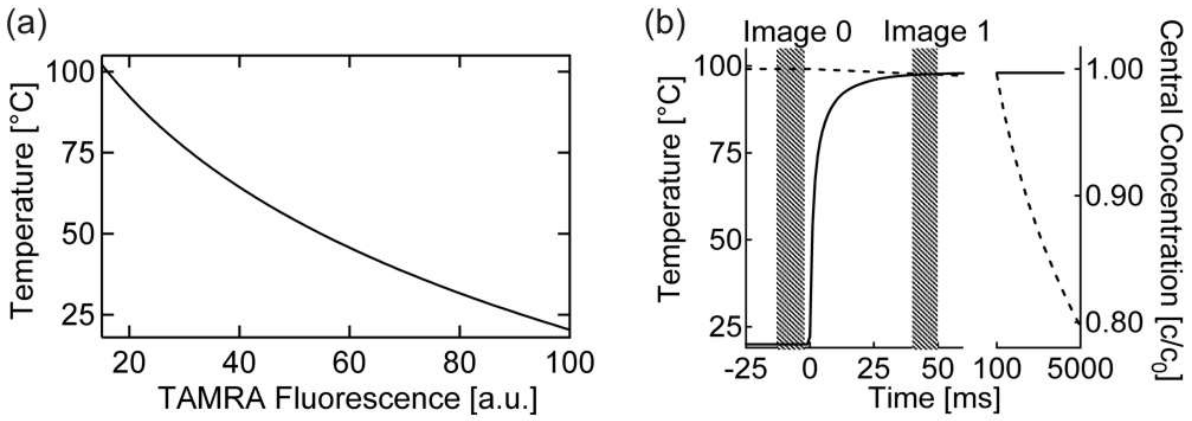

Figure 6. ***Temperature and Timing.*** *(a) Calibration curve of the temperature dependent dye TAMRA in SSC-buffer used to infer the chamber temperature. (b) Simulations show, that a precise synchronisation between laser heating and image exposures is crucial to reach a steady state in temperature (solid line) and not to significantly decrease the molecule concentration in the center of the chamber due to thermophoresis (dotted line)*

Measurements

Considering these timescales the measurements of the melting curves were conducted as described in the following (Figure 6b). First a fluorescence image $I_0(x,y)$ with 10 ms exposure time is taken at ambient temperature. Then, the infrared laser is switched on within 1 ms and a second image $I_1(x,y)$ with the same exposure time is taken after 40 ms. From the ratio $R(x,y)=I_1(x,y)/I_0(x,y)$ of this two images the conformations of the molecular beacons can then be calculated. In principle, the ratio R(x,y) (Figure 7a) could be plotted against the measured temperature T(x,y) for each pixel (Figure 7b). However, the initial radial averaging of both R(x,y) to R(r) and T(x,y) to T(r) with radius r improves the signal to noise ratio since the low signals towards the periphery are averaged over an increased number of pixels. The resulting melting curve $F(T)=(R(T)-R_{min})/(R_{max}-R_{min})$ is plotted in Figure 7c (circles). R_{min} is the fluorescence ratio of the completely closed state and R_{max} of the completely open state, respectively.

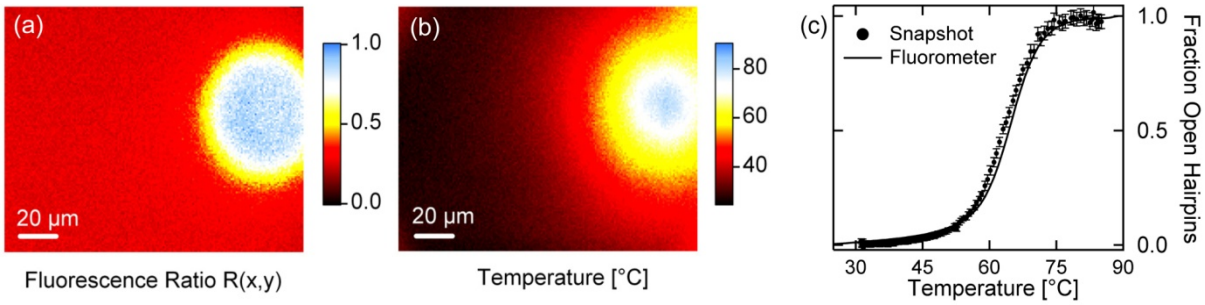

Figure 7. ***Melting curve within a 50ms snapshot.*** *(a) The fluorescence ratio image R(x,y) between heated and unheated conditions for 100 nM DNA hairpins. The fluorescence is increased in the heated spot. (b) The temperature T(x,y) is imposed to a 20 µm thin water film by infrared laser illumination and is measured using temperature sensitive fluorescence. (c) The fraction of open hairpins (circles), derived from the radially averaged fluorescence ratio R(r) is plotted against the radially averaged temperature T(r). It coincides well with a melting curve obtained from a 2h fluorometer measurement (solid line).*

The melting curve measured in only 50 ms agrees well with a 120 minutes lasting melting curve measured using a fluorometer (Figure 7c, solid line).

In the case of molecular beacons the folding and unfolding of the intramolecular DNA hairpin structures equilibrates on the microsecond to millisecond time scale [14]. Therefore, it can be expected that the melting curve is measured in the kinetic equilibrium. Thus, the melting curve was fitted with a two state model to extract the standard change in enthalpy ΔH^0 and entropy ΔS^0 of the reaction according to $\Delta G^0 = -RT\ln(K) = \Delta H^0 - T\Delta S^0$. Standard protocols were used to infer the fraction of closed to open states of the hairpin molecule and thus, the equilibrium constant K [2, 5] from the melting curve. The change in enthalpy and

entropy were ΔH^0 = -253 kJ/mol and ΔS^0 = -754 J/(mol K), respectively and thus a melting temperature of 62°C was calculated. This result is in agreement with calculations of DNA hairpin thermodynamics, predicting ΔH^0 = -275 kJ/mol and ΔS^0 = -813 J/(mol K) and a melting temperature of 65°C [15].

Out-of-Equilibrium Melting Curves

It should be noted that for molecular systems with slower kinetics, the method allows to measure well-defined out-of-equilibrium melting curves, which could show advantages in stability analysis. In the out-of-equilibrium case it is no longer possible to use the equilibrium thermodynamic potentials to describe the binding. However, it is still possible to discriminate between different species of double stranded DNA and to detect for example point mutations in the genetic code. To show this, the melting curves of a 22 bases long single stranded DNA-oligonucleotide hybridized to a fully complementary strand and to a strand containing one single point mutation (Figure 8) were measured.

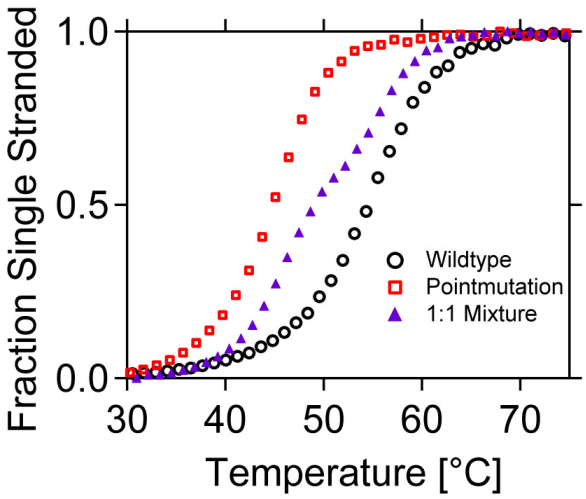

Figure 8. ***Out-of-equilibrium melting curves within a 50ms snapshot:*** *The 22 base oligonucleotide hybridized to its fully complementary strand (wildtype, black circles) can be well discriminated from the oligonucleotid hybridized to a strand containing one point mutation (pointmutation, red squares). Even a mixture of wildtype and pointmutation (1:1 mixture, blue triangles), as it is found in PCR-products, can be well discriminated from the wildtype.*

Because the hybridization between different oligonucleotides is an intermoleculare reaction it is slow compared with intramoleculare reactions. Concentration dependent reaction times $\tau_{hybridization}$ range from 10ms (oligonucleotide concentration>5µM) to several seconds (oligonucleotide concentration<100nM). Thus, the hybridization is too slow to fully equilibrate within the measurement time of only 50ms. However, as the denaturation of

double stranded DNA is an intramoleculare process, the time scales are very fast with τ_{denat}<1ms. Thus, although not in equilibrium, the DNA responds nearly instantaneously to an increase in temperature and allows even to detect single point mutations with an out-of-equilibrium thermal stability analysis.

Conclusion

A method for the fast measurement of high precision melting curves was developed. Based on an all-optically generated spatial temperature distribution, the method circumvents the slow equilibration time of conventional melting curve analysis and accelerates the analysis more than 10000 times from about 10 minutes down to 50 milliseconds. The detection volume is as low as 2 nl and measurements below 100 nM concentration are possible. The method is of particular interest for high throughput screening in biotechnology and fast genotyping in medicine or the area of forensics.

Quantification of Aptamer-Target Binding with Thermophoresis

Aptamers are nucleic acids ligands selected in vitro for their ability to bind to specific molecular targets [1-4]. They are promising candidates for diagnostic applications because of their antibody comparable affinity, specificity and the ease with which novel aptamers can be designed [5]. Aptamers have been implemented in a variety of sensing technologies [6] including optical approaches like "Aptamer Beacons" [7], electronic-sensing strategies [8] mass based sensors [9] and force based assays [10].

Here a novel approach for the quantification of aptamer–target interactions is described, which separates molecular recognition from signal transduction and requires only an aptamer tagged with one dye. It allows to probe the binding with an unspecific label in the native environment of free solution or complex biological fluids like human blood serum.

The approach is based on the directed movement of molecules along temperature gradients, an effect termed "Thermophoresis"[11-14]. In contrast to the method described in the preceding chapter, this approach does not prevent the perturbation of the spatial molecule distribution due to thermophoresis, but uses it to analyze the molecules and to measure the binding equilibrium constant according to the law of mass action. The spatial temperature difference ΔT leads to a well-defined depletion of molecule concentration in the region of elevated temperature, quantified by the Soret coefficient S_T:

$$c_{hot}/c_{cold} = \exp(-S_T \Delta T) \qquad (1)$$

Thermophoresis depends on the interface between molecule and solvent. Under constant buffer conditions, thermophoresis probes the size, charge and solvation entropy of the molecules [13, 14] and is not dependent on the concentration of the probed molecule unless millimolar concentrations are reached [12, 13].

The thermophoresis of an end-labelled aptamer A typically differs significantly from the thermophoresis of an aptamer-target complex AT since the differential contributions from size, charge and solvation entropy do not compensate. This difference in the molecule's thermophoresis is utilized to quantify the binding in titration experiments under constant buffer conditions for a 5.6 kDa aptamer to the 37 kDa protein thrombin as well as the binding of a 8.3 kDa aptamer to the 0.3 kDa AMP or 0.6 kDa ATP. Different binding affinities are

found, which depend on the used buffers, especially in the case of 10% or 50% human blood serum.

Thermophoresis Assay

The thermophoretic movement of the fluorescently end-labelled aptamer is measured by monitoring the fluorescence distribution F(x,y) inside a capillary with an epifluorescence microscope (Figure 9a). The microscopic temperature gradient is generated by an IR-laser (1480 nm), which is focused into the capillary and is strongly absorbed by water [13, 14, 17]. The temperature of the aqueous solution in the laser spot is raised by ΔT=8K. Before the IR-Laser is switched on a homogeneous fluorescence distribution F_{cold} is observed inside the capillary (Figure 9b). When the IR-laser is switched on, two effects, separated by their time-scales, contribute to the changed fluorescence distribution F_{hot}. The thermal relaxation time is fast (≈ 50 ms) and induces a change in fluorescence of the dye due to its intrinsic temperature dependence. On the slower diffusive time scale (≈ 10 s), the aptamers move from the locally heated region to the outer cold regions [14, 18]. The local concentration of aptamers decreases in the heated region until it reaches a steady state distribution (Figure 9b).

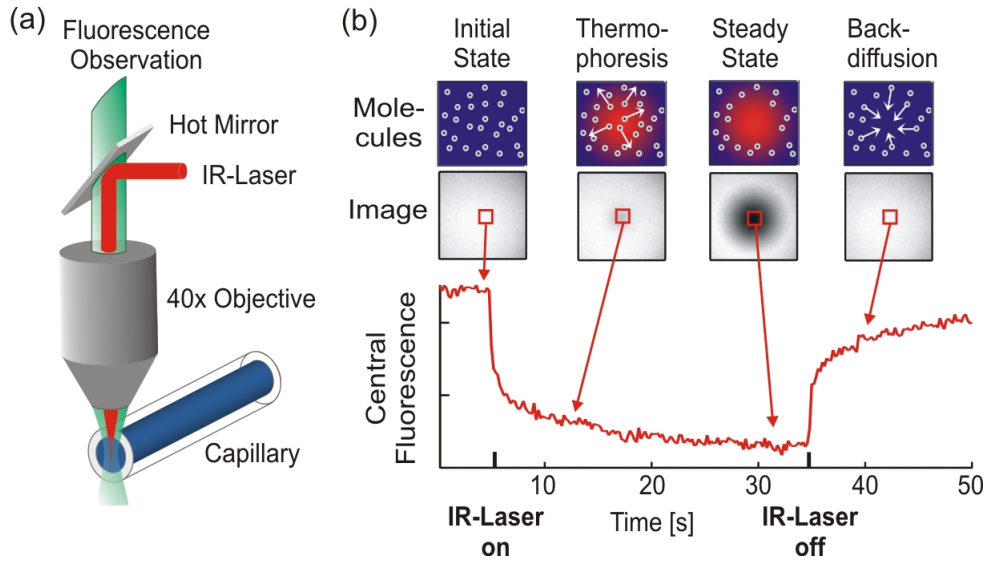

Figure 9. ***Thermophoresis assay****. (a) The blood serum solution inside the capillary is locally heated with a focussed IR-laser, which is coupled into an epifluorescence microscope using a hot mirror. (b) The fluorescence inside the capillary is imaged with a CCD-camera and the normalized fluorescence in the heated spot is plotted against time. The IR-laser is switched on at t=5s and the fluorescence decreases as the temperature increases and the labelled aptamers move away from the heated spot due to thermophoresis. As the IR-laser is switched off the molecules diffuse back.*

While the mass diffusion D dictates the kinetics of depletion, S_T determines the steady state concentration ratio $c_{hot}/c_{cold} = \exp(-S_T \Delta T) \approx 1 - S_T \Delta T$ under a temperature increase ΔT [13, 14]. The normalized fluorescence $F_{norm} = F_{hot}/F_{cold}$ measures mainly this concentration ratio, plus the percentaged temperature dependence of the dye-fluorescence $\partial F/\partial T$. In the linear approximation F_{norm} can be written as: $F_{norm} = 1 + (\partial F/\partial T - S_T)\Delta T$ [14]. Due to linearity of the fluorescence intensity and the thermophoretic depletion, the normalized fluorescence from the unbound aptamer $F_{norm}(A)$ and the bound complex $F_{norm}(AT)$ superpose linearly. By denoting x the fraction of aptamers bound to targets, the changing fluorescence signal during the titration of target T is given by:

$$F_{norm} = (1 - x)F_{norm}(A) + xF_{norm}(AT) \qquad (2)$$

Based on the capacitor model of thermophoresis [13, 19] and neglecting offsets from non-ionic contributions, one can discuss the change in S_T expected from changes in charge Q_{eff} or hydrodynamic radius R upon binding from $S_T \propto Q_{eff}^2/R^2$. Under linear approximation, S_T changes by $\Delta S_T/S_T = 2(\Delta Q_{eff}/Q_{eff} - \Delta R/R)$. Only for the unlikely case of $Q_{eff} \propto R$ no change in S_T would be expected. However contributions from the neglected solvation entropy [13] could reveal the binding even under these conditions.

Measurements

The thermophoresis of 100 nM thrombin-aptamer [21] was measured in 10% human serum (Figure 10). The concentration of thrombin ranges from 0 nM to 19500 nM. The aptamer is labelled with a Cy5 dye at the 5' end. The observed time traces of the pure aptamer differ significantly from the traces of aptamers bound to thrombin (Figure 10a). Plotting the normalized fluorescence F_{norm} at a given time t against the varying thrombin concentration results in a binding curve (Figure 10b) with an EC_{50}=680 nM and a Hill coefficient of 2. Control experiments with a randomly chosen sequence ssDNA show no thrombin dependent changes in the absolut fluorescence and in the thermophoretic signal, both in 10% and 50% human blood serum (Figure 10b).

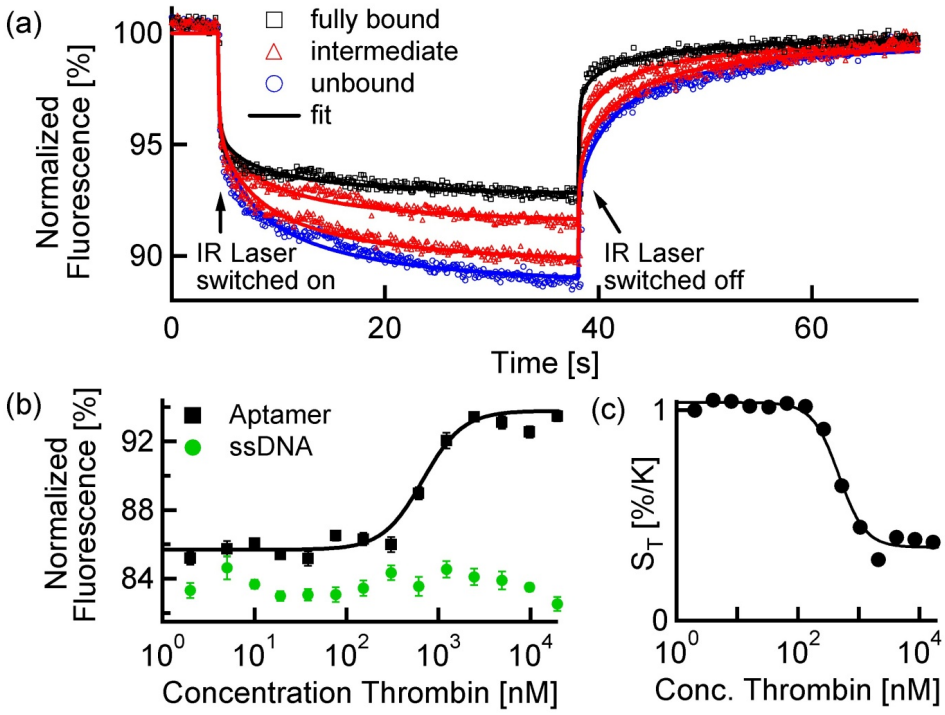

Figure 10. ***Aptamer-thrombin binding in 10% human serum.*** *(a) The thermophoresis of unbound aptamers differs significantly from aptamers bound to thrombin. (b) The normalized fluorescence F_{norm} at t=30s is plotted for different concentrations of thrombin. Random 25mer ssDNA (blue) shows no change in thermophoresis with increasing thrombin concentration. (c) The Soret coefficient S_T equally reports the binding. Fitting of S_T is provided with an analytical model of thermophoresis[16] as shown in (a).*

A 2D finite element simulation was used to infer from the time traces the Soret coefficient S_T, the diffusion coefficient D and the temperature dependence of the fluorescence $\partial F/\partial T$. The binding to thrombin mostly leads to a change in S_T, which drops from 1.05 %/K down to 0.35 %/K (Figure 10c). Both the simple determination using F_{norm} and the fitted Soret coefficient S_T report the binding (Figure 10b,c) due to linear relationship in steady state. Both the temperature dependent fluorescence change $\partial F/\partial T$ and the diffusion coefficient D show no significant binding signal.

As shown in Figure 11a, the approach can be used equally well in buffers as in complex biological liquids like blood serum without significantly loosing sensitivity or specificity, as it is the case with chip based technologies such as surface plasmon resonance (SPR). To further show the broad applicability of the thermophoretic quantification of binding, the binding of ATP/AMP to an aptamer [22] (Figure 11b) was measured in different buffers. In all cases, binding was reported with a high signal-to-noise-ratio (SNR), even in 50% human serum. For example a SNR=93 was found for the case of the 0.3kDa AMP-binding in selection buffer

and SNR=23 was found for thrombin-binding in 50% human serum. As control oligonucleotides almost identical to the aptamer sequences were used (Figure 11a,b "Binucleotide Mutant").

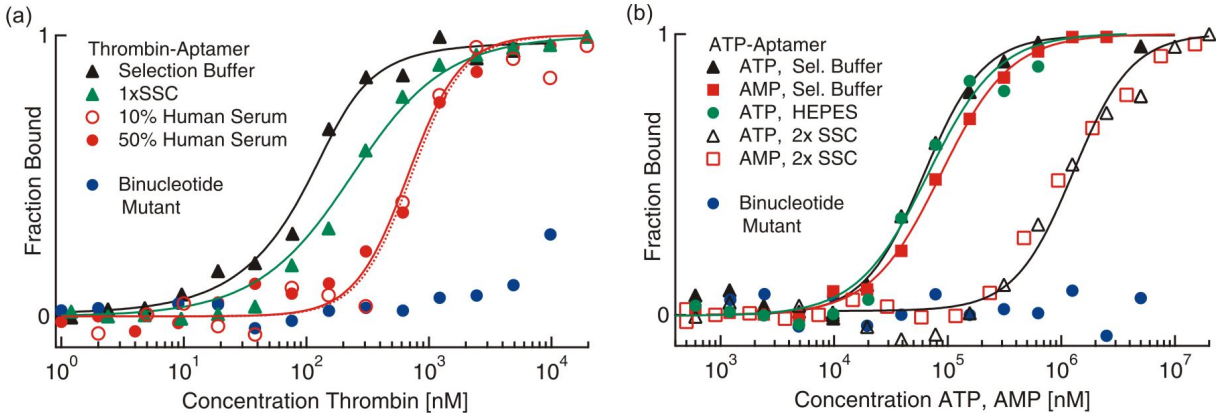

Figure 11. ***Binding curves in various buffers.*** *(a) Aptamer-thrombin binding in selection buffer, SSC and 10% and 50% untreated human serum. (b) Aptamer binding to ATP and AMP in selection buffer, HEPES and 2x SSC. The fraction of bound Aptamers is derived according to equation 2.*

The dissociation constant K_d=30 nM obtained for the aptamer-thrombin binding (Figure 11a) in selection buffer is in good agreement with the reported K_d=25 nM [21] measured in the same buffer. In SSC buffer the dissociation constant increases to K_d=190 nM and in 50% (10%) human serum the binding was best fitted with the Hill equation, yielding an EC_{50}=720 nM (670 nM) and a cooperativity of n=2.

The aptamer-ATP/AMP binding (Figure 11b) shows a cooperative binding of more than one ATP or AMP per aptamer, which is consistent with the literature [7, 23]. In the selection buffer the EC_{50} values for ATP (EC_{50}=60 µM) and AMP (EC_{50}=87 µM) are well within the reported value [7]. Measurements in HEPES buffer with EC_{50}=67 µM confirm these results. In all cases the Hill coefficient was n=1.4. Interestingly, in 2x SSC buffer, the EC_{50} values of the ATP/AMP-aptamer binding were both strongly shifted to lower affinities, resulting in an EC_{50}=1100 µM.

As stated by Cho and Ellington [6], the aptamer-target binding was strongly dependent on the chosen buffer: Binding of the aptamers in the respective selection buffers showed always the highest affinity (Figure 11). For the aptamer-thrombin binding the shift to lower affinities (EC_{50}=720 nM) and enhanced cooperativity (n=1.5) in human serum may be because of interactions of the thrombin with blood serum components. For the ATP-aptamer the

unexpected big shift to lower affinities in the SSC buffer as compared to the TRIS and HEPES buffers can be attributed to a competing interaction of the strongly negative $Citrate^{3-}$ with the Mg^{2+}-ions as the latter are essential for the aptamer-ATP/AMP binding.

Conclusion

An all-optical technique for the screening of aptamer-target interactions in bulk solution with very low material consumption (500 nl out of which only 2 nl are probed) was developed. The dynamic range of the thermophoresis binding assay reaches from nM to mM target concentrations and can also quantify the binding to low molecular weight targets such as AMP. The measurement can be equally well performed in complex liquids such as blood or simple standard buffers. As result, the approach allows to determine the affinity of aptamer based drug candidates, for example Spiegelmers [24], in biological liquids close to physiological conditions. The method is also applicable for in vitro selection of new aptamers, since the binding of unlabelled aptamers to their labelled targets can also be quantified with thermophoresis.

V. A Microthermal Origin of Life?

Hydrothermal Accumulation of Biomolecules

A wide range of studies on the origin of life discuss the chemical synthesis of protobiomolecules [1-4]. Concurrently, the studies of replication systems [5-8] culminated in the RNA-world proposal [9]. All these approaches require fairly high concentrations of small protobiotic molecules, whereas geochemical extrapolations indicate a dilute prebiotic ocean with concentrations comparable to contemporary values [10, 11]. This discrepancy has been termed "the concentration problem of the origin of life" [10, 12]. In the following a robust and efficient solution to the concentration problem is described. The solution is based on heat currents in porous mineral precipitates comprising a hydrothermal mound developed over a moderately warm submarine spring. However, to accumulate molecules from a highly diluted prebiotic ocean a considerable entropic gap has to be bridged. In a rough estimate, at least a 10^6-fold accumulation is required for small protobiomolecules to interact. To fulfill the second law of thermodynamics, such states of exceedingly low entropies can only be siphoned from a larger non-equilibrium system. Contemporary life [13] sustains the required high molecular concentration in a dissipative nonequilibrium state by a wide range of highly evolved strategies. For the evolution of life, an already existing protobiological dissipative environment is required [14]. The most compelling would refer to an accumulation of molecules into preexisting abundant compartments of cellular dimensions [15]. Both requirements are fulfilled by the proposed accumulation mechanism.

Hydrothermal Setting

From a geological point of view, thermal gradients are the most abundant dissipative systems on the early earth. They drive convective water flow with a wide variety of geometries. Contemporary hydrothermal vents [14-20], both black smokers and "Lost City" type vents, are only extreme cases for heat dissipation. Hydrothermal vents are surrounded by highly porous mineral precipitates. Within these structures the ubiquitous millimeter to micrometer sized pores and syneresis cracks (Figure 12a) are considered. A temperature gradient, typically along the horizontal direction, exists across such pore systems. It is shown, that these natural settings can easily accumulate single nucleotides more than 10^8-fold at the bottom of a plugged pore system. Thus, this accumulation is sufficient to step up from the highly diluted prebiotic ocean to molar concentrations within the pore.

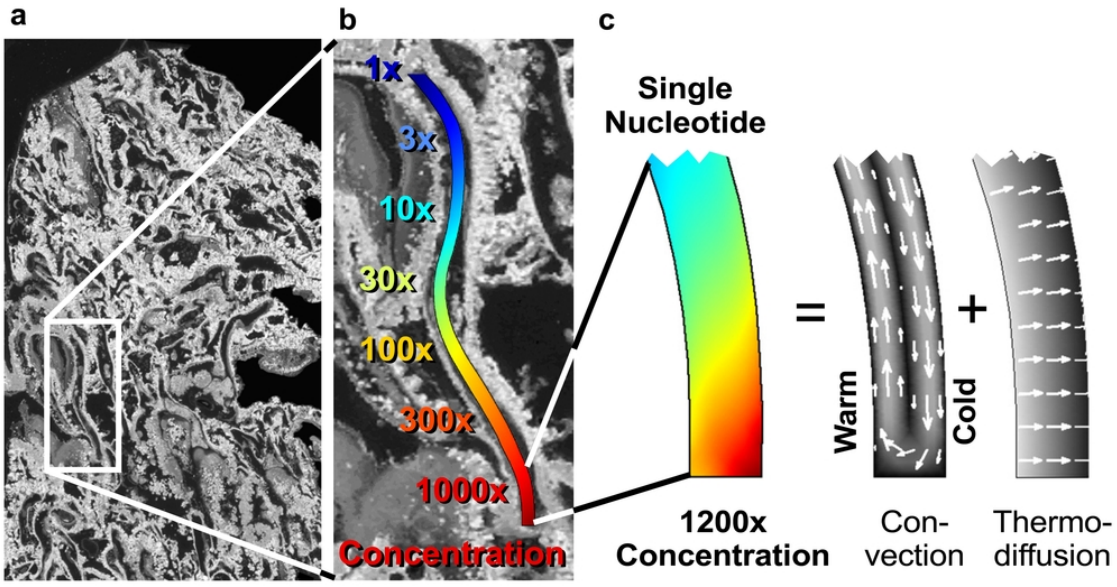

Figure 12. ***Heat driven molecular accumulation in hydrothermal pores.*** *(a) Section through aragonite ($CaCO_3$) from the submarine hydrothermal vent field at Lost City (kindly provided by D. Kelley [20]). (b) Simulation of a part of the pore system. If subjected to a horizontal thermal gradient of 30K, a 1200-fold accumulation of single nucleotides is expected (logarithmic concentration color scale). A concatenation of three of these pore sections leads to a 10^9 fold accumulation. (c) The mechanism of accumulation is driven by heat in a twofold way. Thermal convection shuttles the molecules vertically up and down and thermophoresis pushes the molecules horizontally to the right. The result is a strong molecular accumulation from the top to the bottom (linear concentration color scale).*

Mechanism of Accumulation

The mechanism of accumulation operates as follows. In a hydrothermal vent a plugged pore system is sandwiched between the hot vent interior and the cooling outside ocean (Figure 12b). A temperature gradient across the pore drives two entangled processes: (i) molecules are shuttled up and down the cleft by laminar thermal convection and (ii) thermophoresis drives the molecules along the temperature gradient, i.e. perpendicular to the convection flow. Both processes are indicated by white arrows in Figure 12c. In combination, they lead to a strong vertical accumulation towards the closed bottom of the cleft. This geological setting is analogous to a Clusius-tube or thermogravitational column [21]. Here the behavior of rather rapidly diffusing single nucleotides is simulated. Even with conventional biotechnological or microfluidic laboratory methods, such small molecules are hard to concentrate because of their considerable diffusion. The simulation shows a strong 1200-fold downward accumulation of single nucleotides for the 5mm short, bent cleft of Figure 12b. A concatenation of three of these pores leads even to a $1200^3 = 1.7*10^9$-fold accumulation. A temperature difference of 30 K is applied across the pore and the maximal accumulation occurred in a pore with a cross-section of 145µm. The diffusion of molecules in the

convection flow was calculated by solving the combined Navier-Stokes, diffusion- and heat transfer-equations using commercial finite element software (Femlab, Comsol). The simulated pores feature a closed bottom and an open top end. The biomolecule concentration was fixed at the top, while the bulk fluid was subjected to gravity and restricted by the pore with non-slip boundary conditions. The heat transfer is barely affected by the slow laminar convection, and the temperature drops linearly across the pore structure.

For the simulations the thermophoretic characteristics of nucleotides were measured using the previously described fluorescence techniques [22]: Molecules move along a thermal gradient ∇T with a drift velocity $v=-D_T\nabla T$. The ratio between the thermodiffusion coefficient D_T and the mass diffusion coefficent D is termed the Soret coefficient $S_T=D_T/D$, which typically determines the steady state concentrations. This steady state concentration is measured to determine the Soret coefficient. The diffusion coefficient is measured from the backdiffusion of the molecules as shown in Figure 9b. The experimental results are presented in Table 1.

	Single Nucleotide	ssRNA 22bases	dsDNA 100bp	dsDNA 1000bp
S_T 1.7mM salt	0.015/K	0.014/K	0.075/K	0.3/K
S_T 170 mM salt	0.006/K	0.003/K	0.019/K	0.09/K
D	400 µm²/s	100 µm²/s	45 $\mu m^2/s$	8 $\mu m^2/s$

Table 1. *Soret coefficient S_T and Diffusion coefficient for different molecules.*

Results

A short pore with an aspect ratio of 10:1 accumulates single nucleotides 7-fold (Figure 13). A pore with the same aspect ratio accumulates a 22 bases long single stranded RNA 6-fold, a 100 bases long double stranded DNA 20,000-fold, and a 1000 bases long DNA to 10^{15}-fold levels. For these larger molecules the short pore behaves like a molecule trap: once molecules enter the top of the pore, they are transported to the pore base and are accumulated to molar-level concentrations in a micrometer-sized spot in bulk water.

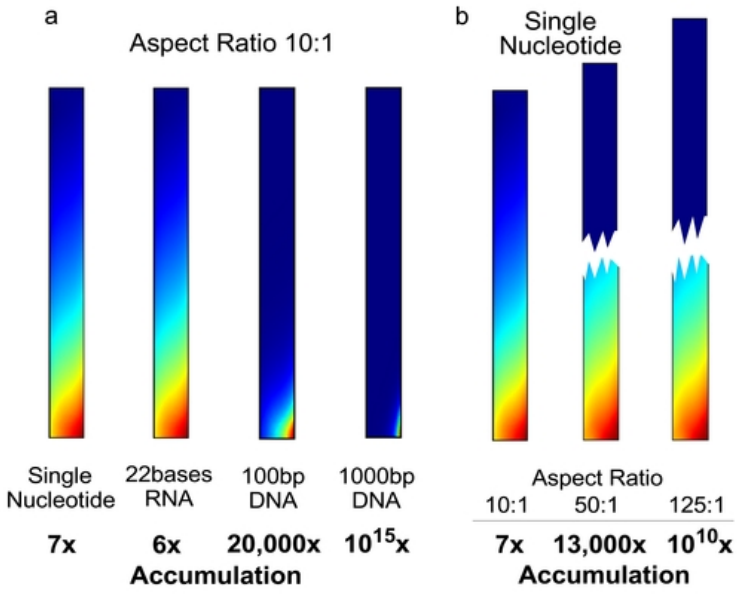

Figure 13. ***Predicted effects of the molecule size and pore length on the accumulation level.*** *The simulations results are based on the experimentally measured Soret coefficients and diffusion coefficients for DNA and RNA (see Table 1). (a) The accumulation increases exponentially with the size of the molecule. While single nucleotides are accumulated 7 fold in a short cleft of aspect ratio 10:1, double stranded DNA comprising 1000 base pairs accumulates 10^{15} fold. The equilibration takes 9min for single nucleotides and 14min for single stranded RNA comprising 22 bases. For DNA polynucleotides of 100bp and 1000bp it takes 18min or 33min, respectively. (b) Elongation of the cleft exponentially increases the accumulation. For example, the accumulation of single nucleotides is raised to a 10^{10} fold levels in a pore with an aspect ratio of 125:1. A linear concentration scale is used in both plots, scaled to the respective maximal concentration. The time to reach steady state is 9min for r=10, 4h for r=50 and 23h for r=125.*

The accumulation grows exponentially both with the size of the molecule and the length of a concatenated pore system. In concatenated pores accumulation of molecules increases exponentially, a result of the considerable concentration independence of thermophoresis below molar concentrations [23-25]. Thus, while single nucleotides accumulate merely 7-fold in the short pore of Figure 13a, concatenating 12 of these pores using a wide variety of orientation angles exponentiate the accumulation to an extreme $7^{12} = 10^{10}$-fold level. Elongation of the pore has exactly the same effect. As shown in Figure 13b, a pore system with a total aspect ratio of r = 125:1 accumulates single nucleotides 10^{10}-fold. Notably, the length of this pore system is only 18 mm, which is below the typical lengths of pore systems in hydrothermal settings.

The analytical solution [26, 27] for the accumulation in a rectangular cleft geometry confirms the above numerical findings. The accumulation is found to be an exponential function given by

$$\frac{c_{bottom}}{c_{top}} = \exp\left(0.42\, S_T\, \Delta T\, r\right) \qquad (1)$$

with the Soret coefficient S_T, the temperature difference ΔT and the aspect ratio r. For $0.42\, S_T\, \Delta T\, r \gg 1$ the molecular accumulation is large and rises exponentially with temperature difference ΔT or pore length. In pores with a sufficient aspect ratio r, substantial accumulation is reached even for small molecules with tiny Soret coefficients (Table 1). The exponential characteristic of equation (1) makes the accumulation robust since a small elongation of the pore leads to a large increase in molecular accumulation. Every linear decrease in the temperature difference ΔT can be compensated by a linear increase in pore aspect ratio r. For example, in order to achieve the same accumulation at just one tenth of the temperature difference, a ten-fold longer pore is needed. To illustrate this the accumulation versus the aspect ratio r is plotted in Figure 14 for single nucleotides, for polynucleotides of 22 single stranded RNA bases, and double stranded DNA comprising 100 and 1000 base pairs.

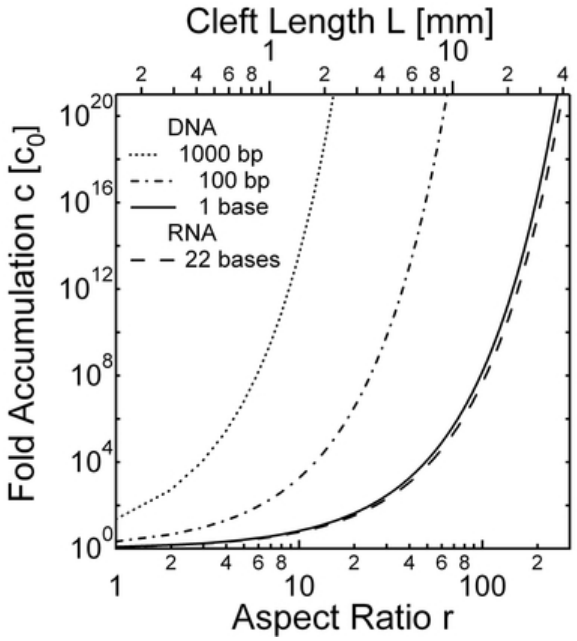

Figure 14. ***Exponential accumulation.*** *The accumulation depends exponentially on the aspect ratio r and the temperature difference ΔT, according to the analytical theory [Equation 1]. Even for single nucleotides it is remarkably easy to reach exceedingly large molecular accumulations. The accumulation is calculated for ΔT=30K*

A critical parameter is the width of the pore. For an extended rectangular cleft [26, 27], the largest accumulation is found for an optimal width d_0 given by

$$d_0 = 8.4\ (\mu D\ /\alpha\rho g_0 \Delta T sin\theta)^{1/3} \qquad (2)$$

with the viscosity of the fluid μ, the diffusion coefficient of the molecule D, the fluid volume expansion coefficient α, the fluid density ρ, the gravitational acceleration g_0, the inclination angle θ to the horizontal plane and the temperature difference ΔT. As the result of the exponent 1/3 in equation (2), values for d_0 fall between 40μm and 400μm for an extensive range of parameters D, θ and ΔT, as shown in Figure 15a.

Figure 15b illustrates the pore size dependence of the accumulation in more detail. DNA molecules of different length are selectively partitioned depending on pore width. For an equivalent value of ΔT (30K), single nucleotides accumulate best for a pore width of 145 μm while a 1000bp DNA fragment accumulates best for a width of 40μm. Therefore the geometry determines the size of the preferentially accumulated molecules. On the other hand, the accumulation of longer polynucleotides is much more efficient and pore widths around 150 μm accumulate a wide range of different DNA lengths equally well.

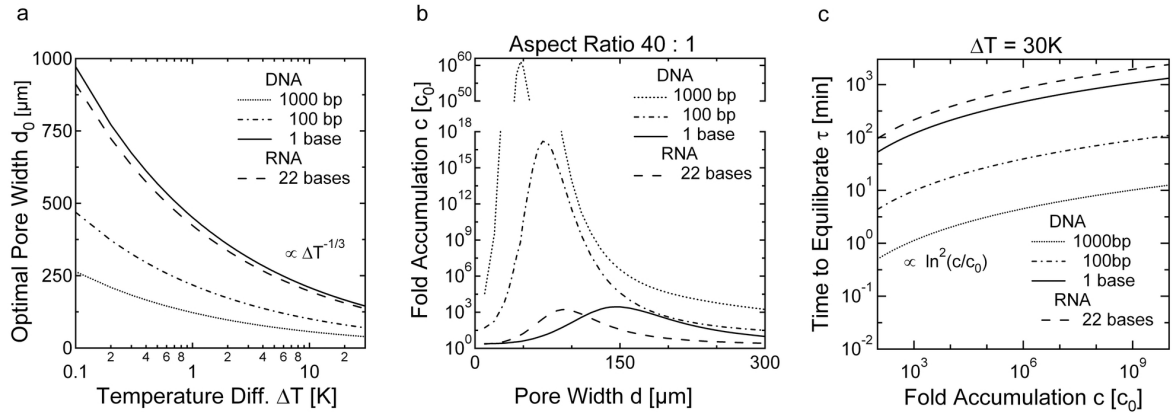

Figure 15. ***Pore width and equilibration time.*** *(a) The optimal cleft width depends moderately on the molecular size and temperature difference. The optimal cleft width is proportional to $D^{1/3}$ and $\Delta T^{-1/3}$ with the diffusion coefficient D and temperature difference ΔT. As a result, much longer nucleotides require only slightly narrower pores. (b) Accumulation drops considerably for pores with a non-optimal width. Nucleotides are selectively accumulated in particularly narrow chambers. For a wider pore width d ≈ 150μm, the accumulation of molecules with different sizes reaches comparable levels. (c) The equilibration towards a 10^8-fold accumulation takes 14 hours for single nucleotides and 25 hours for single stranded RNA comprising 22 bases. For DNA polynucleotides of 100bp and 1000bp it takes 70min or 8min, respectively. This might be counterintuitive, but larger molecules accumulate faster since a considerably shorter cleft is sufficient to achieve the same level of accumulation.*

The time τ to reach a steady state concentration profile is given by the diffusion time along the pore:

$$\tau = r^2 d_0^2 / \pi^2 D \quad (3)$$

As a result a 10^8-fold accumulation of single nucleotides is achieved after τ = 14 hours, and for a 22 base single stranded RNA, after τ = 25 hours. However, the time to reach a comparable accumulation for larger molecules drops to 70min for 100 bp DNA and 8min for 1000 bp DNA (Figure 15c). The reason for this drop in accumulation time is the much shorter cleft length required for longer DNA.

Notably, all these times are extremely short compared to the lifetime of a typical vent chimney or even the Lost City vent system, which operates at least for 30,000 years [20, 28].
In the above calculations, a temperature difference of ΔT=30K is assumed. It is anticipated, that this is a realistic assumption, since temperature gradients are focused inside the clefts due to the considerably lower thermal conductivity of water (0.6 W/mK) as compared to the surrounding rock (>3 W/mK). The thermal conductivity measured for a hydrothermal pyrite-silica precipitate [31] is 14 W/mK, but the isolated pyrite and quartz minerals yield roughly 20 W/mK and 3-4 W/mK, respectively, in laboratory tests [30, 32]. The resulting enhancement of the temperature gradient in the liquid part of the pores is 5- to 200-fold. Thus, in order to obtain the temperature difference of 30 K, assumed in the above simulations, the required overall temperature gradient is of the order of 1 to 40 K/mm, in good agreement with reported values of ΔT for natural hydrothermal settings. Focussing of the temperature gradient in the pores however is not essential for the accumulation process. For lower thermal gradients, the same accumulation can be achieved, if the pore system is elongated linearly for a decreasing temperature difference.

Conclusion

Previously, all experimental approaches, devised in the past to simulate conditions of molecular evolution, required considerable concentrations of biomolecules to work and thus implicitly relied on an efficient accumulation process in bulk water. The pore geometries studied here demonstrate for the first time a strong accumulation of small molecules, such as single nucleotides, in a highly plausible geological setting on the early earth. The approach has the advantage of offering an active accumulation mechanism [34] in an already existing, robust enclosure. Since thermophoretic drift is common within molecules, the accumulation

scheme applies to nucleic acids, amino acids and lipids. Notably, the results from the simulations shown here were recently proved experimentally by JW Szostak [42].

The mineral pores, which are proposed as accumulation centers for the emergence of life, are presently populated with thermophilic prokaryotes, and it is speculated that these sites could have been inhabited by the last common ancestor and its biochemical precursors [15, 39]. Rapid thermal quenching was demonstrated to be able to polymerize both nucleic [40] and amino acids [16] in a setting, in which hydrothermal fluids were injected into cooled (4°C) water. The discussed setting of thermal convection provides comparable temperature interfaces, but now within a single pore. So both the temperature drop and the needed molecule concentration could be found in an enclosure instead of an open flow reactor.

The water inside the pore network is permanently shuttled by laminar thermal convection [34, 35, 36]. Molecules which stochastically escape the accumulation at the bottom of the pore by diffusion are subjected to a rapid periodic temperature variation within a wide range of temperature amplitudes and cycle times inside a single pore. Equally, freshly precipitated mesoscopic mineral grains are subjected to thermal cycling by the convection. Their catalytic surfaces might generate nucleic acid multimers by thermally triggered periodic condensation and unbinding reactions. In a comparable thermal convection setting DNA was shown to replicate exponentially using the albeit protein-catalysed Polymerase Chain Reaction (PCR) [33, 41]. Thus this setting provides a compelling, dissipative microenvironment to promote the first steps in the molecular evolution of life.

Hairpin Replicators: Protein-Free Replication by Hybridization?

In the previous chapter a mechanism was shown which is able to highly concentrate single nucleotides, suitable for operations of an RNA world at the origin of life. The natural setting of hydrothermal pore systems also provides a temperature oscillation mechanism, namely thermal convection. With thermal convection, as shown previously, it is possible to exponentially replicate DNA in the protein-assisted Polymerase Chain Reaction (PCR). In the following the hypothesis, that even a protein-free replication is possible in these hydrothermal pore systems is presented.

From an evolutionary point of view, replication merely amounts to the transfer of information [1-3]. One would argue, that a minimal transfer of information is the memorizing of the succession of two or more short sequences (Figure 16), i.e. the controlled ligation of two oligonucleotides depending on their sequence [4]. Such economy in replication is also found in biotechnology. The sequence detection of a polymerase chain reaction (PCR) can also be implemented by the biologically simpler ligation chain reaction (LCR). PCR and LCR are used to detect the existence of a specific sequence, as the faithful replication of a base sequence is not required [5, 6]. This aspect of amplification of information is also central to evolution, where the central point is detecting and amplifying suitable sequences, which have survived selection. Here it is argued, that the simplest transfer of information is physico-chemical by concatenating sequences together with hybridization (Figure 16) rather than by the chemical fixation of a template sequence base-by-base.

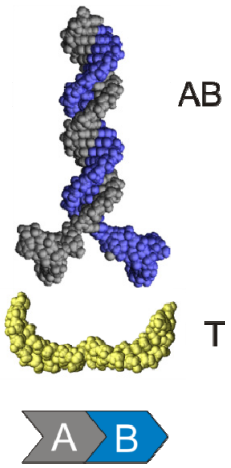

Figure 16. ***Information storage in oligonucleotides.*** *The template **T** contains the information "**A** before **B**". This information is also stored in the single stranded regions of the duplex **AB**. The complex **AB** forms from kinetically trapped hairpins.*

Temperature oscillations are required for exponential replication and can be implemented by microscale thermal convection [7]. For example, they can be provided by the laminar

microconvection in porous rock in the vicinity of hydrothermal vents, in which the synthesis of interesting molecules is likely [8-16]. The thermal cycling of molecules by convection periodically associates and dissociates nucleotides. For example, the template initiated Polymerase Chain Reaction can be driven by convection [17, 18]. As shown in the previous chapter, similar conditions allow for the strong accumulation of even single nucleotides, thus providing a periodically changing environment for the emergence of information-carrying and knowledge-accumulation systems [20].

Replication Scheme

The exponential replication mechanism proposed is driven by a temperature oscillation and the hybridization of hairpins. In a cross-catalytic chain reaction, initiated by a template, metastable RNA hairpins form multimers and replicate a succession of template sequences. The energy to drive the replication is kinetically trapped in the metastable RNA hairpins and is released by the template catalyzed hybridization of hairpins towards more stable multimers. The temperature oscillation prevents product inhibition and allows an exponential replication.

The hairpins **A**, **B**, **a** and **b** are composed of three segments: toehold, stem and loop (Figure 17a). The stem is formed by two self complementary regions within the hairpin sequence. The hybridization energy of the loop is kinetically trapped [21] and can only be released after the stem is opened [22, 23]. The two hairpins **A** and **B** are complementary to each other in the loop and stem segment. Upon activation of their stem, they hybridize to the duplex **AB** with a comparably large and stable base-paired sequence (Figure 17b). The spontaneous hybridization rate of **A** with **B** is very low as long as the stem is closed. So, in spite of the duplex **AB** being the thermodynamically favorable equilibrium conformation, no significant amount of duplex is formed over long times due to the kinetically trapped secondary structure. The template **T** catalyzes the reaction between **A** and **B** (Figure 17c) by hybridizing to both of the toehold regions of the hairpins. As both are kept in proximity, the local concentration for hybridization is increased. This activation can increase the reaction rate of **A** with **B** by at least a factor of 1000 [24].

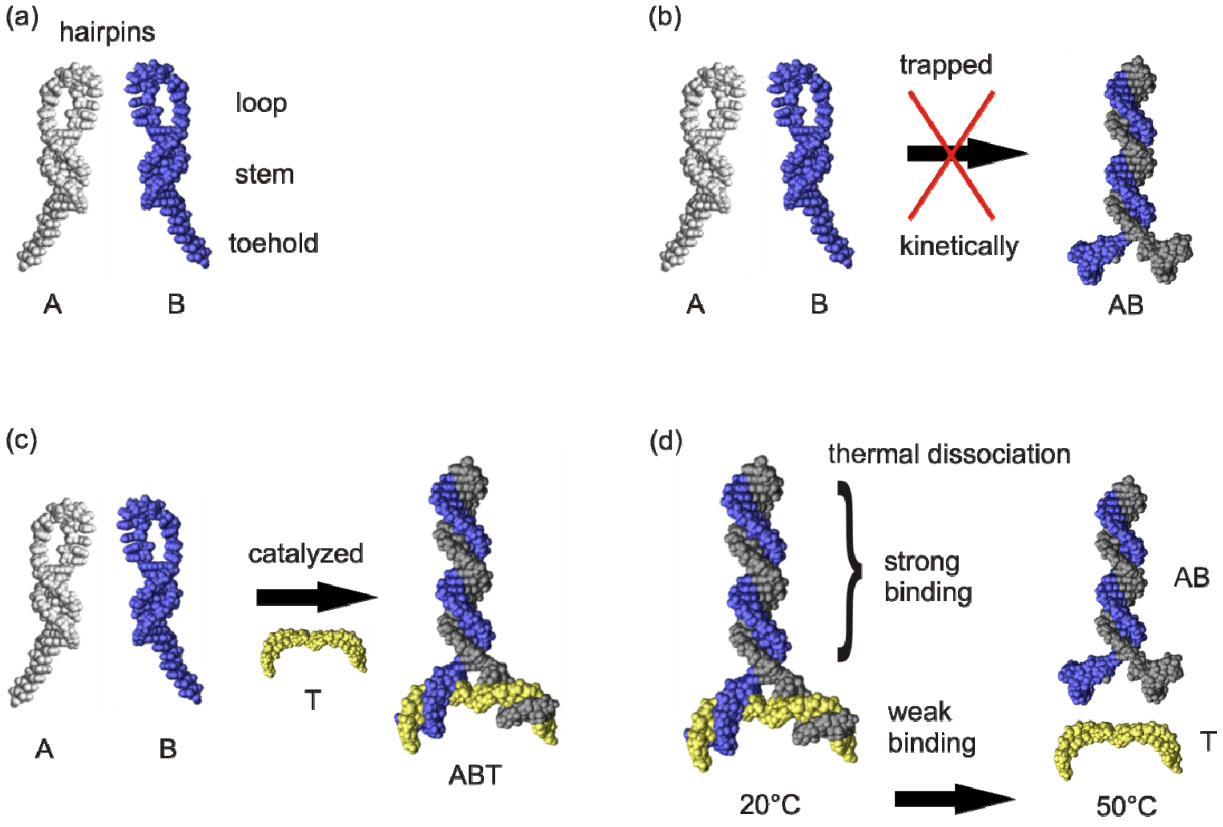

Figure 17. ***RNA hairpin structures.*** *(a) RNA molecules often form a hairpin secondary structure. Generally, the hairpins consist of a loop, storing hybridization energy, a stem, kinetically trapping the stored energy and a toehold. (b) The binding of hairpin **A** with hairpin **B** is kinetically trapped since the loops can only fully hybridize if the stems are opened. (c) At 20°C the single stranded template-strand **T** hybridizes to the toehold region of the hairpins, opens the stems partially and catalyzes the formation of the triplex **ABT**. (d) In the triplex structure **ABT**, the hairpins show a strong binding domain and a weak binding domain. The triplex is stable at 20°C whereas at elevated temperatures the more stable duplex domain **AB** remains hybridized.*

Before the replication scheme is extended to a succession of sequences, the simplest case is analyzed. Starting point is a pool of highly concentrated RNA sequences, **A**, **B**, **a** and **b.** The molecules form an intramolecular metastable hairpin conformation when they are cooled faster than the average time needed to bind to other molecules. The addition of a small amount of the template **T** to this pool of sequences initiates a cross-catalytic chain reaction (Figure 18). At the first step of 20°C the template **T** catalyzes the hybridization reaction of hairpin **A** with hairpin **B**, forming the triplex **ABT**. In a short heating step to 50°C, this triplex dissociates into **T** and the stable duplex **AB** (Figure 18a).

In the next step at 20°C the hybridization reaction of the hairpins **a** and **b** is catalyzed by the duplex **AB** forming the quadruplex **ABab** (Figure 18b). At the same time, the free template **T** again catalyzes the reaction between the hairpins **A** and **B**, forming the triplex **ABT**. A short heating step to 50°C allows the quadruplex **ABab** and the triplex **ABT** to dissociate into the

stable duplexes **AB**, **ab**, and the template **T** (Figure 18b). From this point on, the number of quadruplexes **ABab** doubles after each temperature cycle under ideal conditions (Figure 18c). The temperature cycling overcomes product inhibition, which is a problem in isothermal replication systems [4, 25, 26].

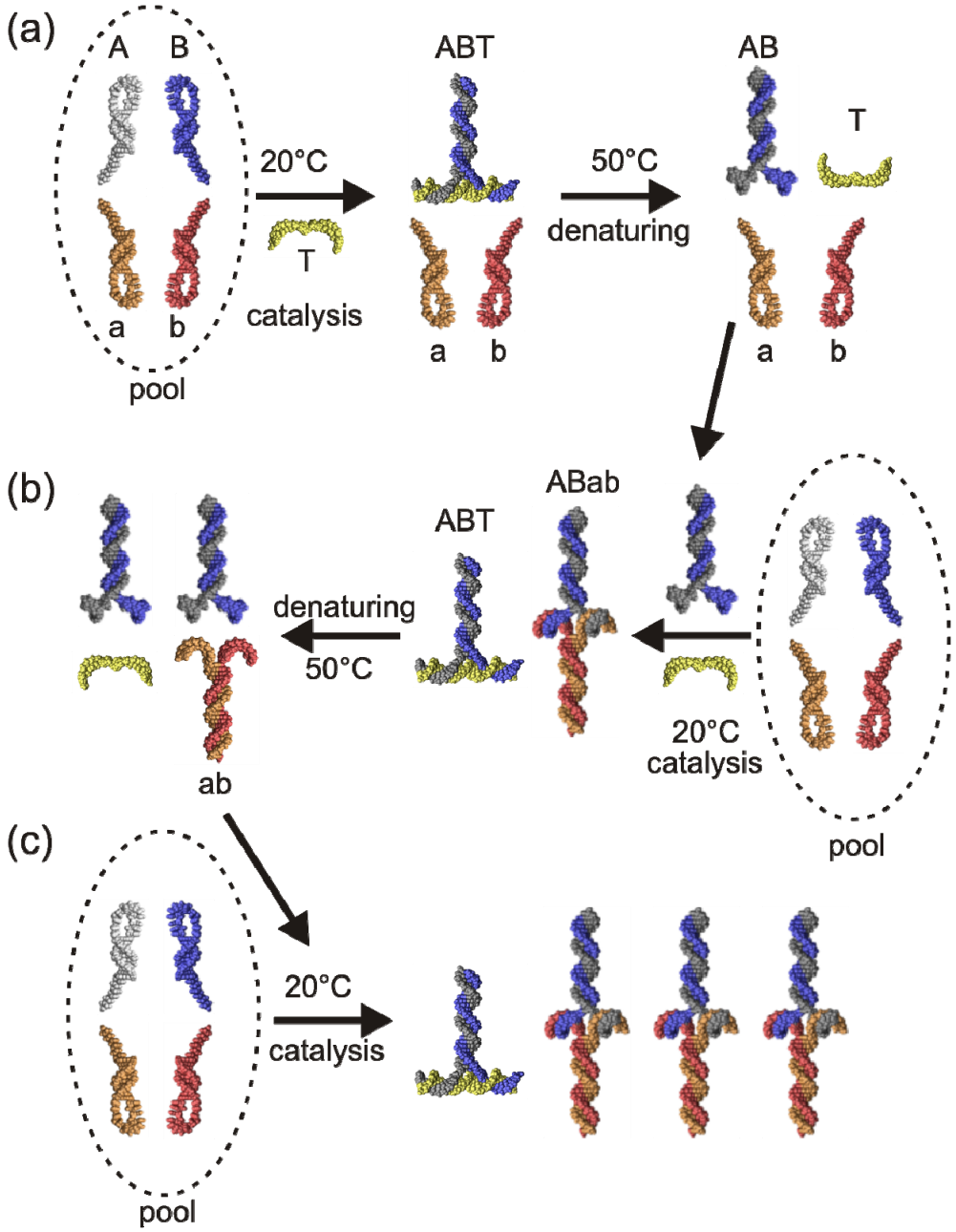

Figure 18. ***Exponential hairpin amplification by thermal cycling.*** *(a) Starting point is a pool of highly concentrated hairpins **A**, **B**, **a**, **b**. The addition of the template **T** catalyses the formation of the Triplex **ABT** at 20°C. At 50°C the template strand **T** dissociates from **ABT** while the duplex **AB** is stable due to its long common sequence. (b) The duplex **AB** catalyzes the formation of the duplex **ab** into a quadruplex **ABab**. At 20°C the products **ABab** and **ABT** form. At 50°C the triplex and quadruplex dissociate into **AB**, **ab** and **T**. (c) Again at 20°C the duplexes **AB** and **ab** catalyze the reactions of **a** with **b** and **A** with **B**, respectively. The information of the template **T** is exponentially amplified into the quadruplex complexes by temperature cycling.*

Boundary Conditions for the Replication Scheme

The first requirement for a replicating system is, that the template molecule **T**, and the products **AB** and **ab**, substantially accelerate the rate of the reaction between the hairpin substrates **A**, **B**, **a** and **b** [27, 28]. This necessitates, that the hairpins are kinetically trapped by the stem, forming an energy barrier before the hairpins can reach the duplex states. The spontaneous hybridization reaction to directly form **AB** and **ab** is slow. Because of the free accessible dangling ends of the catalyzing templates **T**, **AB**, or **ab** the formation of the triplex **ABT** and quadruplex **ABab** structures is quickened. Measurements for DNA show up an acceleration of at least 1000 [24, 29].

The second requirement is the effective dissociation of the products and the template to allow exponential replication [30, 31]. This is implemented by the temperature cycling of thermal convection. For example, at 20°C the triplex **ABT** and quadruplex **ABab** structures are the most stable structures. However, at enhanced temperatures, such as 50°C, the duplexes **AB** and **ab** are more stable than the quadruplex structure and thus the quadruplex splits into the two duplex structures. The templates and products are released to again catalyze the reaction at cooler temperatures, allowing for an exponential replication.

However, the elevated temperatures reached during temperature cycling enhance the chances of false positive reactions. In consequence quadruplexes might be formed independently of the catalyzing sequences of template **T** or, equally, the dangling ends of duplexes **AB** or **ab**. At low temperatures this is prevented by the high catalyzing efficiency, but at higher temperatures the rate of the template-independent reaction is enhanced. While this makes the replication less probable, one should keep in mind, that the four hairpins **A**, **B**, **a**, **b** can have sequences stable enough to keep their secondary structure for temperatures well above 50°C [32, 33]. Of course not all sequences will be suited to such reactions, but hairpin formation is very common for RNA sequences in comparison, for example, to DNA. The pool of molecules that show kinetically frustrated energy-entropy storage are expected to be appreciable even in random sequence pools.

A way to enhance replication is to consider a convection flow, which produces asymmetric temperature spikes, thus making the reaction time $t_{20°C}$ at low temperatures much longer than the reaction time $t_{50°C}$ at high temperatures [18]. Comparable to a PCR reaction the dissociation step at elevated temperatures takes only seconds, while the hybridization reactions require several minutes.

The starting condition for the replication - the hairpin conformation - is set through fast cooling of the RNA from temperatures, at which RNA is in the single stranded random coil

conformation [34, 35]. Cooling rates on the 100 millisecond scale are readily achieved by thermal convection in a vertical pore (Figure 19). Significant to this model is, that the same geometry strongly accumulates even small molecules such as single nucleotides [19, 36]. The mechanism combines thermal convection with thermophoresis - the drift of molecules in a temperature gradient - and is solely driven by a temperature gradient across an elongated pore. As a result, not only are the hairpins closed by fast cooling by the microscale convection, they are also strongly accumulated in the colder lower right corner. The enhanced concentration significantly reduces the entropy required for forming the complexes.

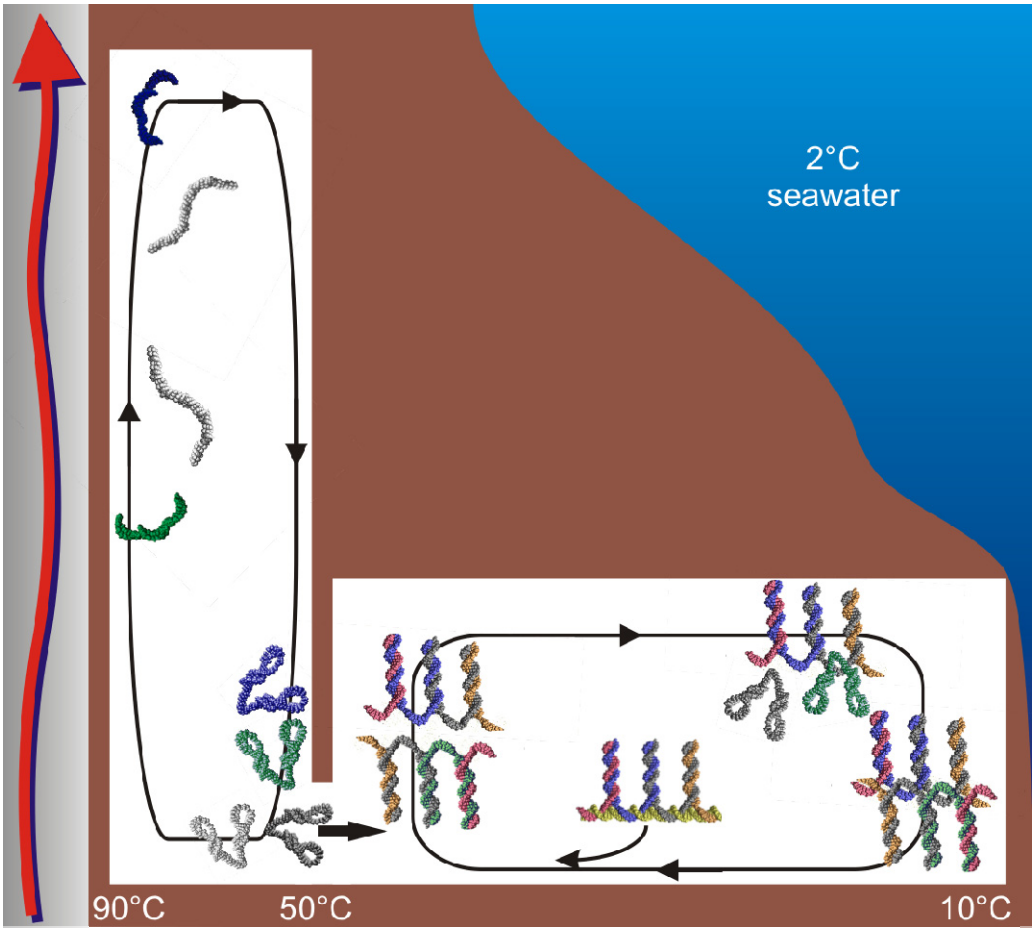

Figure 19. ***Hairpin replication driven by thermal microconvection.*** *A horizontal temperature difference induces thermal convection in two neighboring pores inside a hydrothermal vent. Double hairpins are formed in the left pore by fast cooling from the hot left side to the cooler right side at the top of the chamber. Concurrently, the colder molecules are trapped at the bottom by thermophoresis and convection. From there, they diffuse into the right pore. The first complex is formed by template assisted association of double-hairpins (middle). This complex moves by convection to the warm side, dissociates and is now able to catalyze the hybridization reaction of other double-hairpins, as it is transported towards the cold. The complementarity of double-hairpins drives a cross-catalyzing replication reaction, as the molecules are shuttled repeatedly through different temperatures by the convection. An exponential replication results, similar to a convective polymerase chain reaction.*

Diffusion between the flow lines on the submillimeter to millimeter scale is slow compared to the convective cycling. On the time scale of several hundred temperature cycles different species can exist along neighboring flow lines with differing temperature cycling characteristics. As a result, laminar convection can host a wide range of thermal conditions in parallel. It is expected, that the pore space in the vicinity of hydrothermal vents host convection cells in a wide variety of conditions [37-39]. Because the vents are permeable, all pores are interconnected and thus the convection cells are coupled on slow time scales. One possibility to combine accumulation and replication is sketched in Figure 19.

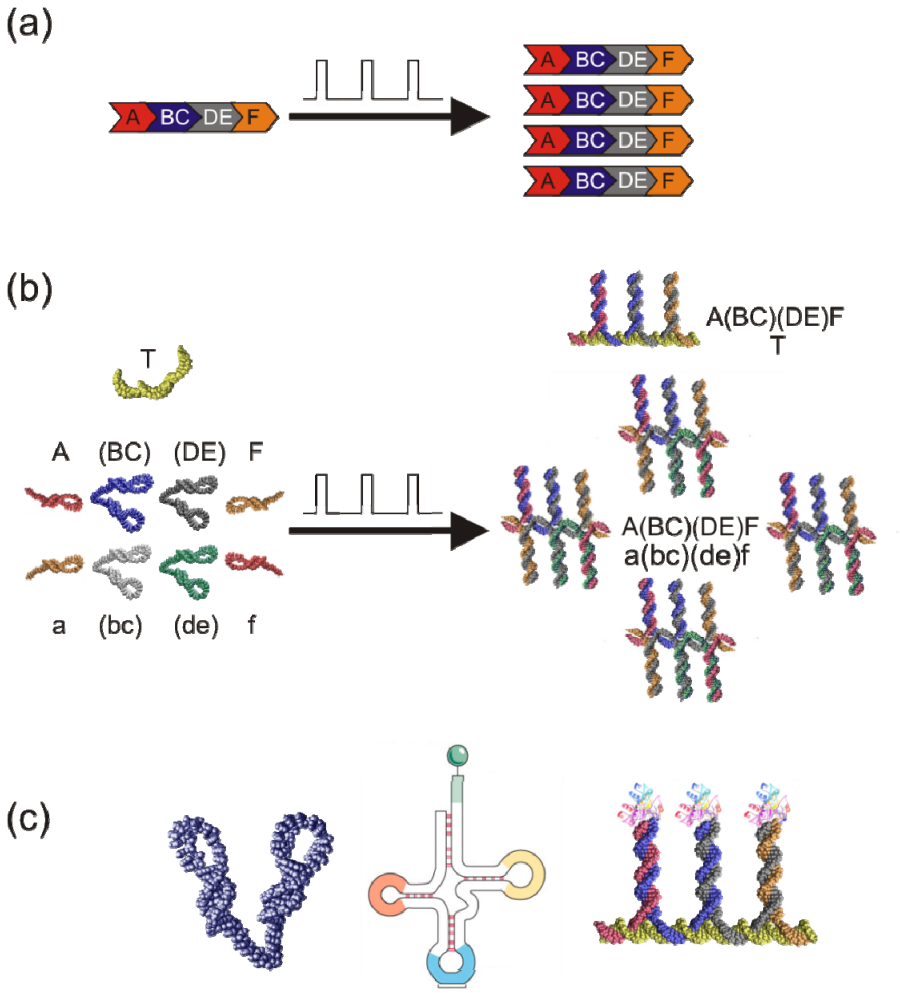

Figure 20. ***Double hairpin replication of sequences.*** *(a) The aim is to replicate a sequence of sequence chunks* ***ABCDEF*** *by the temperature oscillation of microscale thermal convection. (b) To do this, hairpins are joined at the toehold region into double hairpins* ***(BC)***, ***(DE)***, ***(bc)*** *and* ***(de)***. *Upon temperature oscillation and display of template T, we expect linear growth of ABT-structures and exponential growth of complexes of* ***A(BC)(DE)F-a(bc)(de)f***. *Single hairpins* ***A***, ***F***, ***a***, ***f*** *in red and orange start and end the sequence, but could extend the replication, if replaced by double hairpins. (c) The double hairpin shows a strong similarity to modern tRNA, both in its structure and binding geometry. Within the scheme, the codon region is replicated. The double hairpins can be stabilized by amino acid polymerization at the end of the inter-hairpin binding site, showing a direct route towards translation.*

Double Hairpin Replication

Until now only two hairpin binding sequences **A** and **B** were used for replication. In Figure 20, the scheme is extended to the temperature-induced replication sequence **ABCDEF**, given in red, blue, grey and orange. Longer replication requires, that two hairpins are combined into hairpin pairs at their toehold region, as shown in Figure 20b with double hairpins **(BC)**, **(DE)** and their partners **(bc)**, **(de)**. The template sequence is now replicated into more complex structures. On the one hand, the replication will generate a linear increase in the amount of complex consisting of **A**, **(BC)**, **(DE)**, **F** and **T** with capping single hairpins **A** and **F** shown in red and orange, respectively. On the other hand, complexes of **A(BC)(DE)F-a(bc)(de)f** are formed exponentially upon temperature oscillation.

The structural similarity of the replicating hairpin pairs with modern tRNA is compelling (Figure 20c). The codon region of tRNA could be understood as an evolutionarily shortened replicating site [40], while the right and left hairpins of the clover leaf structure would be remainders of the replication hairpin. Sequence analysis has indicated [41-43], that tRNA probably evolved from two independent hairpin sequences, which is in accordance with our argument. Similarities between nucleotides at comparable positions within the two halves of the tRNA molecule have often been taken as evidence, that the modern cloverleaf structure arose through direct duplication of a hairpin [44-47]. This sequence duplication could reflect the evolution from single hairpin to double hairpin replicators.

Conclusion

The initial point was the perceived need for protein-free replication of sequence information using the simplest of mechanisms, namely hybridization, driven by thermal convection. The proposed scheme is based on physical hybridization interaction alone and is a way to motivate and generate double hairpin structures very similar to tRNA. The reaction requires a temperature oscillation, which can be provided by microscale convection in porous mineral precipitates subjected to a temperature gradient, like it can be found in the vicinity of submarine hydrothermal springs. The scheme offers to bridge a wide gap in molecular evolution without excessive assumptions.

VI. Conclusion and Outlook

The determination of the thermal stability of biomolecules is of great interest in red and white biotechnology and molecular medicine. The method described here, allows to measure the thermal stability of DNA molecules within 50ms and can not only be used to detect point mutations in the genetic code, but also to measure the thermal stability of enzymes, chaperons or antibodies. For the fluorescence based method shown here, also the intrinsic fluorescence of biomolecules can be used, for example the fluorescence of tryptophan residues. Thus, the method provides the opportunity to measure the thermal stability of tryptophan containing molecules within several milliseconds without the need to conduct extensive labeling reactions. The described approach may be used in high throughput screening, as it is fast enough to measure the thermal stability of several hundred different molecules per minute.

Besides the thermal stability, which is an intramolecular property, interactions between different molecules are very important in biology and biochemistry. It is shown, that thermophoresis can be used to detect and quantify the interactions between DNA-aptamers and their targets. The described method allows to quantify the binding of high molecular weight molecules, like thrombin, equally well as the binding of low molecular weight molecules, like AMP. In addition, the binding of molecules can be quantified in biological liquids like human blood serum without loosing specificity and sensitivity. The described assay is not limited to aptamers, but can also be used to determine the equilibrium constant of any reaction between molecules. The only precondition for this is, that the reaction alters the thermophoresis of at least one of the binding partners. The assay can be used by researchers to investigate interactions of molecules under close to physiological conditions, meaning complex biological liquids, in which other methods, like surface plasmon resonance, fail to work. For example, the binding affinity of antibody based drug candidates can be quantified in human blood and thus, reliable predictions of the antibodies efficacy in the human body are possible.

One central issue of the Origin of Life theories is the so called concentration problem: The concentration of molecules required for theories, like the RNA world scenario, is much higher than the concentrations found in the prebiotic ocean. A solution to this problem is provided by showing, that molecules can be exponentially accumulated in hydrothermal pore systems, a geological setting wide spread in the prebiotic ocean. These pore systems also provide

temperature oscillations, which can drive enzyme free replication reactions as the proposed hairpin replicators. Thus, it is argued, that these natural settings provide a probable starting point for the molecular evolution of life.

Besides this Origin of Life scenario, the here shown concepts can also find applications in research and biotechnology. The enzyme free hairpin replication scheme can be used as an alternative to the polymerase chain reaction (PCR). As only hybridization reactions and no binding and processing of enzymes are needed, this method can be used for a fast amplification of sequence information, for example in the field of DNA computing.

The described accumulation mechanism, based on the combination of thermal convection and thermophoresis found in the pore systems, can also be used to concentrate DNA/RNA and proteins in laboratories, as only several millimeter long and 100 micrometer thick temperature controlled chambers are needed. With this Clusius-tube for biomolecules a millionfold accumulation of even microRNA will be possible within several hours. JW Szostak [42, Hydrothermal Accumulation] has recently used the described mechanism to accumulate single-chain amphiphiles to foster the concentration dependent formation of protocell-like vesicles.

To conclude, the use of microscopic small temperature fields allows to analyze and to manipulate freely diffusing biomolecules. The microthermal methods are applicable to accumulate biomolecules, to detect point mutations in DNA and even to measure the equilibrium constants of intermolecular reactions.

VII. References

Melting Curve Analysis in a Snapshot

[1] J. Marmur and P. Doty, *J. Mol. Biol.* **1962**, 5, 109.

[2] J. L. Mergny and L. Lacroix, *Oligonucleotides* **2003**, 13, 515.

[3] M. G. Herrmann, J. D. Durtschi, L. K. Bromley, C. T. Wittwer, and K. V. Voelkerding, *Clinical Chemistry* **2006**, 52, 494.

[4] J. M. Akey, D. Sosnoski, E. Parra, S. Dios, K. Hiester, B. Su, C. Bonilla, L. Jin, and M. D. Shriver, *BioTechniques* **2001**, 30, 358.

[5] S. O. Sundberg, C. T. Wittwer, J. Greer, R. J. Pryor, O. Elenitoba-Johnson, and B. K. Gale, Biomed *Microdevices* **2007**, 9, 159.

[6] T. Liedl and F. C. Simmel, *Anal. Chem.* **2007**, 79, 5212.

[7] S. Tyagi and F. R. Kramer, *Nature Biotechnology* **1996**, 14, 303.

[8] G. Bonnet, S. Tyagi, A. Libchaber, and F. R. Kramer, *Proc. Natl. Acad. Sci. USA* **1999**, 96, 6171.

[9] S. Duhr and D. Braun, *Proc. Natl. Acad. Sci. U S A* **2006**, 103, 19678.

[10] S. Duhr, S. Arduini, and D. Braun, *Eur. Phys. J. E Soft Matter* **2004**,15, 277.

[11] C. Ludwig, *SB Akad. Wiss. Wien* **1856**, 20, 539.

[12] S. Duhr and D. Braun, *Phys. Rev. Lett.* **2006**, 96, 168301.

[13] P. Baaske, F. M. Weinert, S. Duhr, K. H. Lemke, M. J. Russell, and D. Braun, *Proc. Natl. Acad. Sci. USA* **2007**, 104, 9346.

[14] G. Bonnet, O. Krichevsky, and A. Libchaber, *Proc. Natl. Acad. Sci. U S A* **1998**, 95, 8602.

[15] M. Zuker, Nucl. *Acids Res.* **2003**, 31, 3406.

[1] G. Mayer, *Angew. Chem. Int. Ed. Engl*. **2009**, 48, 2672.

[2] A. D. Ellington, J. W. Szostak, *Nature* **1990**, 346, 818.

[3] C. Tuerk, L. Gold, *Science* **1990**, 249, 505.

[4] D. L. Robertson, G. F. Joyce, *Nature* **1990**, 344, 467.

[5] B. Boese, K. Corbino, R. Breaker, *Nucleosides, Nucleotides Nucleic Acids* **2008**, 27, 949.

[6] E. Cho, J. Lee, A. Ellington, *Annu. Rev. Anal. Chem.* **2009**, 2, 241.

[7] S. Jhaveri, R. Kirby, R. Conrad, E. Maglott, M. Bowser, R. Kennedy, G. Glick, A. Ellington, *J. Am. Chem. Soc*. **2000**, 122, 2469.

[8] Y. Xiao, A. A. Lubin, A. J. Heeger, K. W. Plaxco, *Angew. Chem. Int. Ed. Engl*. **2005**, 44, 5456.

[9] S. Song, L. Wang, J. Li, C. Fan, J. Zhao, *Trends Anal. Chem.* **2008**, 27, 108.

[10] D. Ho, K. Falter, P. Severin, H. E. Gaub, *Anal. Chem.* **2009**, 81, 3159.

[11] Ludwig, C. *Sitzungsber. Akad. Wiss. Wien: Math.-Naturwiss.* **1856**, 20, 539.

[12] S. Iacopini, R. Piazza, *Europhys. Lett.* **2003**, 63, 247.

[13] S. Duhr, D. Braun, *Proc. Natl. Acad. Sci. U. S. A***. 2006**, 103, 19678.

[14] P. Reineck, C.J. Wienken, D. Braun, Thermophoresis of Single Stranded DNA, *Electrophoresis*, accepted.

[15] Jan K. G. Dhont, *Journal of Chemical Physics*, **2004**, 120, 1632.

[16] J. Rauch and W. Köhler, *Journal of Chemical Physics* **2003**, 119, 11977.

[17] P. Baaske, S. Duhr, D. Braun, *Appl. Phys. Lett.* **2007**, 91, 133901.

[18] S. Duhr, S. Arduini, D. Braun, *Euro. Phys. J. E.* **2004**, 15, 277-286.

[19] J.K.G. Dhont, S. Wiegand, S. Duhr and D. Braun, *Langmuir* **2007**, 23, 1674.

[20] H. Ning, J.K.G. Dhont and S. Wiegand, *Langmuir* **2008**, 24 2426.

[21] L. C. Bock, L. C. Griffin, J. A. Latham, E. H. Vermaas, J. J. Toole, *Nature* **1992**, 355, 564.

[22] D. E. Huizenga, J. W. Szostak, *Biochemistry* **1995**, 34, 656.

[23] C.H. Lin, D.J. Patel, *Chem. Biol*. **1997**, 4, 817-832.

[24] C. Maasch, K. Buchner, D. Eulberg, S. Vonhoff, S. Klussmann, *Nucleic Acids Symp. Ser.* **2008**, 52, 61.

Hydrothermal Accumulation of Biomolecules

[1] S.L. Miller, *Science* **1953**, 15,528.

[2] E. Drobner, H. Huber, G. Wächtershäuser, D. Rose and K. O. Stetter, *Nature* **1990**,346, 742.

[3] G. Zubay, *Origins of Life on the Earth and in the Cosmos.* (Academic Press, 2000)

[4] J.P. Ferris, *Origins Life Evol. Biosph*. **2002**,32, 311.

[5] M. Eigen, *Naturwissenschaften*, **1971**,58, 465.

[6] H. Kuhn, *Naturwissenschaften*, **1976**,63, 68.

[7] D. Sievers and G. von Kiedrowski, *Nature* **1994**,369, 221.

[8] G.F. Joyce, *Nature* **1989**,338, 217.

[9] T.R. Cech, J.F. Atkins and R.F. Gesteland (Eds), *The RNA World* (Cold Spring Harbor, 2000)

[10] K. Dose, *Biosystems* **1975**,6, 224.

[11] S.J. Mojzsis, T.M. Harrison, R.T. Pidgeon, *Nature* **2001**,409, 178.

[12] C. de Duve, *Blueprint for a Cell: The Nature and Origin of Life.*(Neil Patterson Publishers, Burlington, North Carolina, 1991)

[13] R.J. Ellis, *Trends Biochem. Sci.* **2001**,26, 597.

[14] J.B. Corliss, *Nature* **1990**,347, 624.

[15] E.V. Koonin and W. Martin, *Trends in Genetics* **2005**,21, 647.

[16] E. Imai, H. Honda, K. Hatori, A. Brack, K. Matsuno, *Science* **1999**, 283, 831.

[17] M.J. Russell, A.J. Hall, A.G. Cairns-Smith, P.S. Braterman, *Nature* **1988**, 336, 117.

[18] M.J. Russell, A. J. Hall, *Geol. Soc. London*, **1997**,154, 377.

[19] E.G. Nisbet and N. H. Sleep, *Nature* **2001**,409, 1083.

[20] D.S. Kelley et al., *Nature* **2001**,412, 145.

[21] K. Clusius, G. Dickel, *Naturwissenschaften* **1938**,26, 546.

[22] S. Duhr, D. Braun, *Proc. Natl. Acad. Sci. U.S.A.*, **2006**,103, 19678.

[23] S. Duhr, S. Arduini, D. Braun, *Eur. Phys. J. E* **2004**,15, 277.

[24] R. Piazza, S. Iacopini and B. Triulzi, *Phys. Chem. Chem. Phys*. **2004,** 6, 1616.

[25] B.-J. de Gans, R. Kita, S. Wiegand, J. Luettmer-Strathmann, *Phys. Rev. Lett*. **2003**, 91, 245501.

[26] W.H. Furry, R. C. Jones, L. Onsager, *Phys. Rev*. **1939**, 55, 1083.

[27] P. Debye, *Annalen der Physik* **1939**, 36, 284.

[28] D. S. Kelley et al., *Science* **2005**, 307, 1428.

[29] M.J. Russell, et al., *Econ. Geol.* **2005**, 100, 419.

[30] D.A. Stone, R. E. Goldstein, *Proc. Natl. Acad. Sci. U.S.A.* **2004**, 101, 11537.

[31] P.A. Rona, E. E. Davis, R. J. Ludwig, *Proc. Ocean Drilling Program, Scientific Results*, **1998**, 158, 329.

[32] C. Clauser, in Landolt-Börnstein - Numerical Data and Functional Relationships, K. Heinloth Ed. (*New Series, Vol. VIII: Energy Technologies, Subvolume 3: Renewable Energies,* Springer Verlag, Heidelberg-Berlin, 2006)

[33] D. Braun, N.L. Goddard, A. Libchaber, *Phys. Rev. Lett*. **2003**, 91, 158103.

[34] D. Braun, A. Libchaber, *Phys. Rev. Lett.* **2002**, 89, 188103.

[35] D. Braun, A. Libchaber, *Phys. Biol.* **2004**, 1, 1.

[36] S. Duhr, D. Braun,, Appl. *Phys. Lett*. **2005**, 86, 131921.

[37] C.D. Duve and S.L. Miller, *Proc. Natl. Acad. Sci. U.S.A*. **1991**, 88, 10014.

[38] G. Wächtershauser, *Proc. Natl. Acad. Sci. U.S.A.* **1994**, 91, 4283.

[39] W. Martin and M.J. Russell, *Philos. Trans. R. Soc. Lond. B Biol. Sci.* **2003**, 358, 59.

[40] H. Ogasawara, A. Yoshida, E. Imai, H. Honda, K. Hatori and K. Matsuno, *Origins Life Evol. Biosph.* **2000***,* 30, 519.

[41] M. Krishnan, V. M. Ugaz, M. A. Burns, *Science* **2002** 298, 793.

[42] I. Budin, R.J. Bruckner, J.W. Szostak, J. *Am. Chem. Soc.*, **2009**, 131, 9628.

Hairpin Replicators: Protein-Free Replication by Hybridization?

[1] Eigen M, Winkler-Oswatitsch R, *Naturwissenschaften* **1981**, 68, 282.

[2] Rodin S, Ohno S, Rodin A, *Proc Natl Acad Sci USA* **1993**, 90, 4723.

[3] Isenbarger TA, Carr CE, Johnson SS, Finney M, Church GM, Gilbert W, Zuber MT, Ruvkun G, *Orig Life Evol Biosph* **2008**, 38, 517.

[4] Sievers D, von Kiedrowski G, *Nature* **1994**, 369, 221.

[5] Saiki RK, Gelfand DH, Stoffel S, Scharf SJ, Higuchi R, Horn GT, Mullis KB, Erlich HA, *Science* **1988**, 239, 487.

[6] Barany F, *Proc Natl Acad Sci USA* **1991**, 88, 189.

[7] Braun D, Libchaber A, *Phys Biol* **2004,** 1, P1.

[8] Baross JA, Hoffman SE, *Orig Life Evol Biosph* **1985**, 15, 327.

[9] Corliss J, *Nature* **1990**, 347, 624.

[10] Imai E, Honda H, Hatori K, Brack A, Matsuno K, *Science* **1999**, 283, 831.

[11] Imai E, Honda H, Hatori K, Matsuno K, *Orig Life Evol Biosph* **1999**, 29, 249.

[12] Lemke KH, Rosenbauer RJ, Bird DK, Ross DS, *Geochim Cosmochim Acta Suppl* **2003**, 67, 249

[13] Russell MJ, *Science* **2003**, 302, 580.

[14] Koonin E, Martin W, *On Trends in Genetics* **2005**, 21, 647.

[15] Hazen RM, Deamer DW, *Orig Life Evol Biosph* **2007**, 37, 143.

[16] Martin W, Baross J, Kelley D, Russell MJ, *Nat Rev Microbiol* **2008**, 6, 805.

[17] Krishnan M, Ugaz VM, Burns MA, *Science* **2002**, 298, 793.

[18] Braun D, Goddard NL, Libchaber A, *Phys Rev Lett* **2003**, 91, 158103.

[19] Baaske P, Weinert FM, Duhr S, Lemke KH, Russell MJ, Braun D, *Proc Natl Acad Sci USA* **2007**, 104, 9346.

[20] Kuhn H, Waser J, *Angew Chem Int Ed* **1981**, 20, 500.

[21] Simmel F, Dittmer W, *Small* **2005**, 1, 284.

[22] Tyagi S, Kramer FR, *Nat Biotechnol* **1996**, 14, 303.

[23] Bonnet G, Tyagi S, Libchaber A, Kramer FR, *Proc Natl Acad Sci USA* **1999**, 96, 6171.

[24] Green SJ, Lubrich D, Turberfield AJ, *Biophys J* **2006**, 91, 2966.

[25] Orgel LE, *Nature* **1992**, 358:203.

[26] Luther A, Brandsch R, von Kiedrowski G, *Nature* **1998**, 396, 245.

[27] Zielinski WS, Orgel LE, *Nature* **1987**, 327, 346.

[28] Paul N, Joyce GF, *Curr Opin Chem Biol* **2004**, 8, 634.

[29] Yurke B, Mills A, *Genetic Programming and Evolvable Machines* **2003**, 4, 111.

[30] von Kiedrowski G, *Bioorganic Chemistry Frontiers* **1993**, 3, 115.

[31] Bag BG, von Kiedrowski G, *Pure and Appl Chem* **1996**, 68, 2145.

[32] Tuerk C, Gauss P, Thermes C, Groebe D, Gayle M, Guild N, Stormo G, d'Aubenton-Carafa Y, Uhlenbeck O, Tinoco I, *Proc Natl Acad Sci USA* **1988**, 85, 1364.

[33] Baaske P, Duhr S, Braun D, *Appl Phys Lett* **2007**, 91, 133901.

[34] Ares S, Voulgarakis N, Rasmussen K, Bishop A, *Phys Rev Lett* **2005**, 94, 35504.

[35] Viasnoff V, Meller A, Isambert H, *Nano Lett* **2006**, 6, 101.

[36] Koonin EV, *Proc Natl Acad Sci USA* **2007**, 104, 9105.

[37] Russell MJ, Hall A, Cairns-Smith A, Braterman P, *Nature* **1988**, 336, 117.

[38] Kelley DS, Karson JA, Blackman DK, Fruh-Green GL, Butterfield DA, Lilley MD, Olson EJ, Schrenk MO, Roe KK, Lebon GT, Rivizzigno P, *Nature* **2001**, 412, 145.

[39] Nisbet EG, Sleep NH, *Nature* **2001**, 409, 1083.

[40] Di Giulio M, *J Theor Biol* **2004**, 226, 89.

[41] Eigen M, Winkler-Oswatitsch R, *Naturwissenschaften* **1981**, 68, 217.

[42] Eigen M, Lindemann BF, Tietze M, Winkler-Oswatitsch R, Dress A, von Haeseler A, *Science* **1989**, 244, 673.

[43] Widmann J, Di Giulio M, Yarus M, Knight R, *J Mol Evol* **2005**, 61, 524.

[44] Randau L, Munch R, Hohn MJ, Jahn D, Soll D, *Nature* **2005**, 433, 537.

[45] Di Giulio M, *J Theor Biol* **1995**, 177:95.

[46] Dick TP, Schamel WA, *J Mol Evol* **1995**, 41, 1.

[47] Di Giulio M, *J Theor Biol* **2006**, 240, 343.

VIII. Acknowledgements

First of all I want to thank Dieter for the close collaboration and all the great ideas. Thanks for the intense help writing the publications and his never-ending patience with my “Frankonian English”. I have learnt a lot about science from him, especially how to design focused experiments.

Stefan Duhr for all the help and support especially in the beginning of my PhD and for all the ups and downs we had and have with NanoTemper.

Christoph Wienken for every nice hour in the lab and outside the lab. Thank you for programming the measurement software. Thank you for our “label-free in 1 hour” setup building record.
Franz Weinert for lvl18 in wc3 and the three productive years we had together in the lab.
Christof Mast for the nice discussion, the PC administration, the fancy Homepage, the “klick”-simulator and all the other help.
Ingmar for improving all the setups and the programs.
Philipp Reineck for measuring “noch schneller” and the great aptamer measurements we did together.
Hubert and Mario for the nice hours in the lab, the movie evenings and for sharing the setups with me. Good luck for your PhDs!
Uta, Britta, Katja and all the Julia’s for the nice hours together in the lab.
Jan Vogelsang for the fancy fluorescence techniques.
Ralf, Tom and Angelika for the help in the chemistry lab.
Hüyesin for the lab automatation.
Petra for the great coffee.
Ann for all the proofreading.
Special thanks to Hermann Gaub for the supporting and the discussions. Thanks for the great environment including all the great food at the Christmas parties.

Thanks to my parents, Annerose und Gerhard, for all the support and the Frankonian food.

Thanks to my wife Nadine for everything you did for me and for everthing you had to abandon. I love you!

Thank you all! It was one of the greatest times in my life!

Danksagungen

Die Arbeit in Dieters Gruppe war eine sehr schöne und vor allem inspirierende Erfahrung. In dieser Zeit konnte ich, dank Dieters Unterstützung, ein breites Spektrum an wissenschaftlichen Methoden lernen. Dieter hat mich nicht nur wissenschaftlich unterstützt und geformt, sondern auch bei der Gründung der Firma NanoTemper geholfen. Er hat öfters beide Augen zugedrückt wenn die Wissenschaft aufgrund der Aufgaben in der Firma mal wieder zu kurz kam. Vielen Dank Dieter!
Im Folgenden möchte ich mich bei allen bedanken, die mich in den letzten Jahren so tatkräftig unterstützt haben.

Stefan Duhr für die gemeinsamen Firmengründung(en), den siegreichen Kampf gegen widerspenstige Gewächse aus der Ordnung der Arecaceae. Für die gemeinsame Arbeit, die Unterstützung bei biologischen und biochemischen Fragen und einfach für alles. Weist ja, wir Franken sind recht kurz angebunden… Danke Stefan!

Christoph Wienken für die gemeinsamen Kaffee-Pausen, die gemeinsamen Mess-Einsätze mit Fussball Live-Übertragungen und vor allem dafür, immer ein offenes Ohr für alle Probleme zu haben. Ganz besonders auch für die Unterstützung bei NanoTemper!

Franz Weinert für lvl18 in wc3 und die drei spaßigen und produktiven gemeinsamen Jahre im Labor.

Christof Mast für die sehr angenehmen Diskussionen, die Administration der Computer und die coole Homepage.

Ingmar Schön für die Verbesserung der Messaufbauten und Messprogramme.

Philip Severin für die vielen Diskussionen und die Unterstützung bei der Auswahl der richtigen Kameras und LEDs. Und ganz besonders für „Die Ärzte“-Einsätze.

Philipp Reineck für die schnellen Thermophorese Messungen.

Hubert und Sabine die vergeblich versucht haben mir bayrisch beizubringen.

Hüyesin für die Automatisierung der Messungen.

Svenja für lustige Fragen und die Hilfe bei den Messungen.

Jan Vogelsang für all die coolen hochauflösenden Fluoreszenztechniken mit den lustigen Namen.

Uta, Britta, Katja und allen Julias für das Ausleihen von Reagenzien und die vielen lustigen Stunden.

Elias für die Verteidigung des Frankentums und die tiefgehenden wissenschaftlichen Diskussionen.

Petra für den super leckeren Kaffee.

Ralf, Tom und Angelika für die Unterstützung im Chemielabor.

Jose, Hulzer, Michi, Gaucho, Steppenwolf, Sterling, Bettina, Christina und Luenya für die schönen gemeinsamen Kneipenbesuche und Feiern.

Meinen Eltern, Annerose und Gerhard, denen ich Alles verdanke, und die mich immer unterstützt und an mich geglaubt haben. Besonders auch für die Versorgung mit fränkischen Nahrungsmitteln. Meinen Großeltern für die immerwährende Unterstützung. Schön dass es Euch gibt!

Meiner Frau Nadine dass sie meine 80 Stunden Wochen mitgemacht hat und mir nach München gefolgt ist. Ich liebe Dich!

IX. Curriculum Vitae

Philipp Ewald Baaske

Personal data

Adress	Gatterburgstrasse 11
	80689 München
	Germany
E-Mail	philipp.baaske@nanotemper.de

Birth date	April, 19th, 1979 in Kulmbach, Germany
Nationality	German

Education

10/2005-today	PhD student, Ludwig-Maximilians-University Munich, Germany
09/2004-08/2005	Diploma student in biophysics, University Bayreuth, Germany
	Topic: *Messung der DNA-Hybridisierungskinetik an funktionalisierten Oberflächen mittels Förster Resonanz Energie Transfer und evaneszentem Feld*
10/2000-08/2004	Student physics, field biophysics, University Bayreuth, Germany
07/99	Abitur Markgraf Georg Friedrich Gymnasium Kulmbach

Awards

07/2009	2nd place Munich Business Plan Competition
05/2009	Winner of "CyberOne 2009 Hightech Award" with NanoTemper
05/2008	Publication „Extreme accumulation of nucleotides in simulated hydrothermal pore systems" selected for Faculty of 1000 Biology
11/2004	Fellowship Studienstiftung des deutschen Volkes

X. Appendix: Publications

Publications

1. Extreme Accumulation of Nucleotides in Simulated Hydrothermal Pore Systems, Philipp Baaske, Franz M. Weinert, Stefan Duhr, Kono H. Lemke, Michael J. Russell, Dieter Braun, *Proc. Natl. Acad. Sci. U.S.A.* **2007**, 104, 9346–9351.
2. Melting Curve Analysis in a Snapshot, Philipp Baaske, Stefan Duhr and Dieter Braun, *Appl. Phys. Lett.* **2007**, 91, 133901.
3. Optical Thermophoresis quantifies Buffer dependence of Aptamer Binding, Philipp Baaske, Christoph J. Wienken, Philipp Reineck, Stefan Duhr, Dieter Braun, submitted **2009**
4. Accessing the Hydration-Shell: Immobilization-Free Binding Assays in Temperature Gradients, Christoph J. Wienken, Philipp Baaske, Ulrich Rothbauer, Dieter Braun, Stefan Duhr, submitted **2009**
5. Was tRNA a Dual-Hairpin Replicator? A scheme to exponentially replicate RNA by thermal cycling of metastable hairpins, Philipp Baaske, Dieter Braun, submitted **2009**

Patent Applications

1. Fast Thermo-Optical Particle Characterisation, Stefan Duhr, Philipp Baaske, WO/2008/061706 (**2008**)
2. Thermo-Optical Characterisation of Nucleic Acid Molecules, Stefan Duhr, Philipp Baaske, WO/2009/098079 (**2009**)
3. Method and device for particle analysis using thermophoresis , Philipp Baaske, Stefan Duhr, Christoph J. Wienken, Dieter Braun, PCT/EP2009/056162 (**2009**)

Extreme accumulation of nucleotides in simulated hydrothermal pore systems

Philipp Baaske*, Franz M. Weinert*, Stefan Duhr*, Kono H. Lemke†, Michael J. Russell‡, and Dieter Braun*§

*Biophysics Department, Ludwig-Maximilians Universität München, Amalienstrasse 54, 80799 München, Germany; †Geochemistry Group, Institute for Mineralogy and Petrology, Swiss Federal Institute of Technology, ETH-Zürich, 8092 Zürich, Switzerland; and ‡Jet Propulsion Laboratory, California Institute of Technology, Pasadena, CA 91125

Edited by Howard Brenner, Massachusetts Institute of Technology, Cambridge, MA, and approved March 9, 2007 (received for review October 28, 2006)

We simulate molecular transport in elongated hydrothermal pore systems influenced by a thermal gradient. We find extreme accumulation of molecules in a wide variety of plugged pores. The mechanism is able to provide highly concentrated single nucleotides, suitable for operations of an RNA world at the origin of life. It is driven solely by the thermal gradient across a pore. On the one hand, the fluid is shuttled by thermal convection along the pore, whereas on the other hand, the molecules drift across the pore, driven by thermodiffusion. As a result, millimeter-sized pores accumulate even single nucleotides more than 10^8-fold into micrometer-sized regions. The enhanced concentration of molecules is found in the bulk water near the closed bottom end of the pore. Because the accumulation depends exponentially on the pore length and temperature difference, it is considerably robust with respect to changes in the cleft geometry and the molecular dimensions. Whereas thin pores can concentrate only long polynucleotides, thicker pores accumulate short and long polynucleotides equally well and allow various molecular compositions. This setting also provides a temperature oscillation, shown previously to exponentially replicate DNA in the protein-assisted PCR. Our results indicate that, for life to evolve, complicated active membrane transport is not required for the initial steps. We find that interlinked mineral pores in a thermal gradient provide a compelling high-concentration starting point for the molecular evolution of life.

concentration problem | hydrothermal vents | molecular evolution | origin of life problem | RNA world

Starting with Miller and Urey (1), a wide range of studies on the origin of life discuss the chemical synthesis of protobiomolecules (2–4). Concurrently, the studies of replication systems (5–8) culminated in the RNA-world proposal (9). All these approaches require fairly high concentrations of small proto-biotic molecules, whereas geochemical extrapolations indicate a dilute prebiotic ocean with concentrations comparable to contemporary values (10, 11). This discrepancy has been termed the concentration problem of the origin of life (10, 12). In the following, we describe a robust and efficient solution to the concentration problem, based on heat currents in porous mineral precipitates comprising a hydrothermal mound developed over a moderately warm submarine spring.

Living cells are crowded with small molecules which are accumulated as a result of highly evolved active transport mechanisms across the cell membrane (13). A comparably effective transport mechanism is required to solve the concentration problem of the origin of life. However, to accumulate molecules from a highly diluted prebiotic ocean (10, 11), a considerable entropic gap has to be bridged. In a rough estimate, at least a 10^6-fold accumulation is required for small protobiomolecules to interact. To fulfill the second law of thermodynamics, such states of exceedingly low entropies can only be siphoned from a larger nonequilibrium system. Contemporary life sustains the required high molecular concentration in a dissipative nonequilibrium state by a wide range of highly evolved strategies. For the evolution of life, an already existing protobiological dissipative environment is required (14). The most compelling would refer to an accumulation of molecules into preexisting abundant compartments of cellular dimensions (15). Both requirements are fulfilled by the accumulation mechanism we propose here.

Hydrothermal Setting

From a geological point of view, thermal gradients are the most abundant dissipative systems on the early earth. They drive convective water flow with a wide variety of geometries. Contemporary hydrothermal vents, both black smokers and "Lost City" type vents, are only extreme cases for heat dissipation. Hydrothermal vents are surrounded by highly porous mineral precipitates. Within these structures, we consider the ubiquitous millimeter to micrometer sized pores and syneresis cracks (Fig. 1*a*). A temperature gradient, typically along the horizontal direction, exists across such pore systems. We show that these natural settings can easily accumulate single nucleotides $>10^8$-fold at the bottom of a plugged pore system. Thus, this accumulation is sufficient to step up from the dilute hydrothermal solution to molar concentrations within the pore.

It is well known that probiotic reactions can be envisaged to foster molecular evolution and favor synthesis over hydrolysis only when concentrations are sufficiently high (16). Submarine hydrothermal environments were previously envisaged as potential sites for the emergence of life, partly because of their contemporary habitability and partly because essential basic materials can be found in such environments (14, 15, 17–20). The concentration mechanism described here considerably strengthens the scenario for a hydrothermal emergence of life.

Robust Exponential Accumulation

The mechanism of accumulation operates as follows. In a hydrothermal vent a plugged pore system is sandwiched between the hot vent interior and the cooling outside ocean (Fig. 1*b*). A temperature gradient across the pore drives two entangled processes: (*i*) molecules are shuttled up and down the cleft by laminar thermal convection and (*ii*) thermophoresis drives the molecules along the temperature gradient, i.e., perpendicular to the convection flow. Both processes are indicated by white arrows in Fig. 1*c*. In combination, they lead to a strong vertical accumulation toward the closed bottom of the cleft. This geological setting is analogous to a Clusius-tube or thermogravitational column (21). We simulate the behavior of rather rapidly diffusing single nucleotides. Even with conventional biotechno-

Author contributions: D.B. designed research; P.B., F.M.W., and S.D. performed research; P.B., F.M.W., S.D., K.H.L., M.J.R., and D.B. analyzed data; and P.B., K.H.L., M.J.R., and D.B. wrote the paper.

The authors declare no conflict of interest.

This article is a PNAS Direct Submission.

See Commentary on page 9105.

§To whom correspondence should be addressed. E-mail: dieter.braun@physik.lmu.de.

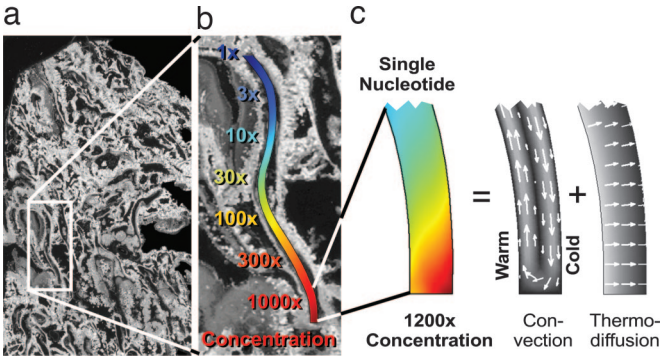

Fig. 1. Heat-driven molecular accumulation in hydrothermal pores. (*a*) Section through aragonite ($CaCO_3$) from the submarine hydrothermal vent field at Lost City (kindly provided by D. Kelley; ref. 20). (*b*) Simulation of a part of the pore system. If subjected to a horizontal thermal gradient of 30 K, a 1,200-fold accumulation of single nucleotides is expected (logarithmic concentration color scale). A concatenation of three of these pore sections leads to a 10^9-fold accumulation. (*c*) The mechanism of accumulation is driven by heat in a twofold way. Thermal convection shuttles the molecules vertically up and down and thermophoresis pushes the molecules horizontally to the right. The result is a strong molecular accumulation from the top to the bottom (linear concentration color scale).

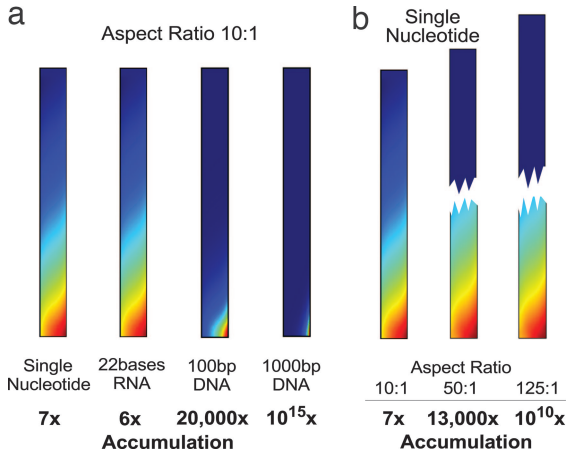

Fig. 2. Predicted effects of the molecule size and pore length on the accumulation level. The simulation results are based on the experimentally measured Soret coefficients and diffusion coefficients for DNA and RNA (see Table 1). (*a*) The accumulation increases exponentially with the size of the molecule. Whereas single nucleotides are accumulated 7-fold in a short cleft of aspect ratio 10:1, double-stranded DNA comprising 1,000 base pairs accumulates 10^{15}-fold. The equilibration takes 9 min for single nucleotides and 14 min for single stranded RNA comprising 22 bases. For DNA polynucleotides of 100 and 1,000 bp it takes 18 or 33 min, respectively. (*b*) Elongation of the cleft exponentially increases the accumulation. For example, the accumulation of single nucleotides is raised to a 10^{10}-fold level in a pore with an aspect ratio of 125:1. A linear concentration scale is used in both plots, scaled to the respective maximal concentration. The time to reach steady state is 9 min for $r = 10$, 4 h for $r = 50$ and 23 h for $r = 125$.

logical or microfluidic laboratory methods, such small molecules are hard to concentrate because of their considerable diffusion. The simulation shows a strong 1,200-fold downward accumulation of single nucleotides for the 5 mm short, bent cleft of Fig. 1*b*. As we will see later, a concatenation of three of these pores leads to a $1{,}200^3 = 1.7 \times 10^9$-fold accumulation.

We applied a 30 K temperature difference across the pore and found that maximal accumulation occurred in a pore with a cross-section of 145 μm. The diffusion of molecules in the convection flow was calculated by solving the combined Navier–Stokes, diffusion and heat transfer equations using commercial finite element software (Femlab, Comsol). The simulated pores feature a closed bottom and an open top end. The biomolecule concentration was fixed at the top, whereas the bulk fluid was subjected to gravity and restricted by the pore with nonslip boundary conditions. The heat transfer is barely affected by the slow laminar convection, and the temperature drops linearly across the pore structure.

Previously, we measured the thermophoretic characteristics of nucleotides using microfluidic fluorescence techniques (22). Molecules move along a thermal gradient ∇T with a drift velocity $v = -D_T \nabla T$. The ratio between the thermodiffusion coefficient D_T and the mass diffusion coefficient D is termed the Soret coefficient $S_T = D_T/D$, which typically determines the steady state concentrations. The values for single nucleotides are measured by using the fluorescent molecule 2′,7′-bis(carboxyethyl)-5 (6)-carboxyfluorescein (BCECF) in a 1 mM Tris buffer. BCECF and single nucleotides are of comparable size and charge. We also obtained S_T values for single stranded RNA of 22 bases in sodium chloride-sodium citrate-buffer with a monovalent salt concentration of 1.7 mM as well as double-stranded DNA of 100 and 1,000 bp in 1 mM Tris buffer. All measurements are performed at pH 7.8. In the experiments, the Soret coefficient S_T changes only by a factor of about three when the concentration of monovalent salt is increased from 1.7 to 170 mM. The Soret coefficient of a single nucleotide is comparable to the considerably larger single-stranded RNA of 22 bases. This is typical for thermodiffusion of charged particles smaller than the debye length and is due to reduced ionic shielding (22). Notably, single stranded RNA with 22 bases shows an ≈3-fold smaller thermodiffusion than single-stranded DNA of the same length. The experimental results are presented in Table 1.

A short pore with an aspect ratio of 10:1 accumulates single nucleotides 7-fold (Fig. 2*a*). A pore with the same aspect ratio accumulates a 22-bases-long single-stranded RNA to 6-fold, a 100-bases-long double-stranded DNA to 20,000-fold, and a 1,000-bases-long DNA to 10^{15}-fold levels. For these larger molecules, the short pore behaves like a molecule trap: once molecules enter the top of the pore, they are transported to the pore base and are accumulated to molar-level concentrations in a micrometer-sized spot in bulk water. As a result, the accumulated molecules diffuse freely and would find chemical reaction partners comparable to the situation within prokaryotic cells (13).

Pertinent to our argument is the fact that accumulation grows exponentially both with the size of the molecule and the length of a concatenated pore system. In concatenated pores accumulation of molecules increases exponentially, a result of the considerable concentration independence of thermophoresis below molar concentrations (23–25). Thus, although single nu-

Table 1. Soret coefficient (S_T) and diffusion coefficient (D) for different molecules

Coefficient	Single nucleotide	ssRNA, 22 bases	ssDNA, 22 bases	dsDNA, 100 bp	dsDNA, 1,000 bp
S_T 1.7 mM salt, per K	0.015	0.014	0.044	0.075	0.3
S_T 170 mM salt, per K	0.006	0.003	0.01	0.019	0.09
D, $\mu m^2/s$	400	100	115	45	8

Table 2. Predicted accumulation depends on the type of molecule and pore aspect ratio

Aspect ratio	Single nucleotide	ssRNA 22 bases	dsDNA 100 bp	dsDNA 1,000 bp
10:1	7	6	2×10^4	10^{15}
25:1	120	89	10^{10}	(10^{37})
50:1	13,000	8,000	(10^{21})	(10^{75})
125:1	10^{10}	6×10^9	(10^{52})	(10^{187})

Accumulation levels that cannot be reached because of steric hindrance are denoted in brackets.

cleotides accumulate merely 7-fold in the short pore of Fig. 2*a*, concatenating 12 of these pores using a wide variety of orientation angles exponentiate the accumulation to an extreme $7^{12} = 10^{10}$-fold level. Elongation of the pore has exactly the same effect. As shown in Fig. 2*b*, a pore system with a total aspect ratio of $r = 125$:1 accumulates single nucleotides 10^{10}-fold. Notably, the length of this pore system is only 18 mm, below the typical lengths of pore systems in hydrothermal settings. A compilation of the simulated accumulation values is given in Table 2.

The analytical solution for the accumulation in a rectangular cleft geometry confirms the above numerical findings. The analytical theory (26, 27) was originally developed for gas separation columns (21). The accumulation is found to be an exponential function given by

$$\frac{c_{\mathrm{BOTTOM}}}{c_{\mathrm{TOP}}} = \exp[0.42 \times S_{\mathrm{T}} \times \Delta T \times r] \qquad [1]$$

with the Soret coefficient S_{T}, the temperature difference ΔT and the aspect ratio r. For $0.42 \times S_{\mathrm{T}} \times \Delta T \times r \gg 1$, the molecular accumulation is large and rises exponentially with temperature difference ΔT or pore length. In pores with a sufficient aspect ratio r, substantial accumulation is reached even for small molecules with tiny Soret coefficients (Table 1). The exponential characteristic of Eq. **1** makes the accumulation robust because a small elongation of the pore leads to a large increase in molecular accumulation. Every linear decrease in the temperature difference ΔT can be compensated by a linear increase in pore aspect ratio r. For example, to achieve the same accumulation at just one tenth of the temperature difference, a 10-fold longer pore is needed. To illustrate this the accumulation versus the aspect ratio, r is plotted in Fig. 3 for single nucleotides, polynucleotides of 22 single stranded RNA bases, and double-stranded DNA comprising 100 and 1,000 base pairs.

The accumulation is highly robust with respect to the changes in the geometry of the pore. Fig. 4*a* shows various geometries that yield equal accumulations. We start with a rectangular pore with an aspect ratio of $r = 10$:1. The accumulation remains at the same level even if the pore is heavily dented, bent, incised, opened toward a bottom molecule repository, or strongly inclined. This insensitivity to geometric variation has two main reasons. First, mass diffusion bridges regions with inferior accumulation. This diffusion between the pores does not require any special geometries between the pore sections. Second, the slowing down of convection resulting from a tilt of the pore section can be easily compensated by a small increase in the pore width, because of the exponent 1/3 in Eq. **2**. For example, a tilt from 90° (vertical) to 1° (basically horizontal) enlarges the optimal cleft width only by a factor of four. Therefore, a wide variety of pore systems accumulate molecules with equal efficiency.

So far, we have discussed only two-dimensional pores with cleft-like geometries. We simulated the cross-section and assumed that the pore extends considerably further into the third

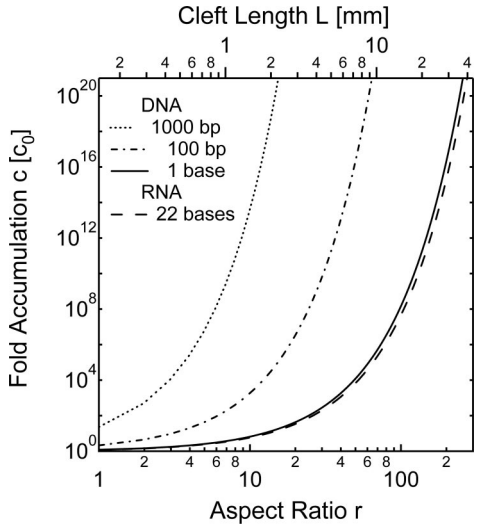

Fig. 3. Exponential accumulation. The accumulation depends exponentially on the aspect ratio r and the temperature difference ΔT, according to the analytical theory (Eq. **1**). Even for single nucleotides, it is remarkably easy to reach exceedingly large molecular accumulations. The accumulation is calculated for $\Delta T = 30$ K.

dimension. However, equal accumulation is also found for pores with only limited extension in the third dimension. Fig. 4*b* shows results for various pore cross-sections with comparable accumulation levels. Also, molecular accumulation is not seen to be significantly lowered over a variety of depths. As noted before, all of the geometries shown in Fig. 4 can be concatenated ad libitum, yielding a wide range of pore system geometries that are capable of an efficient molecular accumulation.

A critical parameter is the width of the pore. For an extended rectangular cleft (26, 27), the largest accumulation is found for an optimal width d_0 given by

$$d_0 = 8.4 \times (\mu D/\alpha\rho g_0 \Delta T \sin\Theta)^{1/3} \qquad [2]$$

with the viscosity of the fluid μ, the diffusion coefficient of the molecule D, the fluid volume expansion coefficient α, the fluid density ρ, the gravitational acceleration g_0, the inclination angle Θ to the horizontal plane, and the temperature difference ΔT. As

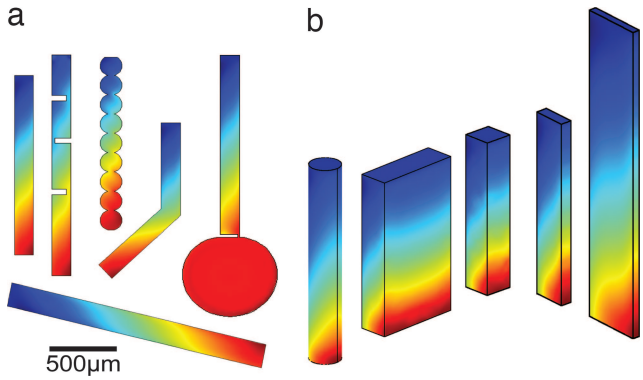

Fig. 4. Robustness of the accumulation. (*a*) Equally efficient accumulation is found for a large variety of geometries. Regions of reduced accumulation are bridged vertically by mass diffusion. Strongly inclined pores accumulate molecules equally well. A linear concentration scale is used in both plots. (*b*) Likewise, a wide range of pore cross-sections yields identical accumulations. As for two dimensional clefts, optimal accumulation is achieved if the convection speed balances the diffusion time across the pore.

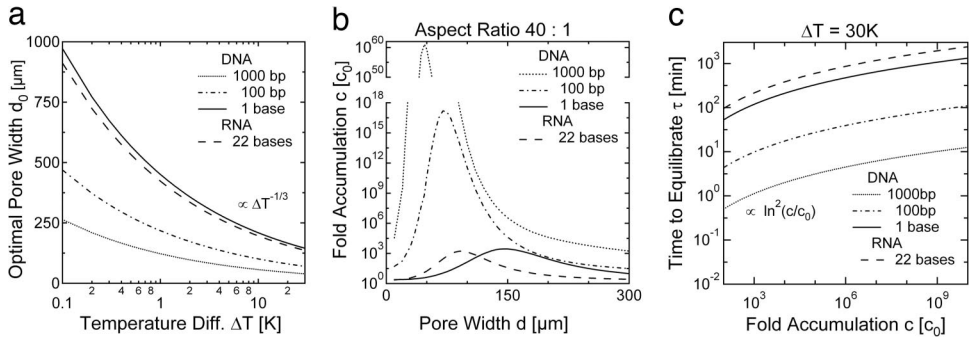

Fig. 5. Pore width and equilibration time. (*a*) The optimal cleft width depends moderately on the molecular size and temperature difference. The optimal cleft width is proportional to $D^{1/3}$ and $\Delta T^{-1/3}$ with the diffusion coefficient D and temperature difference ΔT. As a result, much longer nucleotides require only slightly narrower pores. (*b*) Accumulation drops considerably for pores with a nonoptimal width. Nucleotides are selectively accumulated in particularly narrow chambers. For a wider pore width $d \approx 150$ μm, the accumulation of molecules with different sizes reaches comparable levels. (*c*) The equilibration toward a 10^8-fold accumulation takes 14 h for single nucleotides and 25 h for single-stranded RNA comprising 22 bases. For DNA polynucleotides of 100 and 1,000 bp. it takes 70 or 8 min, respectively. This might be counterintuitive, but larger molecules accumulate faster because a considerably shorter cleft is sufficient to achieve the same level of accumulation.

the result of the exponent 1/3 in Eq. **2**, values for d_0 fall between 40 and 400 μm for an extensive range of parameters D, Θ, and ΔT, as shown in Fig. 5*a*.

Fig. 5*b* illustrates the pore size dependence of the accumulation in more detail. DNA molecules of different length are selectively partitioned depending on the pore width. For an equivalent value of ΔT (30 K), single nucleotides accumulate best for a pore width of 145 μm, whereas a 1,000-bp DNA fragment accumulates best for a width of 40 μm. Therefore, the geometry determines the size of the preferentially accumulated molecules. On the other hand, the accumulation of longer polynucleotides is much more efficient, and pore widths $\approx$150 μm accumulate a wide range of different DNA lengths equally well. Monomers and polymers accumulate to similar levels under all these various pore conditions (Fig. 5*b*).

The time τ to reach a steady state concentration profile is given by the diffusion time along the pore

$$\tau = r^2 d_0^2 / \pi^2 D. \qquad [3]$$

As a result, a 10^8-fold accumulation of single nucleotides is achieved after $\tau = 14$ h, and for a 22-base single-stranded RNA, a 10^8-fold accumulation is achieved after $\tau = 25$ h. However, the time to reach a comparable accumulation for larger molecules drops to 70 min for 100-bp DNA and 8 min for 1,000-bp DNA (Fig. 5*c*), the reason being the much shorter cleft length required for longer DNA.

Notably, all these times are extremely short compared with the lifetime of a typical vent chimney, or even the Lost City vent system, which operates at least for 30,000 years (20, 28).

We also tested the robustness of accumulation against diffusive leakage from the pore. In general, a leak of molecules into an attached closed pore space does not inhibit accumulation. An example is shown in Fig. 4*a*, where a large extension is filled to the same high concentration at the pore base. Only the equilibration time slightly increases as a result of such an extension of the pore. However, leaks into permeable chambers can reduce the accumulation, depending on the concentration gradient ∇c and the resulting diffusive molecular flux, $j = -D\nabla c$. The distance between the leak and the surrounding background concentration $c = 1$ is crucial. This distance is expected to be relatively large for a hydrothermal mound. To characterize the effects of diffusive leaks, we simulated a worst case scenario. A wide diffusive leak is placed at the base of a pore and is connected to the outside over a distance of the pore length itself (Fig. 6*a*). Otherwise the same geometrical condition as illustrated in Fig. 2a is used, namely an aspect ratio of $r = 10{:}1$ with an optimal width d_0. Thus, we effectively simulate a tube which is open to both sides. Compared with a nonleaking pore, the resulting accumulation is reduced from 7 to 3 for single nucleotides, from 6 to 2.6 for single-stranded RNA, from 20,000 to 2,000 for 100-bp DNA and from 10^{15} to 10^{13} for 1,000-bp DNA. These reductions in accumulation that stem from leakage are quite easily compensated for by extending the length of the pore. We conclude that, even if the pore leaks through diffusion, accumulation is maintained at a high level.

In addition to diffusion, slow water flow through pore leakages might hinder accumulation. We focus on an upward flow because this direction is most probable in a hydrothermal mound. We use the same geometry as before (see Fig. 6*a*), but now add an upward flow at the lower end of the leak. This flow is fed with molecules from the outside concentration of $c = 1$. Obviously, such an upward flow through the pore directly competes with the downward accumulation. The accumulation versus flow rate is plotted in Fig. 6*b*. For comparison, the typical convection flow inside the pore is on the 1–10 μm/s scale. Fig. 6*b* shows that the accumulation of single nucleotides is quite robust against the upflow, probably because of the rapid diffusion of these molecules. Slower diffusing molecules are more vulnerable to pore

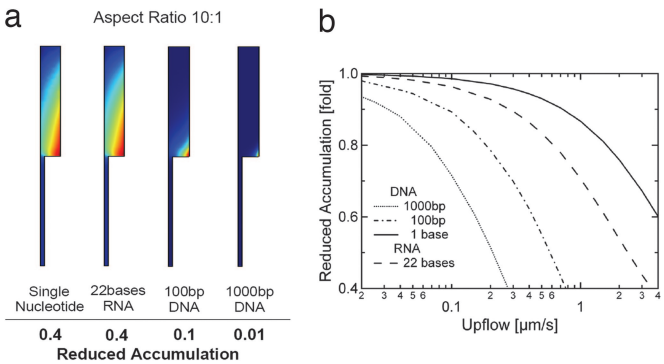

Fig. 6. Reduction of the accumulation by diffusive leakage and upflow. (*a*) A diffusive leak is introduced at the bottom of the pore over 1/5 of the pore width. The numbers beneath indicate the reduction of accumulation relative to the nonleaking pore in Fig. 2*a*. (*b*) Upflow is introduced into the cleft shown on the left side. For longer polynucleotides, the accumulation drops considerably faster with increasing upflow. Short molecules are less affected. The drop in accumulation for both diffusive leaks and upflow drift is readily compensated by a slight elongation of the pore.

flow drift, as can be seen from Fig. 6*b*. For a 22-base single-stranded RNA, the accumulation drops by a factor of two for an upflow of ≈2.5 μm/s. For 100-bp DNA and 1,000-bp DNA, accumulation drops by the same factor for an upflow of 0.6 and 0.2 μm/s, respectively. These flow rates are comparable with the thermal convection speed in the pore. Flow rates in pores of hydrothermal mounds are hard to estimate but are probably slower than these values. As expected, strongest accumulation is found in pores that are well sealed at the bottom. According to our assessment, drift and diffusion in microscopic pore systems in hydrothermal precipitates do not, or only weakly, affect the proposed accumulation mechanism.

Discussion

We compare the assumptions on pore geometry with the geological record. As seen from the representative cross-section in Fig. 1*a*, an aspect ratio between 25 and 50 can be estimated for single elongated pore spaces in the mounds at the Lost City vent site (≈20–100 μm across and ≤1 mm long). Although, at Lost City, pore shapes may be governed by filamentous bacterial growth, chemical garden-like growth with even higher aspect ratios is likely to occur in comparable hydrothermal systems with moderate temperatures. For example, the 500-mm-long hydrothermal pyrite spires from the 352-million-year-old Tynagh zinc-lead sulfide deposit, Ireland, have central cavities that are ≈100 μm in diameter (aspect ratio $r \leq 5{,}000{:}1$) (ref. 29 and Fig. 3*b*). Similar structures have been realized in laboratory simulations (30). Thus, the projected extreme accumulation should be easily reached in natural settings. In any case, the accumulation is exponentiated when low aspect ratio clefts are interconnected. Note that pore concatenation is an especially interesting feature from a geological point of view. During hydrothermal dissolution pores enlarge, become more interconnected (i.e., the value of the aspect ratio increases), and can substantially promote the accumulation of molecules. Based on these results, and given the large number of clefts in any one of multitudinous submarine hydrothermal mounds on the early earth (29), the opportunities would have been manifold for a critical accumulation of organic monomers and polymers synthesized in the same milieu.

In the above calculations, we have assumed a temperature difference of $\Delta T = 30$ K. We anticipate that this is a realistic assumption, because temperature gradients are focused inside the clefts due to the considerably lower thermal conductivity of water (0.6 W/mK) as compared with the surrounding rock (>3 W/mK). The thermal conductivity measured for a hydrothermal pyrite–silica precipitate (31) is 14 W/mK, but the isolated pyrite and quartz minerals yield ≈20 W/mK and 3–4 W/mK, respectively, in laboratory tests (32). The resulting enhancement of the temperature gradient in the liquid part of the pores is 5- to 200-fold. Thus, to obtain the temperature difference of 30 K assumed in the above simulations, the required overall temperature gradient is of the order of 1–40 K/mm, well within reported values of ΔT for natural hydrothermal settings. However, focusing of the temperature gradient in the pores is not essential for the accumulation process. For lower thermal gradients, the same accumulation can be achieved if the pore system is elongated linearly for a decreased temperature difference.

The presented accumulation geometry surpasses previous approaches. Experiments with a circular, laser-heated geometry demonstrated that thermal convection could drive the DNA replicating PCR (33). In the same setting, we observed a considerable accumulation of long DNA (34). Although both of those experiments pointed toward the potential for convection to contribute to the emergence of life (35), no accumulation of short molecules was found or theoretically expected. We now know that this was due to the low aspect ratio of the chamber geometry ($r \approx 0.1$). The pore geometries studied here, however, demonstrate a strong accumulation of small molecules, such as single nucleotides, in a highly plausible geological setting on the early earth.

As we have seen, large molecules accumulate more efficiently. One may ask whether the strong accumulation of solvated organic molecules would lead to the tarring of the pore. This is not expected because thermophoretic coefficients become small for concentrations in the molar range (23–25). As a result, accumulation will level out at similar concentrations and will not lead to tarring. Also, a closing of the pore by microscopic solid particles is unlikely, based on our recent experimental findings (36). It was shown that, for low aspect ratio chambers ($r \approx 0.1$), 2-μm polystyrene spheres became highly concentrated, but still only formed two or three layers of a colloidal crystal. Further accumulation into the volume of the chamber was disrupted by flow interactions of the solid particles with the thermal convection current (36). As a result, convective flow itself is likely to prevent tarring of the pore by larger particles. On the other hand, a minor accumulation of sticky particles at the pore bottom could contribute to the sealing of the leaks (see Fig. 6). Moreover, in this process, any pore shortening would be negligible.

The mechanism provides concentrated molecules in bulk water without requiring molecules to adsorb onto surfaces. Surface-assisted accumulation is often thought to solve the concentration problem, either via drying or specific adsorption. However, biological systems complex enough to evolve a replicating machinery would most likely need to disconnect, at least temporarily, from such restricting adsorbing surfaces (37). During this desorption or wetting process, there is a high risk of losing the replicated molecules into the bulk water (38). In the present scenario, where they would simply be reaccumulated from the pore solution and the catalytic activity of surfaces can be efficiently used. Our approach has the advantage of offering an active concentration mechanism in an already existing, robust enclosure. Because thermophoretic drift is common for molecules, the accumulation scheme applies similarly to nucleic acids, amino acids, and lipids.

The described accumulation in semiclosed microscopic pores has several synergistic advantages that pertain to the molecular evolution of early life. The enclosure of pore space by mineral precipitates frees life from the need to build a semipermeable organic membrane in its very first evolutionary steps. Microbiological evidence indicates that membrane synthesis appears to be a rather late development (15, 18). Moreover, active transport across a membrane to accumulate molecules in a cell is well known to be a highly evolved process, requiring complex proteins to form vesicles and to actively pump molecules across the membrane.

Notably, the mineral pores that we propose as accumulation centers for the emergence of life are presently populated with thermophilic prokaryotes, and it is speculated that these sites could have been inhabited by the last common ancestor and its biochemical precursors (15, 39). Rapid thermal quenching was demonstrated to be able to polymerize both nucleic (40) and amino (16) acids in a setting in which hydrothermal fluids were injected into cooled (4°C) water. The discussed setting of thermal convection provides comparable temperature interfaces, but now within a single pore. Therefore, both the temperature drop and the needed molecule concentration could be found in an enclosure instead of an open flow reactor.

The water inside the pore network is permanently shuttled by laminar thermal convection. Molecules that stochastically escape the accumulation at the bottom of the pore by diffusion are subjected to a rapid periodic temperature variation within a wide range of temperature amplitudes and cycle times inside a single pore. Equally, freshly precipitated mesoscopic mineral grains are subjected to thermal cycling by the convection. Their catalytic surfaces might generate nucleic acid multimers by thermally triggered periodic condensation (4) and unbinding reactions. In

this context, we note that, in a comparable thermal convection setting, DNA was shown to replicate exponentially by using the, albeit protein-catalyzed, PCR (33, 41).

In conclusion, we propose a type of mechanism, driven solely by a temperature gradient, which strongly accumulates even small protobiological molecules in semiclosed hydrothermal pore systems. This setting provides a compelling, dissipative microenvironment to promote the first steps in the molecular evolution of life.

Materials and Methods

Combined solutions of the Navier-Stokes equation (velocity $\vec{u}$, pressure p, density ρ, viscosity η), molecule diffusion (concentration c, diffusion coefficient D), and heat transfer (temperature T, heat conductivity k) were simulated in two dimensions by a finite element solver (Comsol, Femlab). Cross terms induce the thermal convection with the expansion coefficient α and the gravitational acceleration g_0, trigger thermophoresis with the thermodiffusion coefficient D_T and consider the flow-induced heating with the heat capacity c_P. Boundary conditions were nonslip for $\vec{u}$, neutral for c except for fixing the concentration to $c = 1$ at the top opening of the column and a horizontal temperature difference of ΔT across the cleft. Material parameters were as follows: density of water 1,000 kg/m^3, viscosity 0.0012 ($N \times$ s)/m^2, heat capacity 4,200 J/(kg $\times$ K), heat conductivity 0.6 W/(m $\times$ K), volume expansion 3.2×10^{-4}, cold temperature 293 K, temperature difference 30 K, and gravitational acceleration 9.8 m/s^2. The temperature dependence of the above parameters is not significant in the simulations. The Femlab simulation files can be obtained from the authors.

We thank Ludmilla Mendelevitch for initial simulations and Hermann Gaub for hosting D.B.'s Emmy–Noether Nachwuchsgruppe, which was funded by the Deutsche Forschungsgemeinschaft. M.J.R.'s work was conducted at the Jet Propulsion Laboratory, California Institute of Technology, under contract with the National Aeronautics and Space Administration.

1. Miller SL (1953) *Science* 15:528–529.
2. Drobner E, Huber H, Wächtershäuser G, Rose D, Stetter KO (1990) *Nature* 346:742–744.
3. Zubay G (2000) *Origins of Life on the Earth and in the Cosmos* (Academic, New York), 2nd Ed.
4. Ferris JP (2002) *Origins Life Evol Biosph* 32:311–332.
5. Eigen M (1971) *Naturwissenschaften* 58:465–523.
6. Kuhn H (1976) *Naturwissenschaften* 63:68–80.
7. Sievers D, von Kiedrowski G (1994) *Nature* 369:221–224.
8. Joyce GF (1989) *Nature* 338:217–224.
9. Cech TR, Atkins JF, Gesteland RF, eds (2000) *The RNA World* (Cold Spring Harbor Lab Press, Plainview, NY).
10. Dose K (1975) *Biosystems* 6:224–228.
11. Mojzsis SJ, Harrison TM, Pidgeon RT (2001) *Nature* 409:178–181.
12. de Duve C (1991) *Blueprint for a Cell: The Nature and Origin of Life* (Neil Patterson, Burlington, NC).
13. Ellis RJ (2001) *Trends Biochem Sci* 26:597–604.
14. Corliss JB (1990) *Nature* 347:624.
15. Koonin EV, Martin W (2005) *Trends Genet* 21:647–654.
16. Imai E, Honda H, Hatori K, Brack A, Matsuno K (1999) *Science* 283:831–833.
17. Russell MJ, Hall AJ, Cairns-Smith AG, Braterman PS (1988) *Nature* 336:117.
18. Russell MJ, Hall AJ (1997) *J Geol Soc London* 154:377–402.
19. Nisbet EG, Sleep NH (2001) *Nature* 409:1083–1091.
20. Kelley DS et al (2001) *Nature* 412:145–149.
21. Clusius K, Dickel G (1938) *Naturwissenschaften* 26:546.
22. Duhr S, Braun D (2006) *Proc Natl Acad Sci USA* 103:19678–19682.
23. Duhr S, Arduini S, Braun D (2004) *Eur Phys J E* 15:277–286.
24. Piazza R, Iacopini S, Triulzi B (2004) *Phys Chem Chem Phys* 6:1616–1622.
25. de Gans BJ, Kita R, Wiegand S, Luettmer-Strathmann J (2003) *Phys Rev Lett* 91:245501.
26. Furry WH, Jones RC, Onsager L (1939) *Phys Rev* 55:1083–1095.
27. Debye P (1939) *Annalen der Physik* 36:284–294.
28. Kelley DS, Karson JA, Fruh-Green GL, Yoerger DR, Shank TM, Butterfield DA, Hayes JM, Schrenk MO, Olson EJ, Proskurowski G, *et al* (2005) *Science* 307:1428–1434.
29. Russell MJ, Hall AJ, Boyce AJ, Fallick AE (2005) *Econ Geol* 100:419–438.
30. Stone DA, Goldstein RE (2004) *Proc Natl Acad Sci USA* 101:11537–11541.
31. Rona PA, Davis EE, Ludwig RJ (1998) *Proc Ocean Drilling Prog Sci Results* 158:329–336.
32. Clauser C (2006) in *Landolt-Börnstein: Numerical Data and Functional Relationships*, ed Heinloth K (Springer, Heidelberg).
33. Braun D, Goddard NL, Libchaber A (2003) *Phys Rev Lett* 91:158103.
34. Braun D, Libchaber A (2002) *Phys Rev Lett* 89:188103.
35. Braun D, Libchaber A (2004) *Phys Biol* 1:1–8.
36. Duhr S, Braun D (2005) *Appl Phys Lett* 86:131921.
37. Duve CD, Miller SL (1991) *Proc Natl Acad Sci USA* 88:10014–10017.
38. Wächtershäuser G (1994) *Proc Natl Acad Sci USA* 91:4283–4287.
39. Martin W, Russell MJ (2003) *Philos Trans R Soc London B* 358:59–85.
40. Ogasawara H, Yoshida A, Imai E, Honda H, Hatori K, Matsuno K (2000) *Origins Life Evol Biosph* 30:519–526.
41. Krishnan M, Ugaz VM, Burns MA (2002) *Science* 298:793.

Melting curve analysis in a snapshot

Philipp Baaske, Stefan Duhr, and Dieter Braun[a)]
Department of Applied Physics, Ludwig-Maximilians-University, Amalienstrasse 54, 80799 Munich, Germany

(Received 10 July 2007; accepted 10 September 2007; published online 26 September 2007)

The thermal denaturation of molecules is an essential method in biochemistry and diagnostics, including the measurement of single nucleotide polymorphisms and the binding analysis of proteins. We present a method for the all-optical high speed measurement of melting curves. A thin sheet of water is locally heated with an infrared laser to obtain a spatial temperature distribution between 20 and 100 °C. Using a fluorescence microscope a melting curve is recorded within 50 ms. This is about 10 000-times faster than state-of-the-art fluorometry and yields the same results for the validation example of a DNA hairpin. © *2007 American Institute of Physics*.
[DOI: 10.1063/1.2790806]

Measuring the stability of biomolecules and especially of DNA is of great importance in the field of biology, medical diagnostics, and biotechnology. It is often inferred from thermal denaturation experiments[1] and directly provides information about the DNA sequence or the biomolecular structure. In most cases, the conformation of the molecules is recorded by fluorescence and is plotted against temperature, yielding a so-called melting curve.[2] Traditionally, a small sample volume inside a comparably large cuvette or multiwell plate is heated by thermal contact. The thermal mass of the setup results in long equilibration times and slow heating rates. Measurement times on the order of 6–70 min are typical.[3]

We developed an all-optical method to determine the thermal stability of biomolecules in less than 50 ms. The temporal scan of temperatures is replaced by the application of a spatial temperature distribution, generated by heating a 20 μm thin fluid film with an infrared laser. The measurement volume is 2 nl and concentrations in the 100n*M* regime are accessible due to sensitive fluorescence imaging with high numerical aperture optics. Typically, a fluorescence dye reports the conformation of molecules in a melting curve. In our case we measured a DNA hairpin which was labeled with a fluorophore quencher pair, a configuration termed molecular beacon.[4,5]

The melting of biomolecules is often approximated using a two state model, which requires information over a wide temperature range to reach the completely closed and completely open states. In our experiment, a spatial temperature distribution with all temperatures between ambient temperature and 100 °C was achieved with a temperature resolution <1 °C. Such high resolution melting curves can be used for single nucleotide polymorphisms detection, genetic screening, and biomolecule binding assays.[6–8]

We generate a broad spatial temperature distribution by focusing an infrared laser into a 20 μm thin sheet of aqueous solution. Temperatures between 20 and 100 °C are created within several milliseconds in a field of view of 200×200 μm^2. Imaging is provided with a fluorescence microscope with a 40× oil immersion objective and a charge coupled device (CCD) camera (Fig. 1).

The precise timing of events is necessary to prevent artifacts from thermophoresis. Initially, a fluorescence image $I_0(x,y)$ with 10 ms exposure time is taken at an ambient temperature. Then, the infrared laser is switched on within 1 ms. A second image $I_1(x,y)$ is taken after 40 ms. The images I_0 and I_1 are corrected against camera background and bleaching. Measuring the fluorescence ratio $R(x,y)=I_1(x,y)/I_0(x,y)$ ensures the removal of artifacts from an inhomogeneous illumination [Fig. 2(a)].

As described below, the temperature distribution is imaged using temperature dependent fluorescence. The resulting temperature image $T(x,y)$ is shown in Fig. 2(b). In principle, the ratio $R(x,y)$ could be plotted against the temperature $T(x,y)$ for each pixel. However, the initial radial averaging of both $R(x,y)$ to $R(r)$ and $T(x,y)$ to $T(r)$ with radius r improves the signal to noise ratio since the low signals toward the periphery are averaged over an increased number of pixels. The resulting melting curve $F(T)=[R(T)-R_{\min}]/(R_{\max}-R_{\min})$ is plotted in Fig. 2(c) (circles). $R_{\min}$ is the fluorescence ratio of the completely closed state and $R_{\max}$ of the completely open state, respectively. The melting curve measured in only 50 ms agrees well with a 120 min lasting melting curve measured using a fluorometer [Fig. 2(c), solid line]. The slight shift between the curves most likely stems from temperature variations due to differences in the chamber thickness between the hairpin and the temperature measurement.

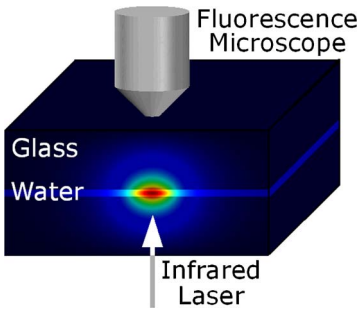

FIG. 1. Setup: Fluorescence from molecules in a 20 μm thin sheet of water is imaged from the top while it is heated with a focused infrared laser from below. Plotting the fluorescence image vs the temperature yields a high speed measurement of a melting curve at low molecule concentration. Color coded is the simulated temperature field.

[a)]Author to whom correspondence should be addressed. Electronic mail: dieter.braun@physik.lmu.de

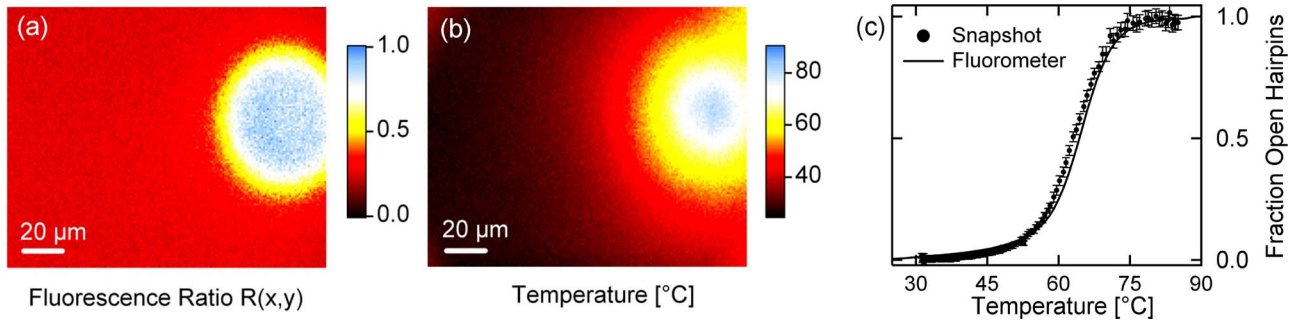

FIG. 2. Melting curve within a 50 ms snapshot: (a) The fluorescence ratio image $R(x,y)$ between heated and unheated conditions for 100nM DNA hairpins. The fluorescence is increased in the heated spot. (b) The temperature $T(x,y)$ is imposed to a 20 μm thin water film by infrared laser illumination and is measured using temperature sensitive fluorescence. (c) The fraction of open hairpins (circles), derived from the radially averaged fluorescence ratio $R(r)$ is plotted against the radially averaged temperature $T(r)$. It coincides well with a melting curve obtained from a 2 h fluorometer measurement (solid line).

The temperature image $T(x,y)$ is measured from a second experiment with the temperature dependent dye tetramethylrhodamine (TAMRA) (Invitrogen). Laser power, chamber geometry, and camera timing are kept fixed. For calibration, the temperature dependent fluorescence signal $F_{\mathrm{TAMRA}}(T)$ of TAMRA is measured in a 0.5× SSC-buffer (75mM NaCl, 7.5mM Na3-citrate, 0.01% TWEEN 20, pH 8.1) with a thermally controlled fluorometer (Fluoromax. 3; Horiba Jobin Yvon GmbH). From $F_{\mathrm{TAMRA}}(T)$ we infer $T(F_{\mathrm{TAMRA}})$ as shown in Fig. 3(a). With this calibration, we can transform the TAMRA fluorescence image $F_{\mathrm{TAMRA}}(x,y)=I_1(x,y)/I_0(x,y)$ into a temperature image $T(x,y)$. As before, the images I_0 and I_1 are corrected against camera background and bleaching.

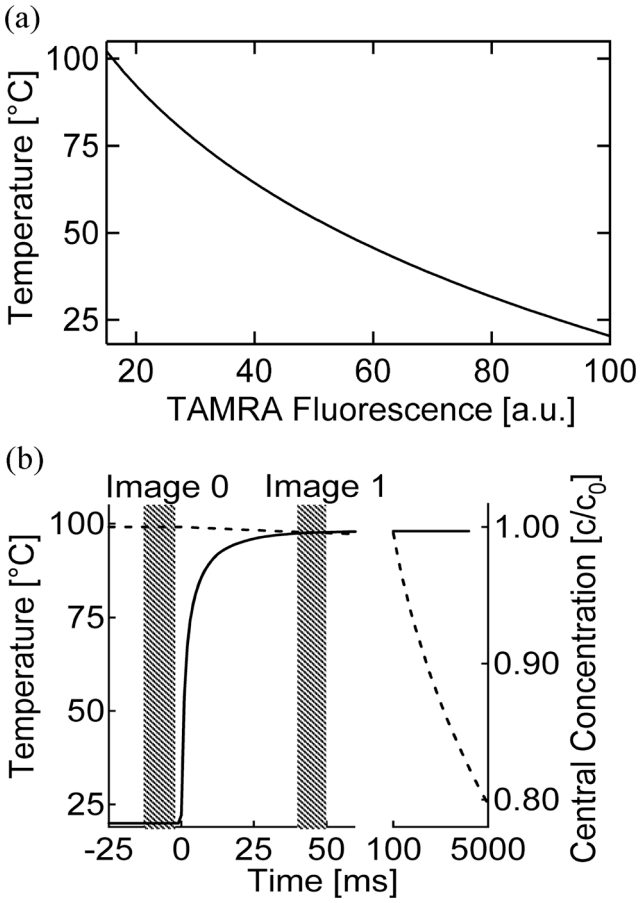

FIG. 3. Temperature and timing: (a) Calibration curve of the temperature dependent dye TAMRA in SSC-buffer used to infer the chamber temperature. (b) Simulations show that a precise synchronisation between laser heating and image exposures is crucial to reach a steady state in temperature (solid line) and not to significantly decrease the molecule concentration in the center of the chamber due to thermophoresis (dotted line).

The spatial temperature distribution was generated by the light absorption in water. We used a fiber coupled IR laser (Raman fiber laser RLD-5-1455; IPG Photonics Corporation) with a wavelength of 1455 nm and typically applied an output power of 1.2 W. Water absorbs at this wavelength with an attenuation length of 305 μm. The laser beam was moderately focused with a lens of 8 mm focal distance and switched on and off by moving the laser spot into the field of view with galvanometric mirrors. A fluorescence microscope (AxioTech Vario; Zeiss) with an oil immersion objective (40×, 1.3 numerical aperture, Zeiss Fluar) was used. Two 170 μm thick coverslips (12 mm diameter) sandwiched 2 μl aqueous solution and were sealed with nail polish to prevent evaporation. Chamber thickness was 20 μm. The sample was illuminated with a mercury lamp (HXP 120, Leistungselektronik Jena GmbH). A TAMRA fluorescence filter set was used (AHF Tübingen, Germany) and the laser was blocked with OD5 using a glass filter (KG 5, AHF Tübingen, Germany). Imaging was provided with a 12-bit CCD camera (Sensicam QE; PCO AG). The DNA hairpin was purchased from biomers.net with the sequence 5′-Hex-GCA CGC ATC GCT CTT CAT TAG AAC TAT GCG TGC-Dabcyl-3′ and diluted to 100nM in 0.5× SSC-buffer.

Several artifacts have to be exluded to be able to measure a melting curve in the described setting. We simulated the heat conduction numerically in the axial symmetric geometry of the chamber.[9,10] The temperature relaxes with a time scale which is essentially given by the heat diffusion relaxation time perpendicular to the chamber,

$$\tau = \frac{d^2}{\pi^2}\frac{C\rho}{k}. \tag{1}$$

We find $\tau=0.32$ ms for a thickness of the chamber of $d=20$ μm, the heat capacity of water $C=4200$ J/(kg K), the thermal conductivity of water $k=0.54$ W/(K m), and the density of water $\rho=1000$ kg/m^3. The glass chamber walls conduct the heat comparably to water with $k\approx 0.8$ W/(K m). This results in an effective increase of the thermal thickness d which changes the thermal relaxation time to 2.2 ms, seen in the numerical simulation [Fig. 3(b), solid line]. The time of 40 ms between the two images therefore ensures a steady state temperature distribution. Due to

the low conducting glass walls the temperature distribution along the z direction follows a flat parabolic profile.[10]

The most important condition is that the molecule concentration within a pixel of the chamber has to remain constant between the two images I_0 and I_1. Due to an effect known as thermophoresis,[9–11] molecules drift along a temperature gradient. Thermophoresis is parametrized with a thermophoretic mobility D_T relating the molecule velocity to the thermal gradient ∇T according to $v=-D_T\nabla T$. In the steady state, the molecule concentration at a given temperature difference ΔT is given by $c/c_0=e^{-S_T\Delta T}$,[12] with the Soret coefficient defined as $S_T=D_T/D$. For the hairpin system, we simulated thermophoresis numerically using $D_T=1.15\ \mu\mathrm{m}^2/(\mathrm{s\ K})$ and $D=115\ \mu\mathrm{m}^2/\mathrm{s}$,[9,13] and find that the temperature gradients along the chamber result only in a $<1\%$ drop of the central concentration within 50 ms [Fig. 3(b), dashed line]. Similarly, the thermophoresis of TAMRA does not affect the temperature measurement. The maximum velocity of thermal convection is calculated to 1.4 μm/s (Ref. 10) and has no effect within the measurement time window.

Epifluorescence in a 20 μm thin chamber averages the fluorescence of the chromophores across the chamber. We probed for thermal lensing effects by comparing objectives with different numerical apertures and found no significant effect under the given defocused laser spot conditions. The IR laser is blocked after the objective; however, tests using dried films of TAMRA with and without laser illumination show no effects of the laser irradiation on imaging.

The folding and unfolding of a DNA hairpin equilibrates on the microsecond to millisecond time scale.[14] Therefore, we can expect that the melting curve is measured in the kinetic equilibrium. As shown in Fig. 4, we fitted the melting curve with a two state model to extract the standard enthalpy ΔH^0 and entropy ΔS^0 of the reaction according to $\Delta G^0=-RT\ln(K)=\Delta H^0-T\Delta S^0$. Standard protocols were used to infer the fraction of closed to open states of the hairpin molecule and thus the equilibrium constant (K) from the melting curve.[2,5] We find $\Delta H^0=-253$ kJ/mol and $\Delta S^0=-754$ J/(mol K) and thus a melting temperature of 62 °C. This result comes very close to the calculations of DNA hairpin thermodynamics, predicting $\Delta H^0=-275$ kJ/mol and $\Delta S^0=-813$ J/(mol K) and a melting temperature of 65 °C.[15]

We developed a method for the fast measurement of high precision melting curves. Based on an all-optically generated spatial temperature distribution, the method circumvents the slow equilibration time of conventional melting curve analysis and accelerates the analysis more than 10 000 times from about 10 min down to 50 ms. The detection volume is as low as 2 nl and measurements at 100nM concentration are demonstrated. The method is of particular interest for high throughput screening in biotechnology and fast genotyping in medicine.

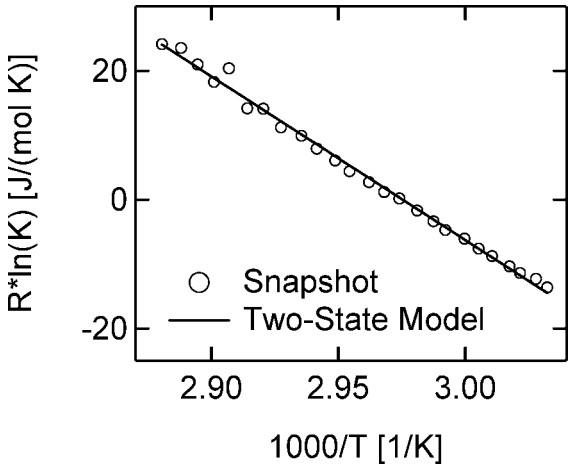

FIG. 4. Thermodynamic analysis: Fitting a two state model to the melting curve data allows one to infer the standard enthalpy and entropy of the reaction.

The authors thank the Deutsche Forschungsgemeinschaft (DFG) for funding through the Emmy Noether Program, the Nanosystems Initiative Munich (NIM), and the SFB 486.

[1] J. Marmur and P. Doty, J. Mol. Biol. **5**, 109 (1962).
[2] J. L. Mergny and L. Lacroix, Oligonucleotides **13**, 515 (2003).
[3] M. G. Herrmann, J. D. Durtschi, L. K. Bromley, C. T. Wittwer, and K. V. Voelkerding, Clin. Chem. **52**, 494 (2006).
[4] S. Tyagi and F. R. Kramer, Nat. Biotechnol. **14**, 303 (1996).
[5] G. Bonnet, S. Tyagi, A. Libchaber, and F. R. Kramer, Proc. Natl. Acad. Sci. U.S.A. **96**, 6171 (1999).
[6] J. M. Akey, D. Sosnoski, E. Parra, S. Dios, K. Hiester, B. Su, C. Bonilla, L. Jin, and M. D. Shriver, BioTechniques **30**, 358 (2001).
[7] S. O. Sundberg, C. T. Wittwer, J. Greer, R. J. Pryor, O. Elenitoba-Johnson, and B. K. Gale, Biomed. Microdevices **9**, 159 (2007).
[8] T. Liedl and F. C. Simmel, Anal. Chem. **79**, 5212 (2007).
[9] S. Duhr and D. Braun, Proc. Natl. Acad. Sci. U.S.A. **103**, 19678 (2006).
[10] S. Duhr, S. Arduini, and D. Braun, Eur. Phys. J. E **15**, 277 (2004).
[11] C. Ludwig, SB Akad. Wiss. Wien **20**, 539 (1856).
[12] S. Duhr and D. Braun, Phys. Rev. Lett. **96**, 168301 (2006).
[13] P. Baaske, F. M. Weinert, S. Duhr, K. H. Lemke, M. J. Russell, and D. Braun, Proc. Natl. Acad. Sci. U.S.A. **104**, 9346 (2007).
[14] G. Bonnet, O. Krichevsky, and A. Libchaber, Proc. Natl. Acad. Sci. U.S.A. **95**, 8602 (1998).
[15] M. Zuker, Nucleic Acids Res. **31**, 3406 (2003).

Optical Thermophoresis quantifies Buffer dependence of Aptamer Binding[**]

Philipp Baaske[*], Christoph J. Wienken, Philipp Reineck, Stefan Duhr and Dieter Braun

Quantification of biomolecular binding in their native environment is crucial for biology and medicine. However, reliable methods are rare. We add a new immobilization-free method by showing that thermophoresis, the movement of molecules in a thermal gradient, can be used to measure binding curves equally well in human blood serum as in various buffers. The assay works without surface contact and requires only an unspecific fluorescence marker on one of the binding partners as no conformational change is needed for signal transduction.

Aptamers are nucleic acid ligands selected in vitro for their ability to bind to specific molecular targets[1-4]. They are promising candidates for diagnostic applications because of their antibody comparable affinity, specificity and the ease with which novel aptamers can be designed[5]. Aptamers have been implemented in a variety of sensing technologies[6] including optical approaches like "aptamer beacons"[7], electronic-sensing strategies[8], mass based sensors[9] and force based assays[10].

In most aptamer based binding assays, the signal transduction mechanism depends on the molecular recognition mechanism. As a result the aptamers not only have to be designed to adopt an appropriate conformation to bind to a target (recognition) but also to undergo a binding induced conformational change, which affects the fluorescence of a dye[8] or the electron-transfer[9] of a redox tag to an electrode (signal transduction). This conjunction between target recognition and signal transduction sets obstacles for the design of aptamers. Often aptamers have to be modified with two labels, resulting in a reduced binding affinity or even complete suppression of binding[11]. These restrictions can be reduced by separating the molecular recognition from the signal transduction by using additional competitor oligonucleotides, complementary to the aptamer, as signal transduction elements[12].

Here we describe a novel approach for the quantification of aptamer–target interactions which separates molecular recognition from signal transduction and requires only an aptamer tagged with one dye. It provides the opportunity to probe the binding with an unspecific label in the native environment of free solution or complex biological fluids.

The approach is based on the directed movement of molecules along temperature gradients, an effect termed thermophoresis[13-16]. A spatial temperature difference ΔT leads to a depletion of molecule concentration in the region of elevated temperature, quantified by the Soret coefficient S_T:

$$c_{hot}/c_{cold} = \exp(-S_T \Delta T) \qquad (1)$$

* P. Baaske, C. J. Wienken, P. Reineck, Prof. D. Braun, Ludwig-Maximilians-Universität München
Systems Biophysics, Department of Physics, Center for NanoScience (CeNS), Munich, DE-80799 Germany,
Fax: ++49 89 218016558, E-mail: philipp.baaske@physik.lmu.de, Homepage: www.biosystems.physik.lmu.de
P. Baaske, S. Duhr, NanoTemper Technologies GmbH, Amalienstr. 54, Munich, DE-80799 Germany

** We thank the LMU Innovative Initiative Functional NanoSystem (FUNS) and the Excellence Cluster NanoSystems Initiative Munich (NIM) for the financial support.

Thermophoresis depends on the interface between molecule and solvent. Under constant buffer conditions, thermophoresis probes the size, charge and solvation entropy of the molecules[15,16] and is not dependent on the concentration of the probed molecule unless millimolar concentrations are reached[17,18]. The thermophoresis of an end-labelled aptamer A typically differs significantly from the thermophoresis of an aptamer-target complex AT due to size, charge and solvation energy differences. We use this difference in the molecule's thermophoresis to quantify the binding in titration experiments under constant buffer conditions for a 5.6 kDa aptamer to the 37 kDa protein thrombin as well as the binding of a 8.3 kDa aptamer to the 0.3 kDa AMP or 0.6 kDa ATP. Different binding affinities are found depending on the buffer conditions or as compared to measurements in 10% or 50% serum.

The thermophoretic movement of the fluorescently end-labelled aptamer is measured by monitoring the fluorescence distribution F inside a capillary with an epifluorescence microscope (Figure 1a). The microscopic temperature gradient is generated by an IR-Laser (1480nm), which is focused into the capillary and is strongly absorbed by water[15,16,19]. The temperature of the aqueous solution in the laser spot is raised by ΔT=8K. Before the IR-Laser is switched on a homogeneous fluorescence distribution F_{cold} is observed inside the capillary (Figure 1b). When the IR-Laser is switched on, two effects, separated by their time-scales, contribute to the new fluorescence distribution F_{hot}. The thermal relaxation time is fast (≈ 50ms) and induces a drop in fluorescence of the dye due to its intrinsic temperature dependence. On the slower diffusive time scale (≈ 10s), the aptamers move from the locally heated region to the outer cold regions[16,20]. The local concentration of aptamers decrease in the heated region until it reaches a steady state distribution (Figure 1b).

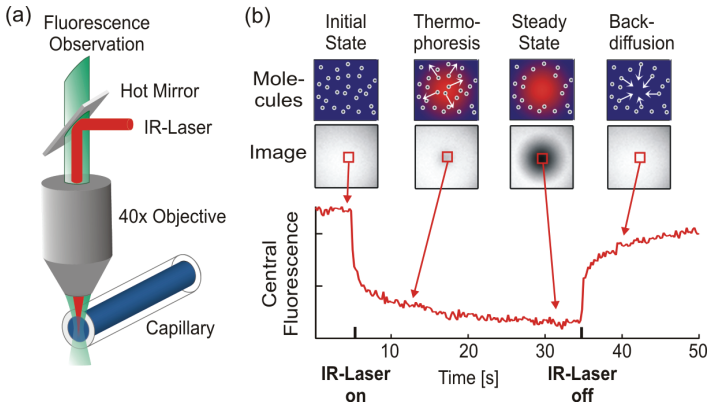

Figure 1. *Thermophoresis assay. (a) The blood serum solution inside the capillary is locally heated with a focused IR-laser, which is coupled into an epifluorescence microscope using a hot mirror. (b) The fluorescence inside the capillary is imaged with a CCD-camera and the normalized fluorescence in the heated spot is plotted against time. The IR-laser is switched on at t=5s and the fluorescence decreases as the temperature increases and the labelled aptamers move away from the heated spot due to thermophoresis. Once the IR-laser is switched off the molecules diffuse back.*

While the mass diffusion D dictates the kinetics of depletion, S_T determines the steady state concentration ratio $c_{hot}/c_{cold} = \exp(-S_T \Delta T) \approx 1 - S_T \Delta T$ under a temperature increase ΔT [15,16]. The normalized fluorescence $F_{norm} = F_{hot}/F_{cold}$ measures mainly this concentration ratio, in

addition to the temperature dependence of the dye fluorescence $\partial F/\partial T$. In the linear approximation we find: $F_{norm}=1+(\partial F/\partial T-S_T)\Delta T$ [16]. Due to the linearity of the fluorescence intensity and the thermophoretic depletion, the normalized fluorescence from the unbound aptamer $F_{norm}(A)$ and the bound complex $F_{norm}(AT)$ superpose linearly. By denoting x the fraction of aptamers bound to targets, the changing fluorescence signal during the titration of target T is given by (see supplementary material):

$$F_{norm}=(1-x)F_{norm}(A)+x\,F_{norm}(AT) \qquad (2)$$

Based on the capacitor model of thermophoresis [15,21], confirmed for thin Debye layers using polystyrene beads[15], double stranded DNA[15], single stranded DNA[16] and Ludox silica particles[22], we can discuss the change in S_T expected from changes in charge Q_{eff} or hydrodynamic radius R upon binding. Assuming negligible offsets from non-ionic contributions, we find $S_T\propto Q_{eff}^2/R^2$. Under linear approximation, S_T changes by $\Delta S_T/S_T=2(\Delta Q_{eff}/Q_{eff}-\Delta R/R)$. Only for the unlikely case of $Q_{eff}\propto R$ no change in S_T would be expected. However contributions from the neglected solvation entropy[15] could reveal the binding even under these conditions.

We measured the thermophoresis of 100nM thrombin-aptamer[23] in 10% human serum (Figure 2). The concentration of thrombin ranges from 0nM to 19,500nM. The low concentrations ensure that the serum and buffer do not change upon addition of thrombin and keep the thermophoresis of the aptamer constant. The aptamer is labelled with a Cy5 dye at the 5' end. The observed time traces of the pure aptamer differ significantly from the traces of aptamers bound to thrombin (Figure 2a). Plotting the normalized fluorescence F_{norm} at a given time t against the varying thrombin concentration results in a binding curve (Figure 2b) with an $EC_{50}=680\pm80$nM and a Hill-coefficient of 2. Control experiments with a randomly chosen sequence ssDNA show no thrombin dependent changes both in the thermophoretic signal (Figure 2b) and the absolute fluorescence, both in 10% and 50% serum . This indicates that neither interactions of thrombin with the Cy5, nor unspecific interactions of thrombin with ssDNA are present.

As detailed before[16], we used a 2D finite element simulation to infer from the time traces the Soret coefficient S_T, the diffusion coefficient D and the temperature dependence of the fluorescence $\partial F/\partial T$. The binding to thrombin mostly leads to a change in S_T, which drops from 1.05 %/K down to 0.35 %/K (Figure 2c). Both the simple determination using F_{norm} and the fitted Soret coefficient S_T report the binding (Figure 2b,c) due to linear relationship in steady state. Both the temperature dependent fluorescence change $\partial F/\partial T$ and the diffusion coefficient D showed no significant binding signal. Notably the determination of D is likely to be hampered by fitting crosstalk with $\partial F/\partial T$.

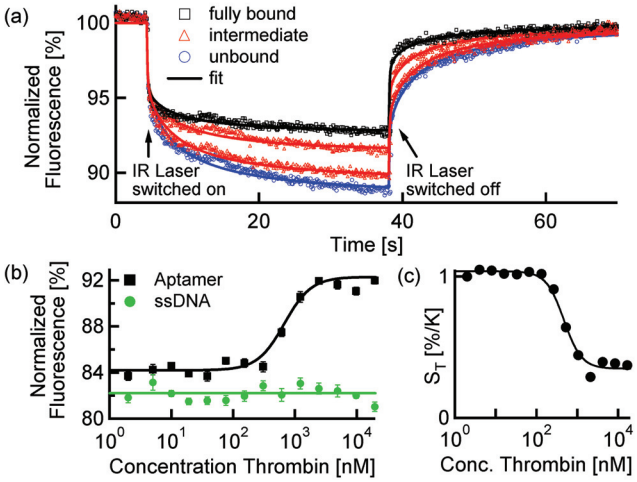

Figure 2. *Aptamer-thrombin binding in 10% human serum. (a) The thermophoretic depletion of unbound aptamer is about 2-fold stronger than for aptamers bound to thrombin. (b) The normalized fluorescence* F_{norm} *t=30s is plotted for different concentrations of thrombin. Random 25mer ssDNA (blue) shows no change in thermophoresis with increasing thrombin concentration. (c) The Soret coefficient* S_T *equally reports the binding. Fitting of* S_T *is provided with an analytical model of thermophoresis*[16] *as shown in (a).*

The thermophoretic perturbation creates a direct fluorescence ratio signal F_{norm} that reveals changes in the observed molecule which stem from changes in size, charge or solvation entropy of the molecule. It does not rely on the notoriously difficult task to observe binding induced size changes by measuring small changes in the diffusion coefficient D as for example in fluorescence correlation spectroscopy (FCS). As shown in Figure 3a, the approach can be used equally well in buffers as in complex biological liquids like blood serum without significantly loosing sensitivity or specificity as it is the case with chip based technologies such as surface plasmon resonance (SPR).

To further show the broad applicability of the thermophoretic quantification of binding, we also measured the binding of aptamer-ATP/AMP[24] (Figure 3b) in different buffers. In all cases, binding was reported with a high signal-to-noise ratio (SNR), even in 50% human serum. For example a SNR=93 was found for the case of the 0.3kDa AMP-binding in selection buffer and SNR=23 was found for thrombin-binding in 50% human serum (supplementary material). As control oligonucleotides we used aptamer sequences, which differed from the respective aptamer only in two nucleotide mutations (Figure 3a,b “Binucleotide Mutant”).

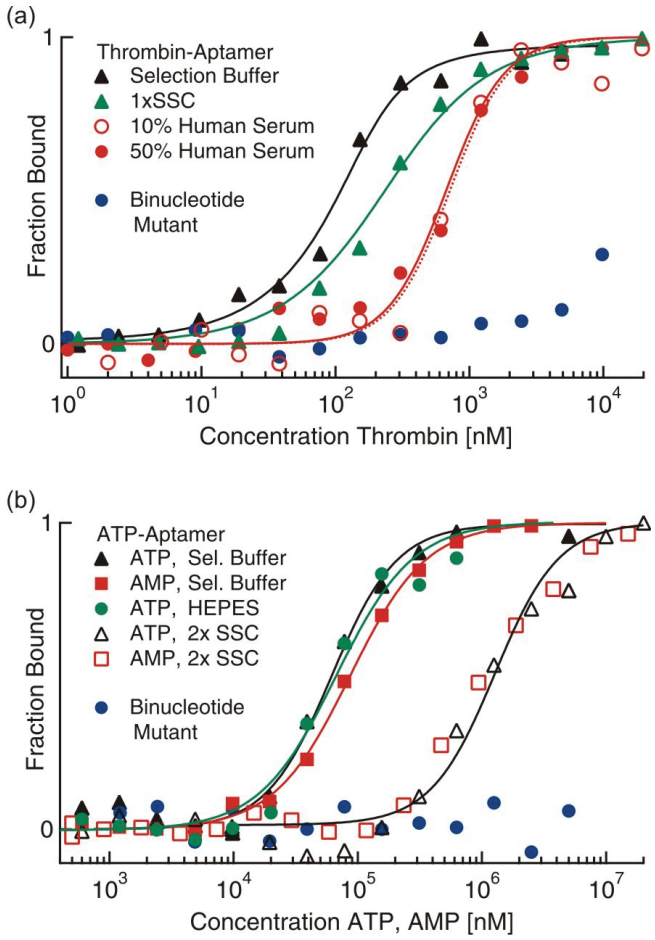

Figure 3. *Binding curves in various buffers. (a) Aptamer-thrombin binding in selection buffer, SSC, 10% and 50% untreated human serum. (b) Aptamer binding to ATP and AMP in selection buffer, HEPES and 2x SSC. The fraction of bound aptamers is derived according to equation 2.*

The dissociation constant $K_D = 30 \pm 19\text{nM}$ obtained for the aptamer-thrombin binding (Figure 3a) in selection buffer is in good agreement with the reported $K_D = 25 \pm 25\text{nM}$ [5] measured in the same buffer. In SSC buffer the dissociation constant increases to $K_D = 190 \pm 20\text{nM}$ and in 50% (10%) human serum the binding was best fitted with the Hill equation, yielding an $EC_{50} = 720 \pm 100\text{nM}$ ($670 \pm 80\text{nM}$) and a cooperativity of n=2.

The aptamer-ATP/AMP binding (Figure 3b) shows a cooperative binding of more than one ATP or AMP per aptamer, which is consistent with the literature [7, 25]. In the selection buffer the EC_{50} values for ATP, $EC_{50} = 60 \pm 4\mu\text{M}$, and AMP, $EC_{50} = 87 \pm 5\mu\text{M}$, are well within the reported values[7,12]. Measurements in HEPES buffer with $EC_{50} = 67 \pm 8\mu\text{M}$ confirm these results. In all cases the Hill coefficient was n=1.4. Interestingly, in 2x SSC buffer, the EC_{50} values of the ATP/AMP-aptamer binding were both strongly shifted to lower affinities, resulting in an $EC_{50} = 1100 \pm 100\mu\text{M}$. Note that the ATP solutions were kept on ice to prevent hydrolysis of ATP.

As stated by Cho and Ellington[6], the aptamer-target binding was strongly dependent on the chosen buffer: The binding of the aptamers in the respective selection buffers always showed the highest affinity (Figure 3). For the aptamer-thrombin binding, the shift to lower affinities

(EC_5=720nM) and enhanced cooperativity (n=1.5) in human serum may be because of interactions of the thrombin with blood serum components. For the ATP-aptamer the unexpected big shift to lower affinities in the SSC buffer as compared to the TRIS and HEPES buffers is likely an effect of a competing interaction of the strongly negative $Citrate^{3-}$ with the Mg^{2+} ions as the latter are essential for the aptamer-ATP/AMP binding.

In conclusion, we have developed an all-optical thermophoretic technique for the screening of aptamer-target interactions in bulk solution with very low material consumption of 500 nl out of which only 2 nl are probed. The signal transduction of binding is separated from the molecular recognition, which provides more freedom in the design of aptamers. The assay is robust and simple as no secondary reactions for detection are required. The dynamic range of the thermophoresis binding assay reaches from nM to mM target concentrations and can also quantify the binding to low mass targets such as AMP. The measurement can be equally well performed in complex liquids such as blood or simple standard buffers. As result, the approach will enable the determination of the affinity of aptamer-based drug candidates, for example Spiegelmers[26], in biological liquids close to physiological conditions. The method is also applicable for screening for new aptamers since the binding of unlabelled aptamers to a labelled target can also be quantified with thermophoresis.

Experimental Section

For imaging, we used a Zeiss Axiotech Vario microscope with a 40x Plan Fluar oil objective, numerical aperture 1.3. The fluorescence was excited with a red high power LED Luxeon III (LXHL-LD3C). Fluorescence filters for Cy5 (F36-523) were purchased from AHF-Analysentechnik (Tübingen, Germany). Detection was provided with the Sensicam EM CCD-camera from PCO AG (Kelheim, Germany). Fused silica capillaries from Polymicro Technologies (Phoenix, USA) with an inner diameter of 100µm containing about 500nl volume were used for the measurements.

The temperature gradients were created with an infrared laser diode (Furukawa FOL1405-RTV-617-1480, wavelength λ=1480nm attenuation length κ=320µm for water, 320mW maximum power), purchased from AMS Technologies AG (Munich, Germany). The IR-Laser beam couples into the path of fluorescence light with a hot mirror (NT46-386) from Edmund Optics (Barrington, USA) and is focused into the fluid with the microscope objective. The temperature inside the capillary was measured via the known temperature dependent fluorescence of the TAMRA-dye[19]. The temperature in the solution was raised by 8K in the beam center with a $1/e^2$ diameter of 25 µm. All measurements were performed at room temperature.

The change in fluorescence were analyzed in a region around the center of heating with a diameter of about 50µm. The images were corrected for background and bleaching of the fluorescence[16,20].

The human α-thrombin was purchased from Haematologic Technologies Inc. (Essex Junction, USA; specific activity 3593 U/mg; MW=36.7 kDa). The human serum, the AMP and the ATP were purchased from Sigma Aldrich (Munich, Germany).

The labeled DNA oligonucleotides were synthesized by Metabion (Martinsried, Germany). The sequences of the oligonucleotides, with mutations as small letters, are:

Thrombin-Aptamer:	5'-Cy5-TGGTTGGTGTGGTTGGT-3'
Thrombin-Binucleotide Mutant:	5'-Cy5-TGGTTGtTGTGGTTtGT-3'
ATP-Aptamer:	5'-Cy5-CCTGGGGGAGTATTGCGGAGGAAGG-3'
ATP-Aptamer-Binucleotide Mutant:	5'-Cy5-CCTtGGGGAGTATTGCGGAtGAAGG-3'
ssDNA:	5'-Cy5-TAGTTCTAATGTGTATCTCAATTTT-3'

Measurements were conducted in the selection buffers of the aptamers and in SSC buffer with different ion concentrations. Thrombin-aptamer: Selection buffer[23]: 20mM Tris-HCl pH 7.4, 150mM NaCl, 5mM KCl, 1mM CaCl2, 1mM MgCl2, 0.01% TWEEN20, 4% BSA. For the human serum measurements this buffer was mixed 1:1 with 100% human serum. 1xSSC: 15mM Na3-citrate, pH 7.4, 150mM NaCl, 5mM KCl, 1mM CaCl2, 1mM MgCl2, 0.01% TWEEN20, 4% BSA.

ATP-aptamer: Selection Buffer[24]: 20mM Tris-HCl pH 7.6, 300mM NaCl, 5mM MgCl2 and 0.01% TWEEN20. 2xSSC: 30mM Na3-citrate, pH 7.4, 300mM NaCl, 5mM MgCL2, 0.01% TWEEN20. HEPES: 20mM HEPES pH 7.5, 300mM NaCl, 5mM MgCl2 and 0.01% TWEEN20. For ATP the pH of the buffers were measured for different ATP concentrations with the pH-sensitive dye BCECF (supplementary).

The aptamer and the mutant concentrations were kept fixed at 100nM (thrombin-aptamer) and 500nM (ATP-aptamer) during all experiments. The aptamers were denatured and renatured prior the experiments to ensure that they reach their active conformation. The solutions were incubated for 2 hours after mixing the oligonucleotides with the different target concentrations.

The K_D values for thrombin were obtained by fitting the fraction of bound aptamers to the quadratic solution of the binding reaction equilibrium, derived from the law of mass action, with K_D as single free parameter [10]. The EC50 value for were obtained from fitting with the Hill equation.

Received: ((will be filled in by the editorial staff))
Published online on ((will be filled in by the editorial staff))

Keywords: aptamers · proteins · immobilization free · drug discovery · DNA

[1] G. Mayer, *Angew. Chem. Int. Ed. Engl.* **2009**, *48*, 2672-2689.
[2] A. D. Ellington, J. W. Szostak, *Nature* **1990**, *346*, 818-822.
[3] C. Tuerk, L. Gold, *Science* **1990**, *249*, 505-510.
[4] D. L. Robertson, G. F. Joyce, *Nature* **1990**, *344*, 467-468.
[5] B. Boese, K. Corbino, R. Breaker, *Nucleosides, Nucleotides Nucleic Acids* **2008**, *27*, 949-966.
[6] E. Cho, J. Lee, A. Ellington, *Annu. Rev. Anal. Chem.* **2009**, *2*, 241-264.
[7] S. Jhaveri, R. Kirby, R. Conrad, E. Maglott, M. Bowser, R. Kennedy, G. Glick, A. Ellington, *J. Am. Chem. Soc.* **2000**, *122*, 2469-2473.
[8] Y. Xiao, A. A. Lubin, A. J. Heeger, K. W. Plaxco, *Angew. Chem. Int. Ed. Engl.* **2005**, *44*, 5456-5459.
[9] S. Song, L. Wang, J. Li, C. Fan, J. Zhao, *Trends Anal. Chem.* **2008**, *27*, 108-117.
[10] D. Ho, K. Falter, P. Severin, H. E. Gaub, *Anal. Chem.* ***2009***, 81, 3159-3164.
[11] S. Beyer, W. Dittmer, F. Simmel, *J. Biomed. Nanotechnol.* **2005**, *1*, 96-101.
[12] N. Li, C. M. Ho, *J. Am. Chem. Soc.* **2008**, *130*, 2380-2381.
[13] Ludwig, C. *Sitzungsber. Akad. Wiss. Wien: Math.-Naturwiss*. **1856**, *20*, 539.
[14] S. Iacopini, R. Piazza, *Europhys. Lett.* **2003**, *63*, 247-253.
[15] S. Duhr, D. Braun, *Proc. Natl. Acad. Sci. U. S. A.* **2006**, *103*, 19678-19682.
[16] P. Reineck, C.J. Wienken, D. Braun, Thermophoresis of Single Stranded DNA, *Electrophoresis*, accepted.
[17] Jan K. G. Dhont, Journal of Chemical Physics, **2004,** 120, 1632-1641
[18] J. Rauch and W. Köhler, Journal of Chemical Physics **2003**, 119, 11977-11988
[19] P. Baaske, S. Duhr, D. Braun, *Appl. Phys. Lett.* **2007**, *91*, 133901.
[20] S. Duhr, S. Arduini, D. Braun, *Euro. Phys. J. E.* **2004**, *15*, 277-286.
[21] J.K.G. Dhont, S. Wiegand, S. Duhr and D. Braun, Langmuir **2007,** 23, 1674-1683
[22] H. Ning, J.K.G. Dhont and S. Wiegand, Langmuir **2008**, 24 2426–2432
[23] L. C. Bock, L. C. Griffin, J. A. Latham, E. H. Vermaas, J. J. Toole, *Nature* **1992**, *355*, 564-566.
[24] D. E. Huizenga, J. W. Szostak, *Biochemistry* **1995**, *34*, 656-665.
[25] C.H. Lin, D.J. Patel, *Chem. Biol.* **1997**, *4*, 817-832.
[26] C. Maasch, K. Buchner, D. Eulberg, S. Vonhoff, S. Klussmann, *Nucleic Acids Symp. Ser.* 2008, 52, 61-62.

Supplementary Material

Signal to Noise Ratio SNR

The signal to noise ratio is calculated from the difference between $F_{norm}(A)$ and $F_{norm}(AT)$ divided by the mean error δ which averages the standard-deviation σ of two independent measurements over N different target concentrations $\delta=(\sum_{i=1}^{N}\sigma_i)/N$:

$$SNR=\left|F_{norm}(A)-F_{norm}(AB)\right|/\delta \quad (1)$$

To quantify the quality of the measurement of a binding reaction the Z-factor[1] can be used:

$$Z=1-\frac{(3\sigma_A+3\sigma_{AT})}{\left|F_{norm}(A)-F_{norm}(AT)\right|} \quad (2)$$

Here σ_A is the standard-deviation of the signal of the aptamer alone and σ_{AT} the standard-deviation of the signal where 100% aptamer are bound to their target. In the case of the aptamer measurements we assume $\sigma_A=\sigma_{AT}=\delta$ and thus equation 2 can be simplified to:

$$Z=1-\frac{6\delta}{\left|F_{norm}(A)-F_{norm}(AT)\right|} \quad (3)$$

From Figure 1a one can derive for the aptamer-AMP binding $\left|F^{AMP}_{norm}(A)-F^{AMP}_{norm}(AT)\right|=2.57$ and $\delta_{AMP}=0.0275$. From Figure 1b one can derive the values for the aptamer-thrombin binding in 50% human serum: $\left|F^{TBA}_{norm}(A)-F^{TBA}_{norm}(AT)\right|=2.86$ and $\delta_{TBA}=0.123$. Using the equations 1 and 2 the Signal-to-Noise ration and the Z-factor is calculated for the aptamer-AMP binding in selection buffer and for the aptamer-thrombin binding in 50% human serum as tabulated below. A value of the Z-factor > 0.5 represents an “excellent assay”[1] for binding detection.

	Signal-to-Noise Ration (SNR)	Z-Factor
Aptamer-AMP	93	0.94
Aptamer-Thrombin	23	0.74

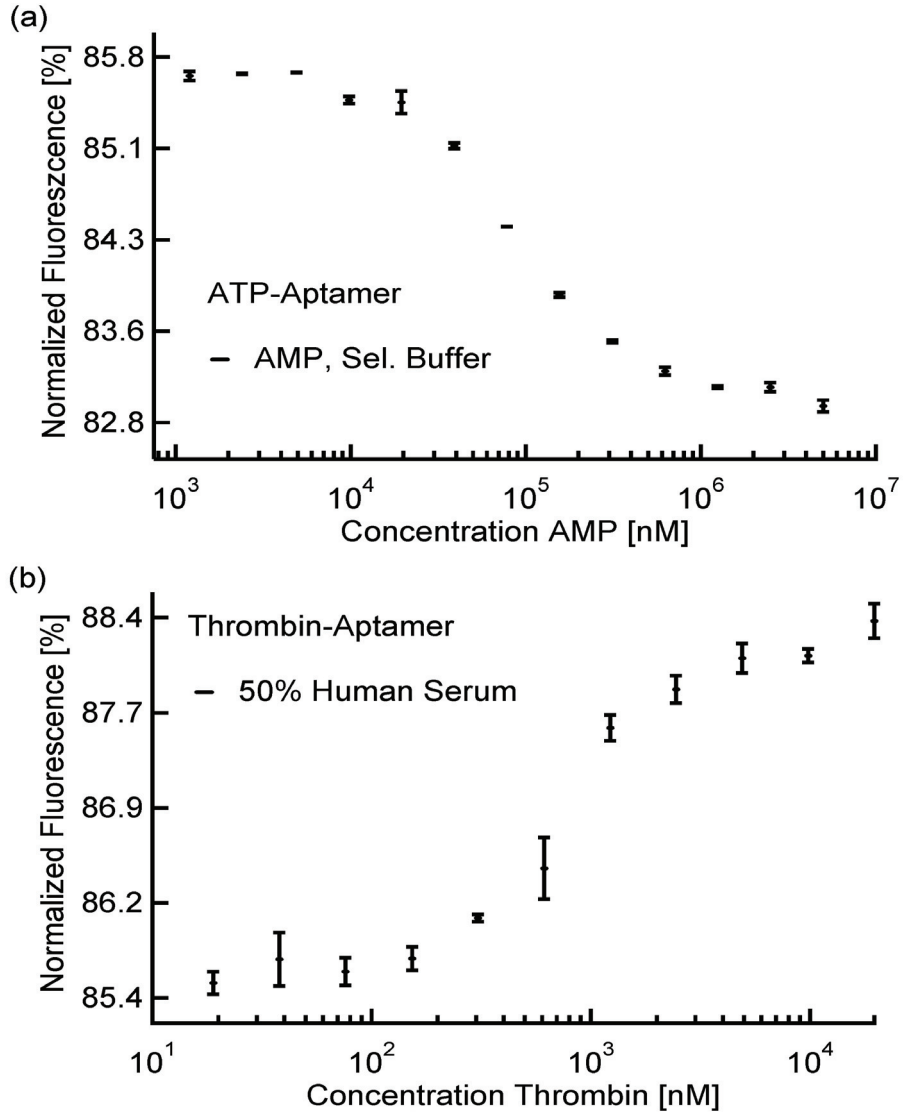

***Figure** 1: Normalized fluorescence signals, including error bars. (a) Aptamer-AMP binding in selection buffer. As expected from the capacitor model of thermophoresis the normalized fluorescence decreases as AMP binds to the aptamer. (b) Aptamer-thrombin binding in 50% human serum.*

Calculation of the normalized fluorescence in steady state

The reaction of an fluorescently labelled aptamer A with its Target T to form the complex AT is measured:

$$A + T \Leftrightarrow AT$$

Due to the labeling the fluorescence is both reported from T and AT. The concentration of aptamer is denoted by c_A , the concentration of target by c_T and the concentration of the formed complex by c_{AT} . The fluorescence of the three molecular states are F_A and F_{AT} . The non-fluorescent target T is not measured. In the used diluted regime, self-quenching of the chromophorese can be excluded and the measured fluorescence is proportional to the concentrations. Thus the measured fluorescence is given by:

$$F = c_A F_A + c_{AT} F_{AT} + F_{Background}$$

Where $F_{background}$ is the background fluorescence of the setup. The background fluorescence can be subtracted, but is typically small compared with the fluorescence of the molecules and will be neglected in the following: $F = c_A F_A + c_{AT} F_{AT}$. When the IR-laser is switched on, the temperature in the solution increases due to the absorption of the laser radiation by the water molecules. The change of fluorescence induced by the change in temperature can be written as total derivative:

$$\frac{\partial F}{\partial T} = F_A \frac{\partial c_A}{\partial T} + c_A \frac{\partial F_A}{\partial T} + F_{AT} \frac{\partial c_{AT}}{\partial T} + c_{AT} \frac{\partial F_{AT}}{\partial T}$$

The concentration change is due to thermophoresis with $\frac{\partial c}{\partial T} = -S_T c$ where the Soret-coefficient describes the percentage of the concentration drop per Kelvin. With S_T^A the Soret-coefficient of A and S_T^{AT} the Soret-coefficient of the complex AT we obtain:

$$\frac{\partial F}{\partial T} = c_A \left(\frac{\partial F_A}{\partial T} - F_A S_T^A\right) + c_{AT} \left(\frac{\partial F_{AT}}{\partial T} - F_{AT} S_T^{AT}\right)$$

A fluorescence signal can be normalized to its cold state before the laser is switched on: $F_{norm} = F_{hot} / F_{cold}$ where F_{cold} is the fluorescence before the heating IR-laser is switched on and F_{hot} is the changed fluorescence measured after the heating IR-laser is switched on. Since the changer fluorescence can be written as $F_{hot} = F_{cold} + \frac{\partial F}{\partial T} \Delta T$ we can denote the normalized fluorescence F_{norm} by:

$$F_{norm} = 1 + \frac{1}{F_{cold}} \frac{\partial F}{\partial T} \Delta T$$

Now we use $c_A + c_{AT} = c_A^0$ where c_A^0 is the total concentration of aptamer which were put into the solution. Thus the the Fraction of Bound aptamer x can be written as: $x := \frac{c_{AT}}{c_A + c_{AT}}$ and thus $\frac{c_A}{c_A + c_{AT}} = 1 - x$.

Dividing the denominator and the enumerator of F_{norm} by c_A+c_{AT} we get:

$$F_{norm}(x)=1+\frac{(1-x)(\frac{\partial F_A}{\partial T}-F_A S_T^A)+x(\frac{\partial F_{AT}}{\partial T}-F_{AT}S_T^{AT})}{F_A+x(F_{AT}-F_A)}\Delta T$$

Dividing the denominator and the enumerator of F_{norm} by F_A and using $y:=\frac{F_{AT}}{F_A}$ we get:

$$F_{norm}(x)=1+\frac{(1-x)(\frac{1}{F_A}\frac{\partial F_A}{\partial T}-S_T^A)+x\,y(\frac{1}{F_{AT}}\frac{\partial F_{AT}}{\partial T}-S_T^{AT})}{1+x(y-1)}\Delta T$$

The correction factor y allows to calculate the fraction of bound molecules from the measurement in the general case where the fluorescence F_A of the aptamer A alone is not equal to the fluorescence F_{AT} of the formed complex AT. During the titration experiments F_A is determined at the beginning where $c_{AT}=0, x=0$. And F_{AT} is determined at high target concentrations $c_T \gg c_A$ where all aptamers are bound to their targets $x=1$. In the most experiments the fluorescence F_A of the aptamer is equal to that of the aptamer-target complex F_{AT} : $F_A=F_{AT}$ and thus: $y=1$. For this case of $F_A=F_{AT}\rightarrow y=1$ the normalized fluorescence F_{norm} simplifies to:

$$F_{norm}(x)=1+((1-x)(\frac{1}{F_A}\frac{\partial F_A}{\partial T}-S_T^A)+x(\frac{1}{F_{AT}}\frac{\partial F_{AT}}{\partial T}-S_T^{AT}))\Delta T$$

Defining $F_{norm}(x=0):=F_{norm}(A)$, the normalized fluorescence of the aptamer alone, and $F_{norm}(x=1):=F_{norm}(AT)$, the normalized fluorescence in the case where all aptamers are bound to their targets, the normalized fluorescence $F_{norm}(x)$ can be denoted as:

$$F_{norm}(x)=((1-x)F_{norm}(A)+x\,F_{norm}(AT))\Delta T$$

Thus the fraction of bound molecules x can directly be calculated from the measured F_{norm} :

$$x=\frac{F_{norm}(x)-F_{norm}(A)}{F_{norm}(AT)-F_{norm}(A)}$$

Calculation of the dissociation constant K_d

The dissociation constant K_d quantifies the equilibrium of the reaction of the aptamer A with its target T to form the complex AT: $A+T\Leftrightarrow AT$ is defined by the law of mass action as:

$$K_d=\frac{c_A c_T}{c_{AT}}$$

where all concentrations are „free“ concentrations. During the titration experiments the added concentration c_A^0 of aptamer A is kept constant and the concentration c_T^0 of added target T is increased. These concentrations are known and can be used to calculated the dissociation constant.

The free concentration c_A of the aptamer is the concentration c_A^0 of aptamer minus the concentration c_{AT} of formed complex AT: $c_A=c_A^0-c_{AT}$. The same holds for the target T: $c_T=c_T^0-c_{AT}$. Thus the K_d is:

$$K_d = \frac{(c_A^0 - c_{AT})(c_T^0 - c_{AT})}{c_{AT}}$$

By solving this quadratic equation for the fraction of bound aptamers $x = c_{AT}/c_A^0$, the titration series can be fitted with the following equation to determine K_d:

$$x = \frac{1}{2c_A^0}(c_A^0 + c_T^0 + K_d - \sqrt{(c_A^0 + c_T^0 + K_d)^2 - 4c_A^0 c_T^0})$$

In the cases where the binding curve could not be fitted with this formula the Hill-equation was used:

$$x = \frac{1}{1 + (EC_{50}/c_T^0)^n}$$

where n is the hill-constant describing the cooperativity of the binding and EC_{50} is the concentration at which half of the aptamers are bound to their respective targets.

ATP-titration: pH-check

A solution of ATP is mildly acidic with a pH of approximately 3.5 (product information sheet for ATP, Sigma Aldrich, product #7699). To ensure that the binding curves are not influenced by a pH-change induced by the titration of ATP-solution, we measured the pH of the buffers with the pH-sensitive dye BCECF ([2',7'-bis-(2-carboxyethyl)-5-(and-6)-carboxyfluorescein])[2]. The fluorescence of BCECF decreases as the pH decreases. So we normalized the fluorescence to the fluorescence value measured in the buffer without ATP.

Additionally we measured the thermophoretic depletion of the ssDNA and the binucleotide mutant at all ATP concentrations. Above 1000µM ATP-concentration, we find a change in the fluorescence of BCECF. Therefore we assume that the pH of the buffer changes. However, since the normalized fluorescence $F_{norm} = F_{hot}/F_{cold}$ of the control ssDNA and the binucleotide mutant did not change even at high ATP concentrations, we assume that a moderate shift in pH does not affect the thermophoresis assay. This would be expected since the ssDNA does not change its charge in this pH regime. Notably, the shift in the pH takes place at an ATP-concentration of 1000µM at which the binding of ATP to the aptamer is already saturated in selection buffer.

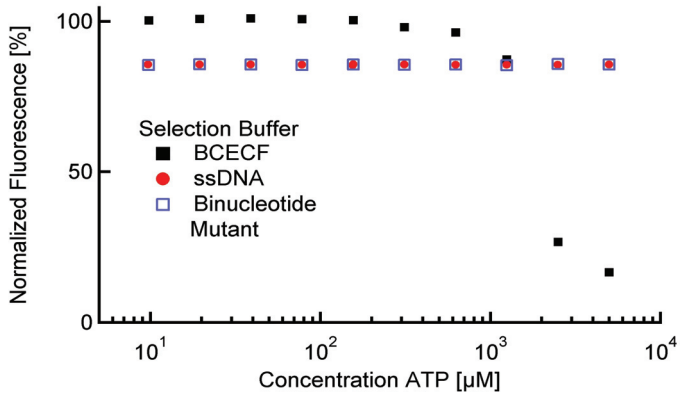

Figure 2. *Normalized fluorescence of BCECF and control oligonucleotides labelled with Cy5. The selection buffer of the ATP-aptamer is stable up to 1000µM ATP. Wheras the BCECF fluorescence reports a change in pH down to mildly acidic values, the normalized fluorescence reporting*

thermophoretic depletion $F_{norm} = F_{hot} / F_{cold}$ *of the oligonucleotides is still constant.*

Temperature dependence of aptamer-fluorescence

To be sure to separate effects of temperature dependent fluorescence and the Soret coefficient, we measured the temperature dependence of the fluorescence of the ATP-aptamer and the thrombin-aptamer in their respective selection buffers in a thermally controlled fluorometer (Fluoromax. 3; Horiba Jobin Yvon GmbH). The fluorescence has a temperature dependence. But this dependence did not change significantly due to target binding. The temperature increase in the experiments was $\Delta T = 8\text{K}$ and the experiments were conducted at 20°C.

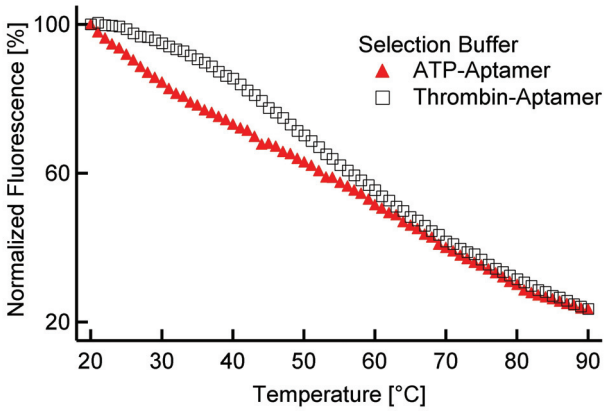

Figure 2. *Temperature dependence of the fluorescence of the ATP-aptamer and the thrombin-aptamer measured in the respective selection buffer. The fluorescence was normalized to the fluorescence value at the temperature 20°C.*

Literature

[1] J. H. Zhang, T.D.Y. Chung, K.R. Oldenburg, *J. Biomol. Screen*. **1999**, 4,67-73.
[2] N. Boens, W. Qin, N. Basaric, A. Orte, E. M. Talavera, J. M. Alvarez-Pez, *J. Phys. Chem. A* **2006**, 110, 9334-9343.

Accessing the Hydration-Shell: Immobilization-Free Binding Assays in Temperature Gradients

Christoph J. Wienken[*], Philipp Baaske[,§], Ulrich Rothbauer[#], Dieter Braun[*] and Stefan Duhr[*,§]*

[*]*Department of Physics and Center for NanoScience (CeNS) Ludwig-Maximilians University Munich, Germany*
[§]*NanoTemper Technologies GmbH, Amalienstr. 54, 80799 Munich, Germany*
[#]*Biocenter at the Department of Biology II, Ludwig Maximilians University Munich, Germany*

Corresponding author:Stefan.Duhr@physik.uni-muenchen.de

In this article, we are introducing an immobilization-free, low volume method to analyze the interactions of biomolecules. The method uses microscale thermophoresis, the directed motion of molecules in local temperature gradients and allows to access important molecular information such as protein-protein or protein small molecule affinity and DNA sequence. In comparison to other techniques, the method is not only sensitive to changes in mass, size or charge of a molecule, but also measures changes of the hydration-shell. Thus, even the binding of small molecules to proteins is readily detectable. The presented experiments highlight the simplicity and broad scope of the method by demonstrating high-resolution measurements of DNA length, sequence specific detection of DNA molecules and accurate quantification of binding affinities of interacting molecules. Microscale thermophoresis has the potential to become a standard technique for antibody based interaction assays, PCR product analysis and assays probing the binding of low molecular weight compounds.

Keywords: Soret Effect, Interaction, Protein, DNA, Hydration Shell, Small Molecule

Methods to detect biomolecules or their interactions are of great importance in cell biology, molecular biology and the development of pharmaceuticals. Today, a variety of in-vitro approaches exist for the analysis of biomolecular interactions, ranging from long established gel-based assays (Electrophoretic-Mobility-Shift-Assay, EMSA) to state-of-the-art surface sensors such as Surface Plasmon Resonance (SPR) or Quartz Crystal Microbalance (QCM) and single molecule techniques like Fluorescence Correlation Spectroscopy (FCS). In general, these techniques rely on changes in mass, size or charge of the molecules of interest. Thus, even using these modern techniques the analysis of low molecular weight compounds interacting with proteins remains challenging. Moreover, these methods analyze molecules far-off their native conditions, as for example using surface-coupled analytes or probing the binding in a gel matrix. Thus, the results may not reflect the native properties of the investigated molecules.
In the field of DNA analytics, Real-time PCR (Polymerase Chain Reaction) is an important and well-established technique, which uses careful designed and empirically validated DNA probes, that typically carry multiple fluorescent dyes. Microscale thermophoresis provides the means for

quantification and specific detection of DNA sequences with simple and less expensive probe molecules.

In this work, we will show that microscale thermophoresis is a versatile tool to analyze protein and DNA molecules providing detailed information about a variety of molecular properties.

Similar to charged molecules in electrical fields, temperature gradients also induce a directed motion of molecules. The effect is known as thermophoresis, thermodiffusion or Soret effect. In liquids it was first observed by Carl Ludwig in 1855, who measured a change in concentration of salt ions caused by inhomogeneous temperatures[1]. To shed light on the theoretical basis of thermophoresis, further experiments were performed, mostly using inorganic molecules or polymers blends[2,3]. Braun and Libchaber[4] as well as Piazza[5], were the first to measure the thermophoresis of biomolecules. Today, the importance of the molecules' charge and nonionic contributions from molecular surface properties or the hydration shell for the thermophoretic effect are widely accepted[6,7,8,9,10].

In this work, we introduce microscale thermophoresis, an all-optical, immobilization-free and low volume method to characterize biomolecules and their interaction in a simple Mix-and-Read fashion. We are demonstrating the feasibility of the method by measuring the length of short DNA molecules with high resolution and detecting DNA-DNA hybridization. Moreover, we measure the dissociation constant of a protein-protein interaction and the affinity of a low molecular weight inhibitor to a cyclic AMP dependent kinase (PKA) in a complex biological background.

Results

Experimental approach

When an aqueous solution is heated locally, molecules start moving along the temperature gradient. This thermophoretical molecule flow is opposed by ordinary mass diffusion (Figure 1a). In steady state, both effects are balanced resulting in a stationary spatial concentration distribution[11, 12]:

$$c/c_0 = \exp[-S_T*(T-T_0)] \qquad (1)$$

where the concentration solely depends on the Soret coefficient S_T of the molecule and the temperature rise $\Delta T=T-T_0$ at the respective position. We established an all-optical approach for both, creation of temperature gradients on the micrometer scale and the detection of the spatial concentration distribution of the molecules. An infrared laser (IR-laser) heats the solution locally (typically by 2-8°C) and fluorescence microscopy is used to measure the changes in concentration of the molecules.

The IR-laser couples into the path of fluorescent light with an infrared dichroic mirror (Figure 1b) and is focused through the same objective. This allows the observation of thermophoresis in

various microfluidic sample compartments. High reproducibility and low sample consumption is achieved using 100 µm glass capillaries with a total volume of about 500 nl.
The IR-laser is focused into the sample and spatial temperature distributions are created with a half width of 20-50 µm. Due to the length scale in the micrometer range, steady state molecule distribution is obtained within seconds, enabling a fast biomolecule analysis. Typically, we visualize the spatial concentration distribution by a fluorescent dye covalently attached to molecules or by intrinsic fluorescence of molecules (e.g. Green Fluorescent Protein, GFP). For a binding analysis, only one binding partner has to be labeled with a single fluorescent tag at an arbitrary position. The read-out signal used throughout this work is the concentration change induced by the local increase in temperature.

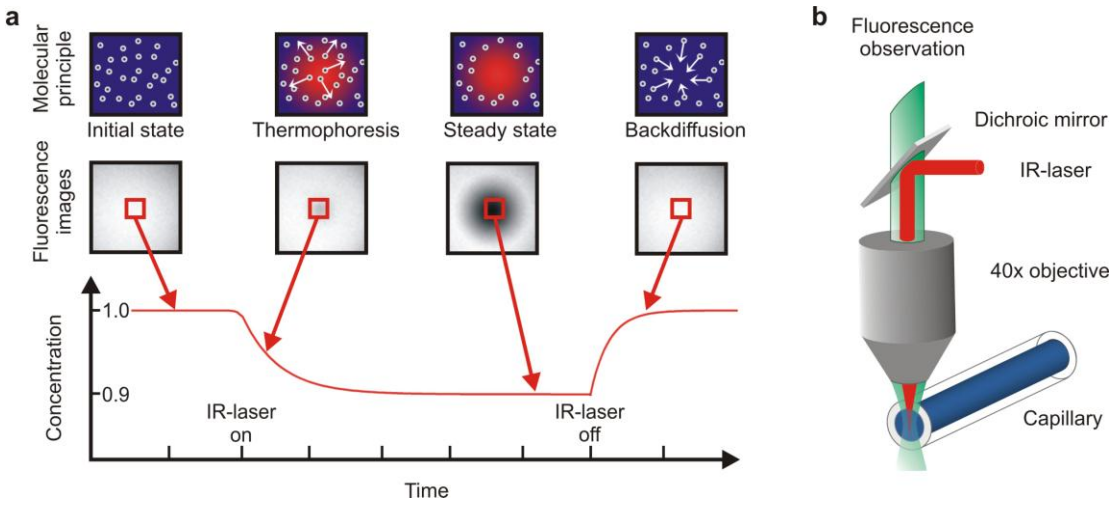

Figure 1. Microscale thermophoresis. (a) Fluorescently labeled molecules or particles are initially distributed evenly and diffuse freely in solution. By switching on the heating with a focused IR-Laser, the molecules experience the thermophoretic force in the temperature gradient and typically move out of the heated spot. In the steady state, this molecule flow is counterbalanced by ordinary mass diffusion. After turning off the laser, the particles diffuse back towards a homogeneous distribution. (b) An epi-fluorescence microscope is used with an additional dichroic mirror inserted into the path of fluorescence light. With this mirror, the heating IR-Laser couples into the path of fluorescence light and is focused with the same objective used for fluorescence detection. This allows observation of thermophoresis in various microfluidic settings.

For an analysis of the molecular properties and binding events, the change in concentration between the initial state and the steady state is measured (Figure 1a). Thus, only two images are required: one image of the initial state before laser heating, showing a homogenous distribution of molecules and a second image of the steady state with an inhomogeneous distribution. This second image is typically recorded within a few seconds after starting the IR-laser irradiation.
Switching off the IR-laser leads to reestablishment of the initial homogeneous concentration profile by diffusion. This provides information about the diffusion coefficient of the particles[13].

However, this is an optional information. The concentration change contains all necessary information about the molecular properties.

Nucleic Acid Length Measurement

We start to demonstrate the capability of the method by measuring the length of DNA oligonucleotides, as they are used as primers in PCR. With our technique, the determination of the oligo length with an accuracy of a single base should be possible within seconds. We conducted experiments for single stranded DNA (ssDNA) with a length from 2 to 50 nucleotides (nts). The infrared laser heats the sample locally with a maximum temperature increase of 8°C. The kinetics of the molecule depletion within the center of the heat spot are shown in Figure 2a. After a few seconds of IR-laser heating, the oligonucleotides became distinguishable. The respective change in concentration is shown in Figure 2b. The fitted calibration curve allows to deduce the length of an unknown oligonucleotide from the measured change in concentration. The length of a 22-mer test oligo with $\Delta c/c=0.2709\pm0.002$ is determined from the fitted curve to 22.0±0.8 bases. This shows that thermophoresis provides a length resolution on the single base level for short single stranded DNA. A single base pair resolution for double stranded DNA molecules up to 100 bp can be expected, since they show a stronger thermophoresis[6].

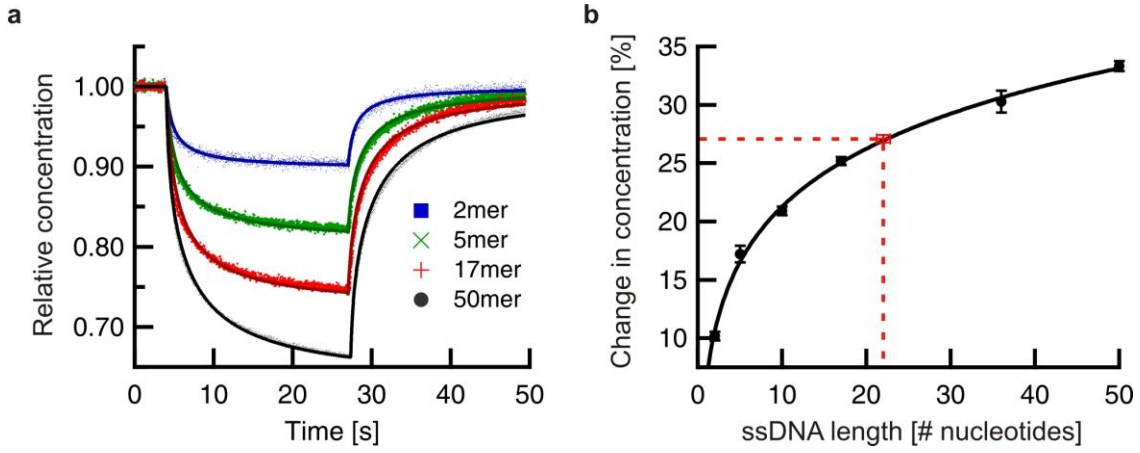

Figure 2. DNA length analysis. (a) Short single stranded DNA oligonucleotides show thermophoretic depletion. Its strength is dependent on the length of the molecules. After a few seconds of laser heating the DNA strands can be distinguished easily. The kinetics of depletion and backdiffusion can be described theoretically and is shown as solid line. (b) The corresponding steady state concentration change of ssDNA follows a power law that makes thermophoresis feasible for a precise discrimination between short DNA molecules of different length. The length of a 22-mer is determined by thermophoresis to 22.0±0.8 bases.

Nucleic Acid Hybridization

For applications in diagnostics and basic research, it is crucial to detect genetic variations like Single Nucleotide Polymorphisms (SNPs). The nucleotide composition of a DNA molecule is typically identified by sequencing, melting curve analysis or allele-specific PCR reactions[14,15,16,17]. The pronounced length dependence of DNA thermophoresis implies that thermophoresis can also discriminate between single and double stranded DNA. This allows the specific detection of a DNA sequence by probe annealing without tedious preparation procedures or special PCR-Primer design and validation.

To test this, we measured the hybridization of a fluorescently labeled 22mer ssDNA to an unlabeled complementary ssDNA molecule of the same length. The experiments were performed at a hybridization temperature of 48°C (sample temperature), a typical temperature used in DNA microarray experiments to resolve SNPs[18]. We measured the average molecule depletion of samples containing a constant concentration of the fluorescently labeled probe molecules (200 nM) at a varying amount of the unlabeled complementary target strand (0 nM to 800 nM). Without target molecule, the concentration change corresponds to that of free diffusible probe molecule. The strength of the thermophoretic depletion increases from 13% to 22% as the concentration of unlabeled target molecule approaches the probe's concentration. When all the probe molecules were hybridized to the target strand, no further increase of the signal was observed. In Figure 3a, we show the concentration decrease normalized to the saturation value obtained for a fully hybridized probe. In contrast, DNA with a single nucleotide mismatch (GC pair to CC) shows a distinctly decreased binding affinity (Figure 3a) as observed by the altered slope of the titration curve. These experimental results were fitted for their dissociation constant K_D, which is related to the ΔG of the DNA hybridization. The fitted values for the perfect match (ΔG = -11.4±0.3 kcal/mol) and for the mismatch (ΔG = -9.1±0.2 kcal/mol) are in good agreement with the theoretical predicted values of ΔG = -12.9 kcal/mol for the match and ΔG = -8.4 kcal/mol for the mismatch[19]. Thus, under stringent hybridization conditions, a single nucleotide polymorphism is readily detected by thermophoresis.

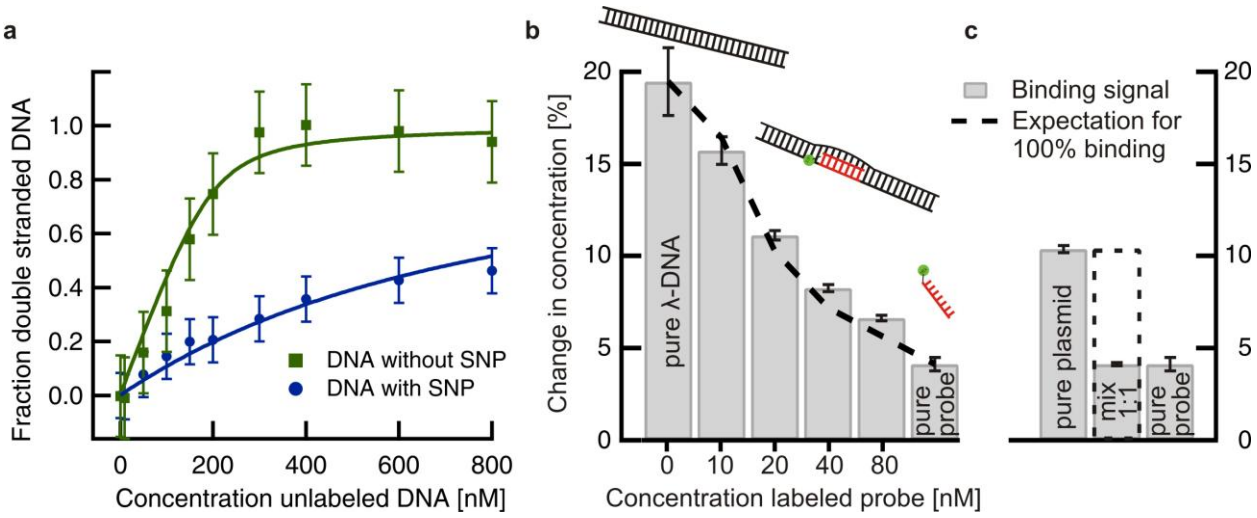

Figure 3. DNA hybridization. (a) The hybridization of a labeled single stranded DNA (22 bases) with its complementary strand is shown. A single nucleotide polymorphism can be easily distinguished from a perfect match. The fitting of the datasets result in a ΔG = -11.4 kcal/mol for the perfect match and ΔG = -9.1 kcal/mol for the single nucleotide polymorphism which is in good agreement with theoretical values. (b) Thermophoresis can detect DNA sequences in large genomes. When a single stranded probe hybridizes to a DNA strand containing its complementary sequence, the probe shows an increased signal, as it adapts the thermophoretical properties of its target strand. (c) The negative control with a DNA molecule not containing the complementary primer sequence proves the sequence specificity. If the primer cannot hybridize to the target, no change in the signal is measurable.

However, products of a PCR reaction are double stranded and therefore a competition between the labeled probe DNA and the strand complementary to the target has to be expected. To test if we can measure the binding of a ssDNA probe to a DNA sequence under these conditions, we performed an experiment similar to the procedure described before: A fluorescently labeled ssDNA probe with a length of 24 bases was used to detect 7.5 nM of the 50,000 base pair long bacteriophage Lambda DNA ("target") in 500 nl of sample (3.75 femtomol). The sequence-matching lambda-probe is provided in a varying molar excess (1.2x to 10x) as compared to the lambda DNA (Figure 3b). When the probe binds to the lambda DNA, the measured thermophoretic properties change as they are now dominated by the properties of the lambda-DNA molecule. A 1.2x excess of the probe leads to a signal comparable to pure lambda-DNA (measured in an independent experiment using an intercalating dye).

With increasing excess of primer DNA, the observed signal decreases and approaches the signal of the unbound probe molecule since an decreasing fraction of labeled primer can hybridize to a lambda DNA strand and dominates the thermophoretic signal. For high excess, the signal of the pure unbound probe is reached. The experimental results at various probe concentrations are in good agreement with the theoretical expectations (Figure 3b, dotted line) for the binding signals, when we assume that all lambda-DNA molecules are bound to a probe.

Control experiments are shown in Figure 3c, where a Plasmid DNA without complementary sequence was mixed with the probe DNA. Thermophoretic depletion shows no binding of the probe molecule to the target: the probe-Plasmid mixture reproduces the value for pure probe. In summary, microscale thermophoresis can be applied to the specific detection of a DNA sequence in solution. Titrating the probe molecule allows to access the target concentration. Furthermore, the technique tolerates a substantial amount of unhybridized probe molecules, allowing analytical assays without any washing procedures. In addition to the detection of single nucleotide polymorphisms, we expect that the method is suited to detect larger genomic deletions.

Protein binding to 5'-biotinylated-DNA

As shown in the first experiments microscale thermophoresis is sensitive to small changes in the molecular properties of biomolecules. Thus, it should be possible to detect the binding of low molecular weight molecules to a protein of significantly higher molecular weight. Upon binding, the mass or size of the labeled target will show only a minimal change.

As a test for the capability of thermophoresis to detect the binding of such molecules, we choose the binding of small ssDNA molecules to streptavidin. Streptavdin is a tetrameric protein (MW = 53 kDa)[20] with four highly affine binding sites for Biotin. To these binding sites, small ssDNA molecules were bound via a biotin tag at their 5'-end. We probed the binding using ssDNA with a length of 10, 40 and 80 nucleotides with molecular weight MW = 3.3 kDa, 13.2 kDa and 26.4 kDa, respectively. The experiment also allowed to discriminate the binding of multiple ligands.

When a biotinylated ssDNA strand binds to the streptavidin molecule, the change in the thermophoretic properties lead to enhanced depletion. Titrating unlabeled ssDNA to the fluorescently labeled streptavidin molecules leads to saturation as soon as all binding sites are occupied (Figure 4a). Upon addition of ssDNA, thermophoretic depletion increases up to an molar excess of 3.2 between streptavidin and biotinylated ssDNA. Due to the high affinity of the streptavidin-biotin system, this saturation value reflects an average of 3.2 active binding sites per molecule. This reduced number of active binding sites can be due to a reduced accessibility of the last binding site, or loss of activity of protein preparation[21]. As expected, the amplitude of the thermophoretic concentration change increases with the length of the DNA (Figure 4b), in agreement with the length dependent DNA thermophoresis shown in Figure 2.

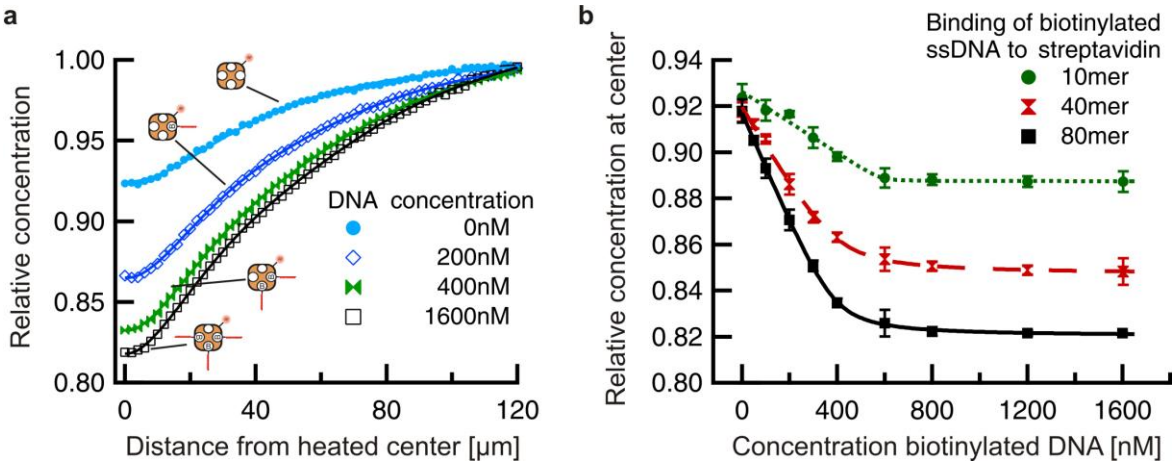

Figure 4. Streptavidin binding to 5'-biotinylated-DNA. The figure shows the binding of biotinylated DNA to tetrameric streptavidin molecules. (a) The spatial concentration profile around the heated spot is plotted for different concentrations of biotinylated ssDNA added to 200 nM of streptavidin. (b) Binding of biotinylated DNA of various lengths (10, 40, 80 bases). The relative concentration in the center of the heated spot is plotted versus the ssDNA concentration. The change in the relative concentration saturates at a concentration of 631nM, which is at a molar excess of approximately 3.2. The thermophoretic amplitude increases with the length of the bound DNA molecule, as expected (see Figure 2).

Interestingly, the binding of a single molecule of only 3kDa in molecular weight still leads to a significant change in the thermophoretic signal. This is consistent with previous findings[6] that not only changes in the size or mass of a molecule are relevant for thermophoresis, but also the solvation energy and surface properties. This sensitivity on surface properties allows an analysis of interactions, which are difficult to address with other techniques: For example, Fluorescence Correlation Spectroscopy (FCS) needs a significant change in the diffusion constant to discriminate differing species of molecules[22] and surface-based methods rely on a measureable change in the molecular weight to provide reliable data[23]. Microscale thermophoresis shows a high sensitivity to probe the surface of molecules and is able to analyze binding events, which only show very small changes in the molecule's size upon binding in bulk solution. In the following, we show that microscale thermophoresis can be used as a screening tool for low molecular weight binders to kinases and other pharmaceutical relevant proteins.

Antibody-Antigen and Kinase Small Molecule Interaction

The specific interactions between proteins play a fundamental role in cellular functions and are also important for biotechnological applications and antibody based assays. Today, most antibody affinities are determined by surface based methods such as Surface Plasmon Resonance[24] or Quartz Crystal Microbalances[25]. Both techniques require the immobilization of either the antigen or the antibody to a solid surface, potentially raising several issues on steric hindrance a molecule activity[26].

With its sensitivity to small molecular changes, thermophoresis allows for binding studies on protein-protein interactions directly in solution. To show the potential of thermophoresis for protein analytics, we determined the affinity of an antibody for its antigen. Therefore, we analyzed a recently described interaction between the green fluorescent protein (GFP) and a small antibody fragment, the GFP-binding protein (GBP), derived from a single domain antibody of a Lama Alpaca. It was previously shown that GBP efficiently binds its antigen (GFP) in living cells as well as in biochemical assays such as immune-precipitation[27]. GFP as an antigen is intrinsically fluorescent, so no fluorescent label is necessary.

We titrated GFP with varying amounts of GBP. For the experiment we increased the temperature locally by 2°C. A measurement was completed within 10 seconds and less than 500 nl of sample was consumed for each datapoint. We analyzed the thermophoretic depletion against the concentration of GBP and find a sharp increase followed by a saturation plateau for an excess of GBP. Figure 5a shows the change in concentration normalized to the difference between saturation value (i.e. >1 µM GBP) and unbound state (i.e. 0.1 nM). To determine the dissociation coefficient K_D the complex formation is related to the absolute antibody concentration in the sample. The dissociation coefficient is measured to $K_D = 5 \pm 4$ nM.

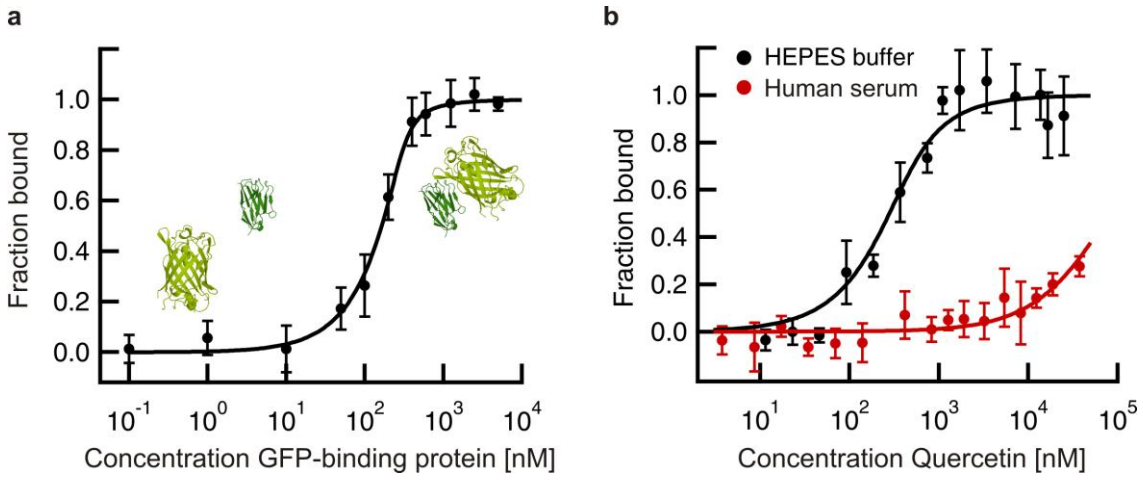

Figure 5. Antibody-Antigen and Kinase-small molecule binding. (a) A titration series with a GFP Binding Antibody (GBP) at constant GFP concentration is performed. The fraction of GFP molecules in a bound state with a GBP is calculated from the measured concentration change. The data are fitted by using equation (2), obtaining a dissociation coefficient of $K_D = 5 \pm 4$ nM. (b) The binding of Quercetin (338 Da) to the cyclic AMP dependent Kinase (PKA) was also measured with thermophoresis. The experiment was performed in buffer (KD = 130 +/- 35 nM) and 30% human serum (KD = 83 +/- 10 µM).

We directly compare the obtained K_D with affinity studies carried out on an Attana surface sensor instrument using QCM (see Supplementary material). For this experiment, GBP was immobilized on the QCM surface and the on- and off-rate of GFP were determined. A dissociation constant of 0.63 nM was observed.

Next, we wanted to investigate whether the binding of a low molecular weight inhibitor can be detected with similar sensitivity as the previously shown protein-protein interaction. For this we have chosen a cAMP dependent kinase (PKA, 38000 Da) as a target protein and analyzed the binding to the low molecular weight inhibitor Quercetin (338 Da). The kinase was fluorescently labeled and its concentration in the binding assay was kept constant. The inhibitor Quercetin was titrated up to 50 µM in a solution containing 50 mM HEPES (4-(2-hydroxyethyl)-1-piperazineethanesulfonic acid) buffer and 5% DMSO (Dimethyl Sulfoxid). The results shown in figure 5b are normalized to the difference between unbound state and the saturation level. The measurement shows that the affinity of Quercetin in HEPES buffer is 130 +/- 35 nM, which is in good agreement with described analyses in the literature, where an affinity of Quercetin to kinases in the nM to µM range is observed[28,28]. Since the binding of Quercetin does not lead to a pronounced change of the mass or size (i.e. diffusion coefficient) of the kinase, this experiment proves that microscale thermophoresis is especially suitable for the detection of small molecule binding. For an analysis with FCS, the change in mass ratio should be at least eight, preferably more than an order of magnitude, due to the approximate cube root dependence of the diffusion coefficient on molecular mass[29]. It is further possible to measure the Quercetin binding in complex biological liquids like blood serum. We performed the titration series in presence of 30% blood serum. The resulting apparent dissociation constant is determined to 83 +/- 10 µM. This reduced apparent affinity can be explained by a reduced active concentration (i.e. free concentration) of Quercetin due to binding to serum proteins.

Such an analysis of protein interactions in bulk solution, without any perturbing effects of a surface immobilization is expected to provide accurate binding data and has the potential to improve our understanding of protein function. In comparison, the analysis of low molecular weight binders has a high potential in pharmaceutical drug screening procedure since it is fast, robust and provides results of the efficacy in biological liquids.

Discussion

In this publication, a broad range of applications of microscale thermophoresis for protein and DNA analytics has been demonstrated. We showed its potential for the determination of the absolute length of short DNA, sequence detection by probe hybridization and the quantification of biomolecule affinities. The method allows the analysis of complex binding events with only a single fluorescence dye, while the exact position of the dye on the molecule is not important for the analysis and the label can be added to a position that does not interfere with the binding sites. In addition, the technique renders the immobilization to a surface unnecessary, which is

inevitable for SPR analysis. Thus, more reliable information about the binding behavior of biomolecules is obtained, as binding partners have unhindered access to their respective binding sites. The robust optics, simple sample preparation and low volume consumption of less than 500 nl make this method suitable for the routine analysis of biomolecules. In contrast to fluorescence correlation spectroscopy, another immobilization free method, thermophoresis is not reliant on significant changes in size or diffusion coefficient, but instead is sensitive to the molecule's surface and can detect the binding of low molecular weight binders with high sensitivity. Furthermore, microscale thermophoresis provides a high dynamic concentration and affinity range in which the method is successfully applied. Even a measurement in complex biological liquids like cell lysate, blood serum or plasma is possible.

Since an analysis takes typically less than 10 seconds, high-throughput applications are possible. Thus, further developments will comprise applications of microscale thermophoresis in the field of pharmaceutical drug screening.

In the future, we expect the method to find applications to measure enzyme and interaction kinetics, as the measurements are fast and thus can provide information about the current state of the binding process.

Methods

Fluorescence imaging and bleaching correction. The method is based on fluorescence microscopy. For imaging, we use a Zeiss Axiotech Vario microscope with a 40x Plan Fluar oil objective, with a numerical aperture (NA) of 1.3. The fluorescence is excited with Luxeon high power LEDs with cyan and red illumination, fluorescence filters were from AHF-Analysentechnik (Tübingen, Germany) for HEX (F36-542) and Alexa Fluor 647 (F36-523). Detection was provided with a 12-bit PCO sensicam qe camera.

Infrared laser heating. The temperature gradients used to induce a thermodiffusive motion were created by focusing infrared laser radiation (λ = 1480nm) into a chamber containing aqueous solution. Water strongly absorbs at this wavelength with an attenuation length of κ=320 μm. We used a fiber-coupled solid-state laser diode Furukawa FOL1405-RTV-317 yielding 320 mW maximum power. The IR-Laser beam couples into the path of light with a dichroic mirror (Edmund Optics, Barrington, USA) and is focused into the fluid with the microscope objective also used for fluorescence imaging. Typically, the temperature in the solution is raised by 2 – 8 K in the beam center with a $1/e^2$ diameter of 25 μm. All measurements were performed at room temperature of about 20°C.

Microfluidic chambers. For a most simple measurement approach, we used fused silica capillaries (Polymicro Technologies, Phoenix, USA) with an inner diameter of about 100 µm and an outer diameter of 370 µm. The well-defined thickness allows a good control and repeatability of the temperature. The volume enclosed in the capillary is about 500 nl.

Data analysis. The change in concentration was analyzed in a rectangle region around the center of heating with a diameter of about 25 µm. Hence, the measured concentration corresponds to an average concentration in the heated spot. To correct the fluorescence signal for the temperature dependency of the fluorescence emission, a separate fluorimeter experiment was used to obtain the behavior of the fluorescence dye at various temperature rises[31].

To provide a calibration curve for the length discrimination of DNA oligonucleotides, we fitted the data excluding the 22-mer to a power function $c/c_0 = A*n^P+C$ with number of nucleotides n, amplitude A=96.242±0.4, exponent P=0.067±0.002 and offset C=-90 (Figure 2b, solid line).

For binding studies, the relative change in concentration by thermophoresis is normalized to the saturation value where all molecules are in the bound state. The binding of ligands to a specific receptor is characterized by the equilibrium dissociation constant (K_D) and the total concentration of binding sites [B_0]. The determination of these two parameters can be achieved using saturation-binding curves obtained at equilibrium. [L_0] equals the amount of added ligand at each data point and [BL] the concentration of formed complexes between the binding sites [B] and the ligand [L]. The fitting function was derived from the law of mass action:

$$[BL] = 1/2*(([L_0]+[B_0]+K_D) - (([L_0]+[B_0]+K_D)^2-4*[L_0]*[B_0])^{1/2}) \qquad (2)$$

For an analysis of the binding behavior of DNA to streptavidin all binding sites where considered being of equal affinity. Hence, we can use the equation (2) as the parameter [B] used to calculate the dissociation constant is not the amount of binding molecules but the amount of actual binding sites. The changes in Gibbs free energy ΔG for the DNA hybridization were calculated from the definition of Gibbs free energy $\Delta G^0 = -RT(\ln K_{eq})$.

Nucleic acid characterization. The single stranded DNA molecules were purchased from biomers.net GmbH (Ulm, Germany). All were labeled at the 5' end with a HEX dye, a hexachloro derivative of carboxyfluorescein with a weight of about 744Da. The experiment was performed in 1 mM TRIS (Tris(hydroxymethyl)-aminomethan)-HCl buffer at a pH 7.8.

DNA hybridization. The signal of pure λ-DNA was measured by labeling the DNA with the intercalating fluorescent dye POPO-3 from Invitrogen (Carlsbad, California). The corresponding DNA-probe contains a HEX at its 5'-end. The measurements were done in 1x SSC (15mM Saline Sodium Citrate, 150 mM NaCl) buffer pH 7.8. The hybridization of probe DNA and lambda DNA was measured after an annealing procedure (94°C for 5 minutes followed by 72°C

for 5 minutes) and subsequent rapid cooling to 0°C on ice to minimize the displacement of hybridized primer with the original complementary strand.

Biotin mediated DNA binding to streptavidin. The streptavidin (S32357, Invitrogen, Carlsbad, USA) was labeled with an Alexa Fluor 647, a fluorescent dye with a molecular weight of 1300Da. The label-free, biotin-modified DNA oligos were bought from IBA BioTAGnology (Goettingen, Germany). The binding measurements were performed in 1x PBS (Phosphate buffered saline, 150 mM NaCl) at pH 7.8. Biotinylated DNA was titrated into a solution with 200 nM Streptavidin with up to 8-fold excess of the DNA molecules.

Protein-Protein interaction. Chromotek GmbH (Martinsried, Germany) provided the GFP and GBP (GFP Binding Protein). GFP is a 28 kDa protein with intrinsic fluorescence. The GBP is a small 13.7 kDa protein originally isolated from the lymphocytes of a Lama Alpaca (Lama Pacos) immunized with purified GFP[27]. The measurements were performed in PBS using 300 nM GFP and titrating 0.1 nM to 4 µM of GBP.

Protein-Small Molecule interaction

The Crelux GmbH (Martinsried, Germany) provided the Protein Kinase A and the Quercetin. The kinase was labeled with Alex Fluor 647 and used at a final concentration of 300 nM. The binding was measured in 50 mM HEPES pH 7.5 containing 5% DMSO. The Quercetin was titrated from 11.5 nM to 50 µM, close to the solubility limit of the substance. After mixing of the protein and Quercetin, the serum was added and incubated for 1h at room temperature.

Acknowledgements

The authors thank Moran Jerabek-Willemsen and Philipp Mertins for reading the manuscript and many thoughtful discussions. We gratefully acknowledge financial support from the Emmy-Noether Program of the Deutsche Forschungsgemeinschaft, of the LMU initiative Functional NanoSystems (FuNS), the Excellence Cluster NanoSystems Initiative Munich (NIM) and the NanoTemper Technologies GmbH. We also want to express our gratitude to the Center for Nanoscience (CeNS). We thank the Crelux GmbH (Martinsried, Germany) for providing the kinase and the small molecule Quercetin.

References

1. Ludwig, C. Diffusion zwischen ungleich erwärmten Orten gleich zusammengesetzter Lösungen. *Sitzungsber. Akad. Wiss. Wien: Math.-Naturwiss*. **20**, 539 (1856).
2. Rauch, J. and Köhler, W. Diffusion and thermal diffusion of semidilute to concentrated solutions of polystyrene in toluene in the vicinity of the glass transition. *Phys. Rev. Lett.* **88**, 185901 (2002).

3. Wiegand, S. and Köhler, W. *Thermal Nonequilibrium Phenomena in Fluid Mixtures* (Springer, Berlin, 2002).

4. Braun, D. and Libchaber, A. Trapping of DNA by thermophoretic depletion and convection. *Phys. Rev. Lett.* **89**, 188103 (2002).

5. Iacopini, S. and Piazza, R. Thermophoresis in protein solutions. *Europhys. Lett.* **63**, 247-253 (2003).

6. Duhr, S. and Braun, D. Why molecules move along a temperature gradient. *Proc. Natl. Acad. Sci. U.S.A.* **103**, 19678-19682 (2006).

7. Piazza, R. and Guarino, A. Soret effect in interacting micellar solutions. *Phys. Rev. Lett.* **88**, 208302 (2002).

8. Dhont, J.K.G., Wiegand, S., Duhr, S., Braun, D. Thermodiffusion of charged colloids: single-particle diffusion. *Langmuir* **23**,1674-1683 (2007).

9. Dhont, J.K.G. Thermodiffusion of interacting colloids. II. A microscopic approach. *J. Chem. Phys.* **120**, 1642-1653 (2004).

10. Weinert, F.M. and Braun, D. Observation of slip flow in thermophoresis. *Phys. Rev. Lett.* **101**, 168301 (2008).

11. Duhr, S. and Braun, D. Thermophoretic Depletion Follows Boltzmann Distribution. *Phys. Rev. Lett.* **96**, 168301 (2006).

12. de Groot, S. R. and Mazur, P. *Non-Equilibrium Thermodynamics* (North-Holland, Amsterdam, 1962).

13. Sperling, R. *et al.* Size Determination of (Bio)conjugated Water-Soluble Colloidal Nanoparticles: A Comparison of Different Techniques. *J. Phys. Chem. C*, **111**, 11552–11559 (2007).

14. Baaske, P., Duhr, S. and Braun, D. Melting curve analysis in a snapshot. *Appl. Phys. Lett.* **91**, 133901 (2007).

15. Sanger, F. and Coulson, A.R. A rapid method for determining sequences in DNA by primed synthesis with DNA polymerase. *J. Mol. Biol.* **94**, 441-446 (1975).

16. Marmur, J. and Doty, P. Determination of the base composition of deoxyribonucleic acid from its thermal denaturation temperature. *J. Mol. Biol.* **5**, 109-118 (1962).

17. Kaufmann, T. et al. Genetic basis of human complement C8 beta deficiency. *J. Immunol.* **150**, 4943-4947 (1993).

18. Naiser, T. et al. Position dependent mismatch discrimination on DNA microarrays – experiments and model. *BMC Bioinformatics* **9**, 509 (2008).

19. Markham, N.R. and Zuker, M. DINAMelt web server for nucleic acid melting prediction. *Nucleic Acids Res.* **33**, W577-W581 (2005).

20. Green, N.M. Avidin. *Adv. Protein Chem.* **29**, 85-133 (1975).

21. Sano, T. and Cantor, C.R. Expression of a cloned streptavidin gene in Escherichia coli. *Proc. Natl. Acad. Sci. USA* **87**, 142-146 (1990)

22. Chen, Y., Müller, J.D., Tetin, S.Y., Tyner, J.D. Gratton, E. Probing Ligand Protein Binding Equilibria with Fluorescence Fluctuation Spectroscopy. *Biophys. J.* **79**, 1074-1084 (2000).

23. Shankaran, D.R., Gobi, K. and Miura, N. Recent advancements in surface plasmon resonance immunosensors for detection of small molecules of biomedical, food and environmental interest. *Sensors and Actuators B: Chemical* **21**, 158-177 (2007).

24. Fägerstam, L.G. *et al.* Detection of antigen – antibody interactions by surface plasmon resonance. Application to Epitope Mapping. *J. Mol. Recognit.* **3**, 208-214 (1990).

25. King, W.H. Piezoelectric Sorption Detector. *Anal. Chem.* **36**, 1735-1739 (1964).

26. Bornhop D.J. *et al.* Free-Solution, Label-Free Molecular Interactions Studied by Back-Scattering Interferometry. Science 317, 1732-1736 (2007)

27. Rothbauer, U. et al. Targeting and tracing antigens in live cells with fluorescent nanobodies. *Nature Methods* **3**, 887-889 (2006).

28. Walker, E.H. et al. Structural Determinants of Phosphoinositide 3-Kinase Inhibition by Wortmannin, LY294002, Quercetin, Myricetin, and Staurosporine. *Molecular Cell* **6**, 909–919, (2000)

29. Hemmings, H.C. *Protein Kinase and Phosphatase Inhibitors, Applications in Neuroscience*, (Humana Press, New York, 1997)

30. Schwille P. and Haustein E. *Fluorescence Correlation Spectroscopy,* (Biophysics Textbook Online, Biophysical Society, Maryland, USA, 2004)

31. Duhr, S., Arduini, S. and Braun, D. Thermophoresis of DNA determined by microfluidic fluorescence. *Eur. Phys. J. E* **15**, 277-286 (2004).

32. Swillens, S. Interpretation of binding curves obtained with high receptor concentrations: practical aid for computer analysis. *Mol. Pharmacol.* **47**, 1197-1203 (1995).

33. Probst, B. and Hermkes, A. Quantitative characterization of hormone receptors by a nonlinear regression approach. J. Steroid Biochem. *Molec. Biol.* **39**, 299-302, (1991).

34. De Gans, B., Kita, R., Wiegand, S. and Luettmer-Strathmann, J. Unusual thermal diffusion in polymer solutions. *Phys. Rev. Lett.* **91**, 245501 (2003).

35. Giglio, M. and Vendramini, A. Soret-type motion of macromolecules in solution. *Phys. Rev. Lett.* **38**, 26-30 (1977).

Supplementary Material

Thermophoresis

As first observed by Carl Ludwig and later confirmed by Charles Soret, molecules respond to a temperature inhomogeneity by changing their concentration distribution. To do so, the molecules move along a temperature gradient with a velocity v according to $v = -D_T*gradT$, with temperature gradient gradT and a thermophoretic mobility, often termed thermodiffusion coefficient D_T. This thermophoretic mobility is an intrinsic property of the molecule, highly dependent on its size, charge and chemical surface composition. The dependence on size of rigid spheres and the length of flexible polymers has been systematically measured for polystyrene beads and double stranded DNA molecules longer than 50 base pairs (bp) [6]

When an aqueous solution of molecules is heated locally, molecules with a positive thermophoretic mobility D_T move from hot to cold or vice versa in case the thermophoretic mobility is negative [34,35]. In steady state, the mass flow induced by thermophoresis is balanced by ordinary diffusion with diffusion coefficient D. Thus, an extended Fick's law for diluted solutions describes the flow: $j = - D*gradc – D_T*c*gradT$. This leads to an expression for the steady state concentration distribution, which only depends on the temperature difference but is independent of the temperature gradient [11]:
$c/c_0 = \exp(-S_T*\Delta T)$ with Soret coefficient $S_T = D_T/D$. For simplicity, the results in this paper are discussed in terms of relative concentration change c/c0, not in terms of the Soret coefficient S_T.

Imaging and IR-Laser heating

The fluorescence is excited with Luxeon high power LEDs (cyan illumination: LXHL-LE5C, dominant wavelength: 505nm for the HEX dye and red illumination: LXHL-LD3C, dominant wavelength: 627nm for the Alexa Fluor 647 dye). The LED were built into a standard halogen lamp housing and driven at a current of 10-200mA by an ILX Lightwave LD-3565 constant current source, providing low illumination noise levels. Detection was provided with a 12-bit PCO sensicam qe camera with a pixel size of 8µm x 8µm, a maximum quantum efficiency of 65% and a typically applied 8x8 pixel binning. Exposure times times ranged between 100 ms and 500 ms.

The IR-Laser is mounted on an ILX Light-wave LDM-4984 laser base. Current and cooling are controlled by an ILX Lightwave LDC-3744B. The current is modulated by a computer-controlled analog output using a DAQPAD-6070E (National Instruments, USA) using LabView 8.2 (National Instruments, USA).

To determine the temperature distribution, we utilize the pH drift of 10mM TRIS buffer upon temperature increase. This pH shift is imaged with a pH-sensitive fluorescent probe, in our case

the fluorescent dye BCECF. The temperature dependence of the dye was calibrated in a temperature-controlled fluorometer (HORIBA Jobin Yvon GmbH, Unterhaching, Germany).

The measurement of relative concentration changes in microscale thermophoresis does not sensitively depend on the precise knowledge of the chamber thickness, but only on the knowledge of the temperature in the chamber. The temperature is checked before every set of measurements using fluorescent imaging of the temperature (see above). To obtain a nearly uniform temperature distribution in z-direction the infrared laser is only moderately focused by illuminating only a fraction of the objective's back aperture. As discussed before, a thin chamber height and a relatively small temperature rise also minimizes possible artifacts from optical trapping, thermal lensing and thermal convection [4,9]

Data analysis

For the analysis of saturation binding curves, standard fitting formulas require that the free ligand concentration does not significantly differ from the total added ligand concentration. To meet this constraint, the concentration of the fluorescent binding partner (i.e. the binding partner with constant concentration) must be rather low compared with the K_D value [32]. For the analysis of the binding behavior of high affinity binders, a fitting equation was derived to extend the standard K_D-Fit function [33]. The definition of the dissociation constant K_D is $K_D = [L]*[B]/[BL]$ where [B] is the concentration of free binding sites and [L] the concentration of free ligands at equilibrium. As the concentrations of [L] and [B] are not accessible in our experiments we substitute $[L] = [L_0] - [BL]$ and $[B] = [B_0] - [BL]$ with the total number of binding sites $[B_0]$ and the total amount of ligands $[L_0]$. This leads to a quadratic fitting function for [BL]:

$$[BL] = 1/2*(([L_0]+[B_0]+K_D) - (([L_0]+[B_0]+K_D)^2-4*[L_0]*[B_0])^{1/2}) \qquad (2)$$

The normalized measurement signal corresponds to the relative concentration of bound complexes $[BL]/[B_0]$, which can be easily fitted with the derived equation. The equation does not include unspecific binding which could be included using a linear unspecific binding proportional to the total amount of ligands available $[L_0]$.

DNA Length Measurement

The following oligos were used for the experiment: 2mer: 5'-HEX-TA, 5mer: 5'-HEX-TA GTT, 10mer: 5'-HEX- TA GTT CTA AT, 17mer: 5'-HEX-GTA GCG GCG CAT TAA GC, 22mer: 5'-HEX-AT TGA GAT ACA CAT TAG AAC TA, 35mer: 5'-HEX-CCT GGG GGA GTA TTG CGG AGG AAG GTT TTT TTT TT 50mer: 5'-HEX-AT AAT CTG TAG TAC TGC AGA AAA CTT GTG GGT TAC TGT TTA CTA TGG GGT.

DNA Hybridization

For the of the detection of single nucleotide polymorphisms a 22mer single stranded probe labeled with HEX at its 5'-end was bought from Metabion International AG (Martinsried, Germany). The corresponding complementary perfect match and mismatch DNA strands were purchased from Biomers.net GmbH (Ulm, Germany). For the hybridization experiments, 48502bp □-DNA was bought from Fermentas GmbH (St.Leon-Rot, Germany).
The probe sequence for the DNA hybridization experiments was 5'-HEX-AT TGA GAT ACA CAT TAG AAC TA-3'. The sequence for the perfect match target 5'-TAG TTC TAA TGT GTA TCT CAA T-3' and for the single mismatch target 5'-TAG TTC TAA TGT CTA TCT CAA T-3'. The probe for sequence detection in lambda DNA was sequence 5'-HEX-GAT GAG TTC GTG TCC GTA CAA CTG G-3' and was bought from Metabion International AG (Martinsried, Germany)

DNA-Protein Binding

For the binding of DNA molecules with various lengths, DNA was purchased by IBA BioTAGnology (Goettingen, Germany). The sequence was Bio-5'-GTC TGG C TTTT-3' for the 10mer, Bio-5'-TTTTTTTTTT CTG CAG GAA TTC GAT ATC AAG CTT ATC GAT-3' for the 40mer and Bio-5'-TTT TTG ACG TCC TTA AGC TAT GTT CGA ATA GCT ACT TTT TTT TTT CAT CGA TAA GCT TGA TAT CGA ATT CCT GCA GTT TTT -3' for the 80mer.

Protein-Protein binding

For reference affinity measurements purified GFP-binding protein (GFP-binder) was immobilized on an Attana Carboxyl Chip by amine-coupling according to manufacturer's instructions. Binding kinetic of GFP to the immobilized GFP-binder were performed on an Attana A 100 Quartz Crystal Microbalance (Attana AB, Sweden) by injection of 5 different concentrations of GFP (0,313 µg, 0,625 µg, 1,25 µg, 2,5 µg and 5 µg, two times replicates). The binding kinetics were evaluated with the ClampXP software (Attana AB, Sweden) which resulted in a Kon rate of 1,42 x 105[1/Ms] and a Koff rate of 9,00 x 10-5[1/Ms]. Taken together this measurement lead to a dissociation constant KD of 0,63 nM.

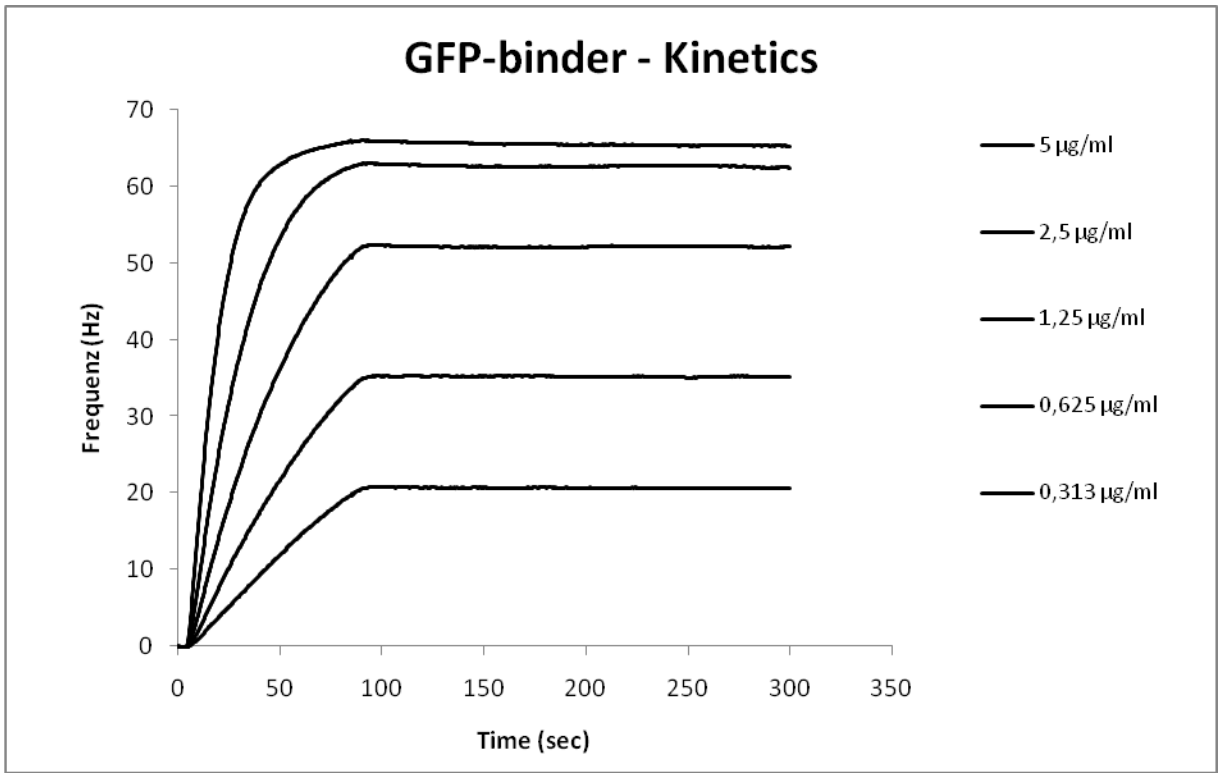

Supplementary Figure 1. Determination of the GFP binding affinity of the GFP-binder. GFP-Binder was immobilized on an Attana-Carboxyl Chip by amine-coupling. Binding kinetics were determined by injection of increasing concentrations of GFP (0,313 µg, 0,625 µg, 1,25 µg, 2,5 µg and 5 µg).

Kinase Quercetin binding

The PKA was fluorescently labeled with Alexa Fluor 647 and a stock solution with 600 nM in 50 mM HEPES buffer pH 7.5 was prepared. The Quercetin was obtained from Sigma Aldrich (No.: 32782) and dissolved to 1 mM in 100% DMSO. The stock solution was diluted to 100 µM using aq. dest and a dilution series with steps of two or three was prepared. 15 µl of the protein stock solution (100 mM HEPES pH 7.5) and 15 µl of the Quercetin solution were mixed, followed by addition of 15 µl of blood serum. Serum was obtained from the researchers. The sample was incubated for 1 hour at room temperature.

Was tRNA a dual-hairpin replicator? A scheme to exponentially replicate RNA by thermal cycling of metastable hairpins

Philipp Baaske and Dieter Braun
Systems Biophysics, Functional Nanosystems
Department of Physics, Center for NanoScience
Amalienstr. 54, 80799 München
Ludwig Maximilians University München, Germany

Abstract

Background Replication is fundamental to the origin of life and evolvability, however its implementation in an RNA world and the transition to an RNA-protein world is unclear. At the core of these processes is transfer RNA (tRNA). We try to address how translational tRNA evolved from a hairpin replication mechanism. Studies have suggested that the modern cloverleaf structure of tRNA has arisen through a combination of two single hairpins. RNA, more than DNA, has the tendency to form intramolecular hairpin structures. These metastable hairpins can store free energy for subsequent intermolecular hybridization reactions. As boundary conditions for the replication we consider reversible hybridization cycles triggered by microconvective temperature oscillation and the length selective accumulation of replication products by thermophoresis and convection.

Result We propose an exponential replication mechanism driven by a temperature oscillation and the hybridization of hairpins. Essentially we try to implement a protein-free ligation chain reaction (LCR) based solely on hybridization. An exponential replication mechanism is proposed which is driven by a temperature oscillation and the hybridization of hairpins. In a cross-catalytic chain reaction, initiated by a template, metastable RNA hairpins form multimers and replicate a succession of template sequences. Microscale thermal convection is a natural setting for the temperature oscillation and is found in the vicinity of submarine hydrothermal vents. The energy to drive the replication is kinetically trapped in metastable RNA hairpins and is released by the template catalyzed hybridization of hairpins towards more stable multimers. The temperature oscillation prevents product inhibition and allows an exponential replication. By combining two hairpins, a succession of templates is replicated. The addition of amino acids may further increase the stability of the replication products.

Conclusion The replicating double hairpins strongly resemble the cloverleaf structure of tRNA. The template binding is located at the modern codon region and the binding of amino acids helps stabilizing the elongated replication products. Thus the hairpin amplification scheme suggests that tRNA evolved from a primitive replication mechanism driven by thermal microconvection.

This article was reviewed by XX, YY and ZZ.

BACKGROUND

Arguably, one of the most mysterious molecules in biology and biochemistry is transfer RNA (tRNA). While it is located at the strongly conserved interface between DNA and proteins, the molecule's large structure appears unnecessarily inflated. As indicated by its function it must be an old molecular relict of ancient evolution [1,2]. And sequence analysis also indicates this as the family of tRNA sequences is widely conserved [3]. Why has a molecule with such a complicated structure and considerable redundant information evolved? Here we propose a replication scheme that uses hairpins, which strongly resemble tRNA. We argue that the section of the RNA world which led to the evolution of tRNA, might have been a highly robust yet simple RNA replication reaction.

What is the core process of replication? From an evolutionary context, replication merely amounts to the transfer of information. We would argue that a minimal transfer of information is the memorizing of the succession of two or more short sequences (Figure 1), i.e. the controlled ligation of two oligonucleotides depending on their sequence [4]. Such economy in replication is also found in biotechnology where the sequence detection of a Polymerase Chain Reaction (PCR) can also be implemented by the biologically simpler Ligation Chain Reaction (LCR). PCR and LCR are used to detect the existence of a specific sequence where the faithful replication of a base sequence is not required [5,6]. This aspect of amplification of information is also central to evolution where is all about detecting and amplifying suitable sequences which have survived selection. We argue here that the simplest transfer of information is physico-chemical by concatenating sequences together with hybridization (Figure 1) rather than by the chemical fixation of a template sequence base-by-base.

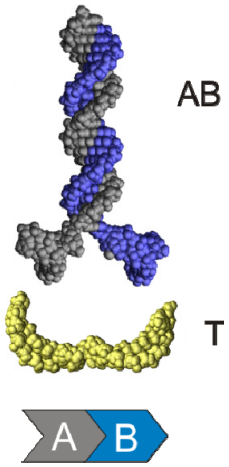

Figure 1 The template **T** contains the information "A before B". This information is also stored in the single stranded regions of the duplex **AB**. The complex AB forms from kinetically trapped hairpins.

Temperature oscillations are required for exponential replication and can be implemented by microscale thermal convection [7]. For example, they can be provided by the laminar microconvection in porous rock in the vicinity of hydrothermal vents where the synthesis of interesting molecules are likely [8-16]. The thermal cycling of molecules by convection periodically associates and dissociates nucleotides. For example, the template initiated Polymerase Chain Reaction can be driven by convection [17,18]. Interestingly, similar conditions allow for the strong accumulation of even single nucleotides with thermal convection and thermophoresis [19], thus providing a periodically changing environment for the emergence of information-carrying and knowledge-accumulation systems [20].

PRESENTATION OF THE HYPOTHESIS

Hairpin Structure

The hairpins **A**, **B**, **a** and **b** are composed of three segments: the toehold, stem and loop (Figure 2a). The stem is formed by two self complementary regions within the hairpin sequence. The hybridization energy of the loop is kinetically trapped [21] and can only be released after the stem is opened [22,23]. The two hairpins **A** and **B** are complementary to each other in the loop and stem segment. Upon activation of their stem, they hybridize to the duplex **AB** with a comparably large and stable base-paired sequence (Figure 2b). The spontaneous hybridization rate of **A** with **B** is very low as long as the stem is closed. So, in spite of the duplex **AB** being the thermodynamically favorable equilibrium conformation, no significant amount of duplex is accumulated over long times due to the kinetically trapped secondary structure.

The template **T** catalyzes the reaction between **A** and **B** (Figure 2c) by hybridizing to both of the toehold regions of the hairpins. As both are kept in proximity, the local concentration for hybridization is increased. This activation can increase the reaction rate of **A** with **B** by at least a factor of 1000 [24].

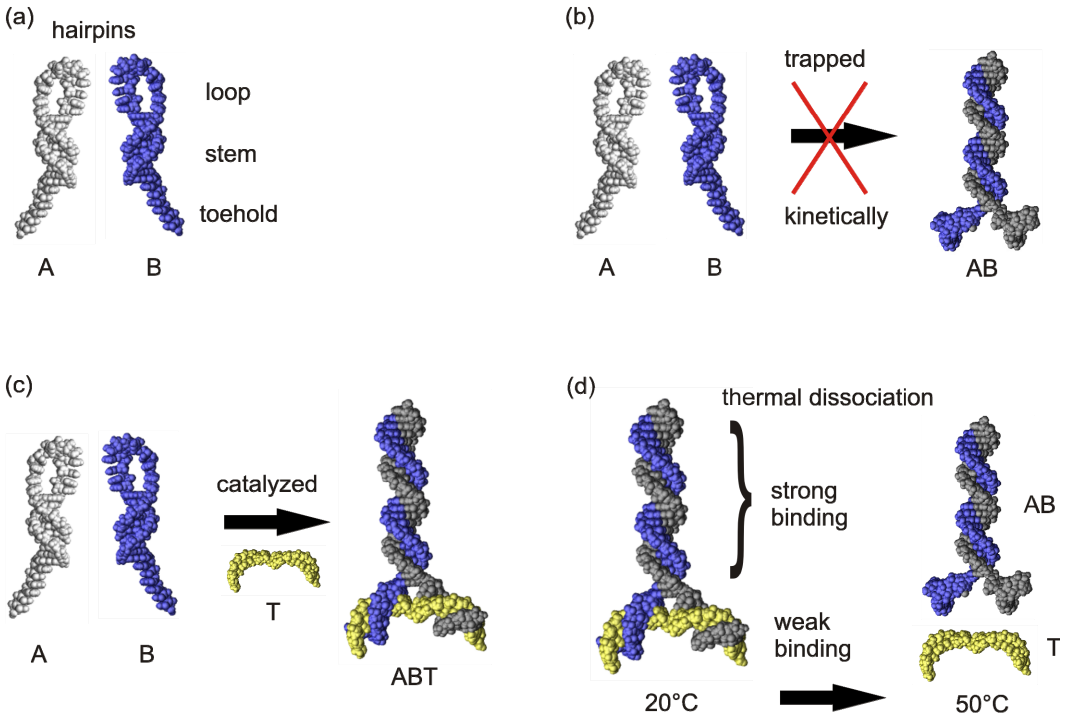

Figure 2 RNA hairpin structures. (a) RNA molecules often form a hairpin secondary structure. Generally, the hairpins consist of a loop, storing hybridization energy, a stem, kinetically trapping the stored energy and a toehold. (b) The binding of hairpin **A** with hairpin **B** is kinetically trapped since the loops can only fully hybridize if the stems are opened. (c) At 20°C the single stranded template-strand **T** hybridizes to the toehold region of the hairpins, opens the stems partially and catalyzes the formation of the triplex **ABT**. (d) In the triplex structure **ABT,** the hairpins show a strong binding domain and a weak binding domain. The triplex is stable at 20°C whereas at elevated temperatures the more stable duplex domain **AB** remains hybridized.

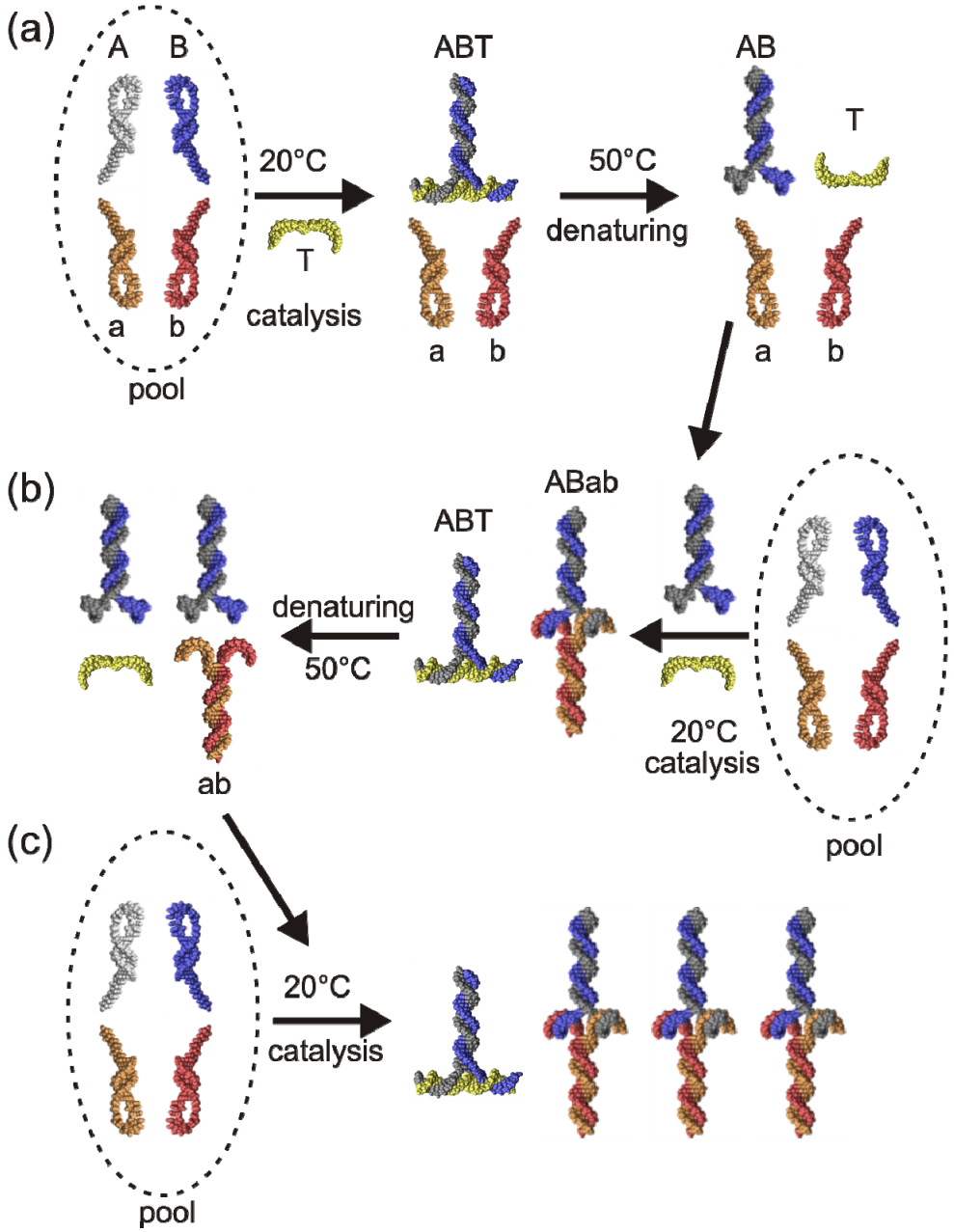

Figure 3. Exponential hairpin amplification by thermal cycling. (a) Starting point is a pool of highly concentrated hairpins **A**, **B**, **a**, **b**. The addition of the template **T** catalyses the formation of the Triplex **ABT** at 20°C. At 50°C the template strand **T** dissociates from **ABT** while the duplex **AB** is stable due to its long common sequence. (b) The duplex **AB** catalyzes the formation of the duplex **ab** into a quadruplex **ABab**. At 20°C the products **ABab** and **ABT** form. At 50°C the triplex and quadruplex dissociate into **AB**, **ab** and **T**. (c) Again at 20°C the duplexes **AB** and **ab** catalyze the reactions of **a** with **b** and **A** with **B**, respectively. The information of the template **T** is exponentially amplified into the quadruplex complexes by temperature cycling.

Replication Reaction

Before we extend the replication scheme to a succession of sequences, we will analyze the simplest case. We start with a pool of highly concentrated RNA sequences, **A**, **B**, **a** and **b.** The molecules form an intramolecular metastable hairpin conformation when they are cooled faster than the average time needed to bind to other molecules. The addition of a small amount of the template **T** to this pool of sequences initiates a cross-catalytic chain reaction

(Figure 3). At the first step of 20°C the template **T** catalyzes the hybridization reaction of hairpin **A** with hairpin **B**, forming the triplex **ABT**. In a short heating step to 50°C, this triplex dissociates into **T** and the stable duplex **AB** (Figure 3a).

In the next step at 20°C the hybridization reaction of the hairpins **a** and **b** is catalyzed by the duplex **AB** forming the quadruplex **ABab** (Figure 3b). At the same time, the free template **T** again catalyzes the reaction between the hairpins **A** and **B**, forming the triplex **ABT**. A short heating step to 50°C allows the quadruplex **ABab** and the triplex **ABT** to dissociate into the stable duplexes **AB**, **ab**, and the template **T** (Figure 3b). From this point on, the number of quadruplexes **ABab** doubles after each temperature cycle under ideal conditions (Figure 3c). The temperature cycling overcomes product inhibition, which is a problem in isothermal replication systems [4,25,26].

TESTING THE HYPOTHESIS

Requirements

The first requirement for a replicating system is that the template molecule **T**, and the products **AB** and **ab**, substantially accelerate the rate of the reaction between the hairpin substrates **A**, **B**, **a** and **b** [27,28]. This necessitates that the hairpins are kinetically trapped by the stem, forming an energy barrier before the hairpins can reach the duplex states, the spontaneous hybridization reaction to directly form **AB** and **ab** is slow. With the dangling ends of the catalyzing templates **T**, **AB**, or **ab** is the formation of the triplex **ABT** and quadruplex **ABab** structures quickened. Measurements for DNA show up an acceleration of at least 1000 [24,29].

The second requirement is the effective dissociation of the products and the template to allow exponential replication [30,31]. We implement this by the temperature cycling of thermal convection. For example, at 20°C the triplex **ABT** and quadruplex **ABab** structures are the most stable structures. However at enhanced temperatures such as 50°C the separated duplexes **AB** and **ab** are more stable than the quadruplex structure. The templates and products are released to again catalyze the reaction at cooler temperatures, allowing for an exponential replication.

However, the elevated temperatures reached during temperature cycling enhance the chances of false positive reactions so that quadruplexes might be formed independently of the catalyzing sequences of template **T** or, equally, the dangling ends of duplexes **AB** or **ab**. At low temperatures this is prevented by the high catalyzing efficiency. At the higher temperatures the rate of the template-independent reaction is enhanced. While this makes the replication less probable, one should keep in mind that the four hairpins **A**, **B**, **a**, **b** can have sequences stable enough to keep their secondary structure for temperatures well above 50°C [32,33]. Of course not all sequences will be suited to such reactions. But hairpin formation is very common for RNA sequences in comparison, for example, to DNA. The pool of molecules that show kinetically frustrated energy-entropy storage are expected to be appreciable even in random sequence pools.

Convection boundary conditions

A way to enhance replication is to consider a convection flow which produces asymmetric temperature spikes, thus making the reaction time t_{20} at low temperatures much longer than the reaction time t_{50} at high temperatures [18]. Comparable to a PCR reaction the dissociation step at elevated temperatures takes only seconds while the hybridization reactions require several minutes.

The starting condition for the replication, the hairpin conformation, is set through fast cooling of the RNA from temperatures where RNA is in the single stranded random coil

conformation [34,35]. Cooling rates on the 100 millisecond scale are readily achieved by thermal convection in a vertical pore (Figure 4). Significant to this model is that the same geometry strongly accumulates even small molecules such as single nucleotides [19,36]. The mechanism combines thermal convection with thermophoresis, the drift of molecules in a temperature gradient, and is solely driven by a temperature gradient across an elongated pore. As a result, not only are the hairpins closed by fast cooling by the microscale convection, they are also strongly accumulated in the colder lower right corner. The enhanced concentration significantly reduces the entropy required for forming the complexes.

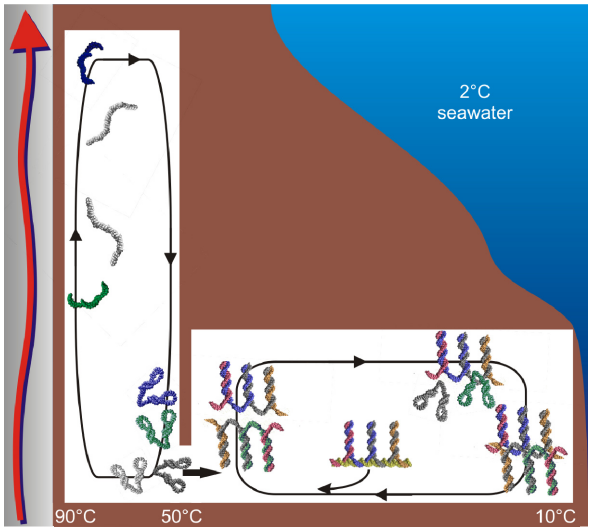

Figure 4 Hairpin replication driven by thermal microconvection. A horizontal temperature difference induces thermal convection in two neighboring pores inside a hydrothermal vent. Double hairpins are formed in the left pore by fast cooling from the hot left side to the cooler right side at the top of the chamber. Concurrently, the colder molecules are trapped at the bottom by thermophoresis and convection. From there, they diffuse into the right pore. The first complex is formed by template assisted association of double-hairpins (middle). This complex moves by convection to the warm side, dissociates and is now able to catalyze the hybridization reaction of other double-hairpins as it is transported towards the cold. The complementarity of double-hairpins drives a cross-catalyzing replication reaction as the molecules are shuttled repeatedly through different temperatures by the convection. An exponential replication results, similar to a convective polymerase chain reaction.

Diffusion between the flow lines on the submillimeter to millimeter scale is slow as compared to the convective cycling. On the time scale of several hundred temperature cycles different species can exist along neighboring flow lines with differing temperature cycling characteristics. As a result, laminar convection can host a wide range of thermal conditions in parallel. We expect that the pore space in the vicinity of hydrothermal vents host convection cells in a wide variety of conditions [37-39]. Because the vents are permeable, all pores are interconnected and thus the convection cells are coupled on slow time scales. One possibility to combine accumulation and replication is sketched in Figure 4.

IMPLICATIONS OF THE HYPOTHESIS

Replication by double hairpins

We think that the above replication scheme gives a direct route toward understanding the generation of codons, the replication process and the structure of tRNA. Until now we replicated two hairpin binding sequences A and B. In Figure 5, we extend the scheme to the temperature-induced replication sequence ABCDEF, given in red, blue, grey and orange. Longer replication requires that two hairpins are combined into hairpin pairs at their toehold region as shown in Figure 5b with double hairpins **(BC)**, **(DE)** and their partners **(bc)**, **(de)**. The template sequence is now replicated into more complex structures. On the one hand, the replication will generate a linear increase in the amount of complex consisting of **A**, **(BC)**, **(DE)**, **F** and **T** with capping single hairpins **A** and **F** shown in red and orange. On the other hand, complexes of **A(BC)(DE)F-a(bc)(de)f** are formed exponentially upon temperature oscillation.

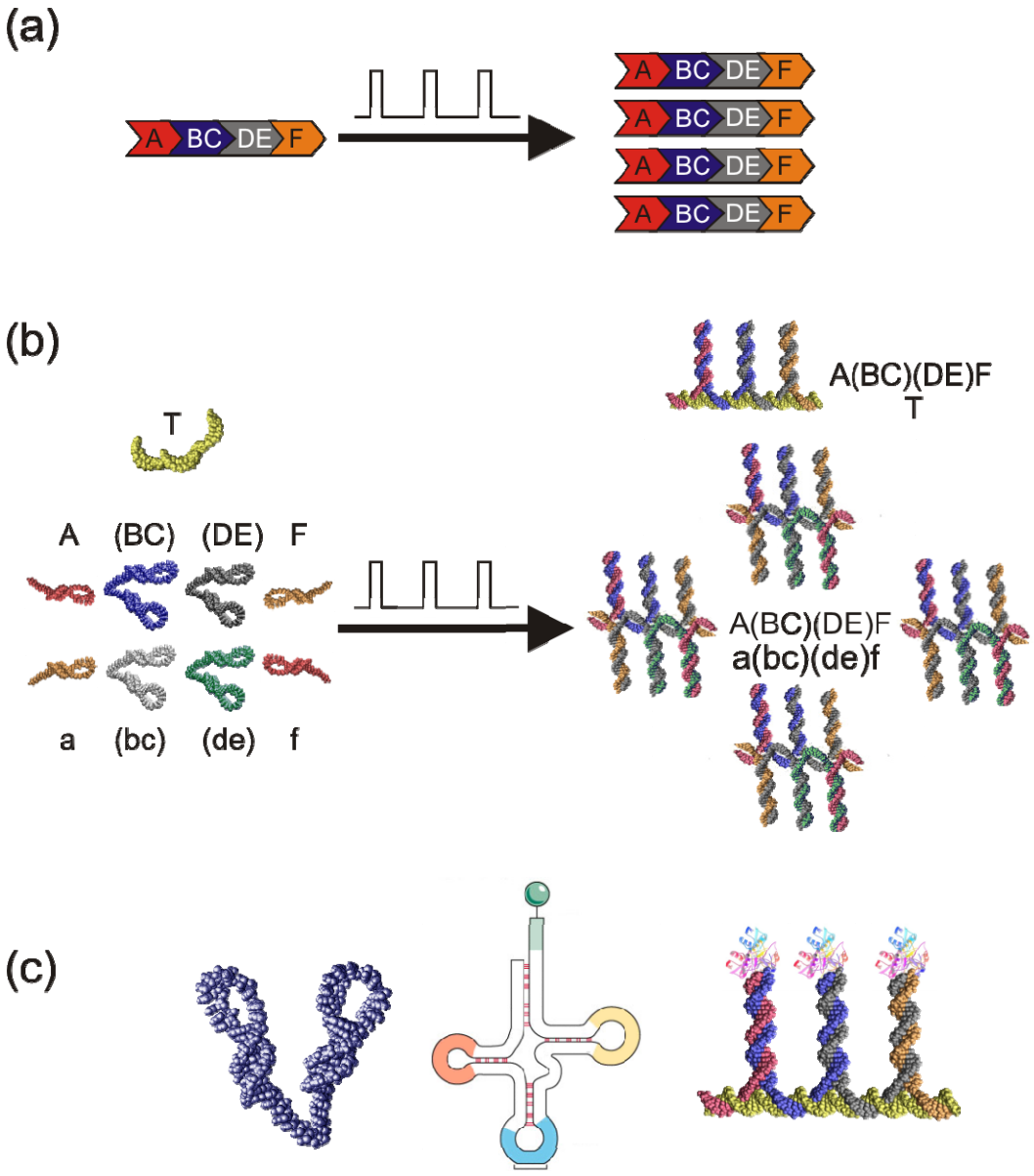

Figure 5 Double hairpin replication of sequences. (a) We aim to replicate a sequence of sequence chunks **ABCDEF** by the temperature oscillation of microscale thermal convection. (b) To do this, hairpins are joined at the toehold region into double hairpins **(BC)**, **(DE)**, **(bc)** and **(de)**. Upon temperature oscillation and display of template **T**, we expect linear growth of ABT-structures and exponential growth of complexes of **A(BC)(DE)F-a(bc)(de)f**. Single hairpins **A**, **F**, **a**, **f** in red and orange start and end the sequence but could extend the replication if replaced by double hairpins. (c) The double hairpin shows a strong similarity to modern tRNA, both in its structure and binding geometry. Within the scheme, the codon region is replicated. The double hairpins can be stabilized by amino acid polymerization at the end of the inter-hairpin binding site, showing a direct route towards translation.

The possible origin of tRNA

The structural similarity of the replicating hairpin pairs with modern tRNA is compelling (Figure 5c). The codon region of tRNA could be understood as an evolutionarily shortened replicating site [40] while the right and left hairpin of the clover leaf structure would be remainders of the replication hairpin. Sequence analysis has indicated [41-43] that tRNA probably evolved from two independent hairpin sequences, in accordance with our argument.

More recently, it has been shown that the archean *Nanoarchaeum equitans* can create functional tRNA from the 3-prime and 5-prime tRNA halves, which are encoded by different loci and trans-spliced to form the final product [44]. Similarities between nucleotides at comparable positions within the two halves of the tRNA molecule have often been taken as evidence that the modern cloverleaf structure arose through direct duplication of a hairpin [45-47]. This sequence duplication could reflect the evolution from single hairpin to double hairpin replicators.

The strong binding between hairpin pairs along the sequence is a limiting factor in the replication of longer sequences in the proposed scheme. The high temperature step in convection have to be increased to foster the unbinding of the template from the product. Since modern tRNA has modified bases, one could assume that unusually locked base bindings might have offered additional inter-hairpin stabilization, similar to LNA or similar structures [48]. However more importantly, the binding of amino acids [49] and the possible polymerization of amino acids between the hairpins offers a direct route to stabilize the binding between neighboring double hairpin sequences. Such a stabilizing connection of the proto-tRNA is exactly what is later used as translational coding of amino acids into protein.

We therefore speculate that hairpins subjected to temperature oscillations by convection allow replication of sequences and give a direct path to the evolution of tRNA. In the past, the structure of tRNA was discussed in terms of translation rather than replication [20,50,51,52], however recent analysis point towards to pre-translation origins [53]. Kuhn for example discussed the derivation of tRNA from backbone interaction of long and tight single hairpins along the sequence [50] to motivate the introduction of codons and tRNA. In contrast we invert the binding structure and can offer a replication origin which does not require amino acid polymers in its early steps.

Selection pressure

With the above findings, our appraisal is that the base-by-base replication is a relatively late development. We rather consider a pool of previously synthesized RNA molecules of length 30-80 bases which, initially, do not need to have a highly detailed sequence because RNA has a strong tendency to form hairpins. The idea is that the scheme can work initially even with strongly mutated sequences. A possible mechanism to polymerize RNA would be the sequence-unspecific surface catalysis pioneered by Ferris [54].

A rather simple selection pressure is conjectured to evolve more and more efficient replicators. We would argue that a faster decay of single stranded molecules rather than double stranded molecules [55,56] offers an advantage to fast replicating sequences under oscillating temperature conditions [57]. With equal effect, thermophoretic traps are expected to accumulate double stranded nucleotides to exponentially higher concentrations, offering significant advantages for the trapping of complexes against ubiquitous fluid drift and molecule diffusion into the ocean [19]. Under these conditions, survival becomes a kinetic quest to hybridize as fast as possible after the single stranded RNA molecule is released from synthesis or is cooled after unfolding from passing a hot convection site. The proposed hairpin replication is an exponentially fast way to transform as many single stranded molecules with fitting sequence as possible into double stranded molecules.

Conclusion

We started from the perceived need for protein-free replication of sequence information using the simplest of mechanisms, namely hybridization, driven by thermal convection. The scheme we propose is based on physical hybridization interaction alone and is a way to motivate and generate double hairpin structures very similar to tRNA. We proposed that

tRNA may have evolved from sequence replication under the selection pressure of dilution or decomposition. The reaction requires a temperature oscillation which can be provided by microscale convection in porous mineral precipitates subjected to a temperature gradient which is obtained in the vicinity of submarine hydrothermal springs. The scheme offers to bridge a wide gap in molecular evolution without excessive assumptions.

Competing Interests

The authors declare no competing interest.

Author's contributions

PB and DB equally contributed to the development of the hypothesis. Both read and approved the final manuscript.

Acknowledgements

We thank Stefan Duhr, Franz Weinert, Hubert Krammer, Friedrich Simmel, Ann Fornhof and Michael Russell for discussions and corrections. Financial help from the Emmy Noether program of the Deutsche Forschungsgemeinschaft (DFG), the Center for Nanoscience (CENS) and the Nanosystems Initiative Munich (NIM) is gratefully acknowledged.

References

1. Eigen M, Winkler-Oswatitsch R: Transfer-RNA, an early gene? Naturwissenschaften 1981, **68:**282-92.
2. Rodin S, Ohno S, Rodin A: Transfer RNAs with complementary anticodons: could they reflect early evolution of discriminative genetic code adaptors? Proc Natl Acad Sci USA 1993, **90:**4723-4727.
3. Isenbarger TA, Carr CE, Johnson SS, Finney M, Church GM, Gilbert W, Zuber MT, Ruvkun G: The most conserved genome segments for life detection on Earth and other planets. Orig Life Evol Biosph 2008, **38:**517-533.
4. Sievers D, von Kiedrowski G: Self-replication of complementary nucleotide-based oligomers. Nature 1994, **369:**221-224.
5. Saiki RK, Gelfand DH, Stoffel S, Scharf SJ, Higuchi R, Horn GT, Mullis KB, Erlich HA: Primer-directed enzymatic amplification of DNA with a thermostable DNA polymerase. Science 1988, **239:**487-491.
6. Barany F: Genetic disease detection and DNA amplification using cloned thermostable ligase. Proc Natl Acad Sci USA 1991, **88:**189-193.
7. Braun D, Libchaber A: Thermal force approach to molecular evolution. Phys Biol 2004, **1**:P1-P8.
8. Baross JA, Hoffman SE: Submarine hydrothermal vents and associated gradient environments as sites for the origin and evolution of life. Orig Life Evol Biosph 1985, **15**:327-345.
9. Corliss J: Hot springs and the origin of life. Nature 1990, **347**:624-624.
10. Imai E, Honda H, Hatori K, Brack A, Matsuno K: Elongation of Oligopeptides in a Simulated Submarine Hydrothermal System. Science 1999, **283**:831-833.
11. Imai E, Honda H, Hatori K, Matsuno K: Autocatalytic synthesis of oligoglycine in a simulated submarine hydrothermal system. Orig Life Evol Biosph 1999, **29**:249-259.
12. Lemke KH, Rosenbauer RJ, Bird DK, Ross DS: Equilibrium formation of oligoglycines from glycine in aqueous hydrothermal media. Geochim Cosmochim Acta Suppl 2003, **67**:249
13. Russell MJ: Geochemistry. The importance of being alkaline. Science 2003, **302**:580-1.
14. Koonin E, Martin W: On the origin of genomes and cells within inorganic compartments. Trends in Genetics 2005, **21**:647-654.
15. Hazen RM, Deamer DW: Hydrothermal reactions of pyruvic acid: synthesis, selection, and self-assembly of amphiphilic molecules. Orig Life Evol Biosph 2007, **37**:143-152.

16. Martin W, Baross J, Kelley D, Russell MJ: Hydrothermal vents and the origin of life. Nat Rev Microbiol 2008, **6**:805-814.
17. Krishnan M, Ugaz VM, Burns MA: PCR in a Rayleigh-Benard convection cell. Science 2002, **298**:793.
18. Braun D, Goddard NL, Libchaber A: Exponential DNA replication by laminar convection. Phys Rev Lett 2003, **91**:158103.
19. Baaske P, Weinert FM, Duhr S, Lemke KH, Russell MJ, Braun D: Extreme accumulation of nucleotides in simulated hydrothermal pore systems. Proc Natl Acad Sci USA 2007, **104**:9346-9351.
20. Kuhn H, Waser J: Molecular self-organization and the origin of life. Angew Chem Int Ed 1981, **20**:500-520.
21. Simmel F, Dittmer W: DNA Nanodevices. Small 2005, **1**:284-299.
22. Tyagi S, Kramer FR: Molecular beacons: Probes that fluoresce upon hybridization. Nat Biotechnol 1996, **14**:303-308.
23. Bonnet G, Tyagi S, Libchaber A, Kramer FR: Thermodynamic basis of the enhanced specificity of structured DNA probes. Proc Natl Acad Sci USA 1999, **96**:6171-6176.
24. Green SJ, Lubrich D, Turberfield AJ: DNA hairpins: Fuel for autonomous DNA devices. Biophys J 2006, **91**:2966-2975.
25. Orgel LE: Molecular replication. Nature 1992, **358**:203-209.
26. Luther A, Brandsch R, von Kiedrowski G: Surface-promoted replication and exponential amplification of DNA analogues. Nature 1998, **396**:245-248.
27. Zielinski WS, Orgel LE: Autocatalytic synthesis of a tetranucleotide analogue. Nature 1987, **327**:346-347.
28. Paul N, Joyce GF: Minimal self-replicating systems. Curr Opin Chem Biol 2004, 8:634-639.
29. Yurke B, Mills A: Using DNA to power nanostructures. Genetic Programming and Evolvable Machines 2003, **4**:111-122.
30. von Kiedrowski G: Minimal replicator theory I: Parabolic versus exponential growth. Bioorganic Chemistry Frontiers 1993, **3**:115–146.
31. Bag BG, von Kiedrowski G: Templates, autocatalysis and molecular replication. Pure and Appl Chem 1996, **68**:2145-2152.
32. Tuerk C, Gauss P, Thermes C, Groebe D, Gayle M, Guild N, Stormo G, d'Aubenton-Carafa Y, Uhlenbeck O, Tinoco I: CUUCGG hairpins: Extraordinarily stable RNA secondary structures associated with various biochemical processes. Proc Natl Acad Sci USA 1988, **85**:1364-1368.
33. Baaske P, Duhr S, Braun D: Melting curve analysis in a snapshot. Appl Phys Lett 2007, **91**:133901.
34. Ares S, Voulgarakis N, Rasmussen K, Bishop A: Bubble nucleation and cooperativity in DNA melting. Phys Rev Lett 2005, **94**:35504.
35. Viasnoff V, Meller A, Isambert H: DNA nanomechanical switches under folding kinetics control. Nano Lett 2006, **6**:101-104.
36. Koonin EV: An RNA-making reactor for the origin of life. Proc Natl Acad Sci USA 2007, **104**:9105-9106.
37. Russell MJ, Hall A, Cairns-Smith A, Braterman P: Submarine hot springs and the origin of life. Nature 1988, **336**:117.
38. Kelley DS, Karson JA, Blackman DK, Fruh-Green GL, Butterfield DA, Lilley MD, Olson EJ, Schrenk MO, Roe KK, Lebon GT, Rivizzigno P: An off-axis hydrothermal vent field near the Mid-Atlantic Ridge at 30 degrees N. Nature 2001, **412**:145-149.
39. Nisbet EG, Sleep NH: The habitat and nature of early life. Nature 2001, **409**:1083-1091.
40. Di Giulio M: The origin of the tRNA molecule: implications for the origin of protein synthesis. J Theor Biol 2004, **226**:89-93.
41. Eigen M, Winkler-Oswatitsch R: () Transfer-RNA: the early adaptor. Naturwissenschaften 1981, **68**:217-228.
42. Eigen M, Lindemann BF, Tietze M, Winkler-Oswatitsch R, Dress A, von Haeseler A: How old is the genetic code? Statistical geometry of tRNA provides an answer. Science 1989, **244**:673-679.

43. Widmann J, Di Giulio M, Yarus M, Knight R: tRNA creation by hairpin duplication. J Mol Evol 2005, **61**:524-530.
44. Randau L, Munch R, Hohn MJ, Jahn D, Soll D: Nanoarchaeum equitans creates functional tRNAs from separate genes for their 5'- and 3'-halves. Nature 2005, **433**:537-541.
45. Di Giulio M: Was it an ancient gene codifying for a hairpin RNA that, by means of direct duplication, gave rise to the primitive tRNA molecule? J Theor Biol 1995, **177**:95-101.
46. Dick TP, Schamel WA: Molecular evolution of transfer RNA from two precursor hairpins: implications for the origin of protein synthesis. J Mol Evol 1995, **41**:1-9.
47. Di Giulio M: The non-monophyletic origin of the tRNA molecule and the origin of genes only after the evolutionary stage of the last universal common ancestor (LUCA). J Theor Biol 2006, **240**:343-352.
48. Koshkin A, Singh S, Nielsen P, Rajwanshi V, Kumar R, Meldgaard M, Olsen C, Wengel J: LNA (Locked Nucleic Acids): Synthesis of the adenine, cytosine, guanine, 5-methylcytosine, thymine and uracil bicyclonucleoside monomers, oligomerisation, and unprecedented nucleic acid recognition. Tetrahedron 1998, **54**:3607-3630.
49. Bernhardt, HS and Tate, WP: Evidence from glycine transfer RNA of a frozen accident at the dawn of the genetic code. Biology Direct 2008, **3**:53
50. Kuhn H, Waser J: Evolution of early mechanisms of translation of genetic information into polypeptides. Nature 1982, **298**:585-586.
51. Wolf YI, Koonin EV: On the origin of the translation system and the genetic code in the RNA world by means of natural selection, exaptation, and subfunctionalization. Biology Direct 2007, **2**:14.
52. Poole AM, Jeffares DC, Penny D: The Path from the RNA World. Journal of Molecular Evolution 1998, **46**:1-17
53. Rodin AS, Szathmary E, Rodin SN: One ancestor for two codes viewed from the perspective of two complementary modes of tRNA aminoacylation. Biology Direct 2009, **4**:4.
54. Ferris JP, Hill AR, Jr., Liu R, Orgel LE: Synthesis of long prebiotic oligomers on mineral surfaces. Nature 1996, **381**:59-61.
55. Soukup GA, Breaker RR: Relationship between internucleotide linkage geometry and the stability of RNA. Rna 1999, **5**:1308-1325.
56. Abo-Riziq A, Grace L, Nir E, Kabelac M, Hobza P, de Vries MS: Photochemical selectivity in guanine-cytosine base-pair structures. Proc Natl Acad Sci USA 2005, **102**:20-23.
57. Lehman N: A recombination-based model for the origin and early evolution of genetic information. Chem Biodivers 2008, **5**:1707-1717.

(12) INTERNATIONAL APPLICATION PUBLISHED UNDER THE PATENT COOPERATION TREATY (PCT)

(19) World Intellectual Property Organization
International Bureau

(43) International Publication Date
29 May 2008 (29.05.2008)

PCT

(10) International Publication Number
WO 2008/061706 A1

(51) International Patent Classification:
G01N 21/64 (2006.01) *G01N 15/14* (2006.01)
G02B 21/00 (2006.01) *B01L 3/00* (2006.01)

(21) International Application Number:
PCT/EP2007/010037

(22) International Filing Date:
20 November 2007 (20.11.2007)

(25) Filing Language: English

(26) Publication Language: English

(30) Priority Data:
06024057.9 20 November 2006 (20.11.2006) EP
07020650.3 22 October 2007 (22.10.2007) EP

(71) Applicants *(for all designated States except US)*: **LUDWIG MAXIMILIANS UNIVERSITÄT MÜNCHEN** [DE/DE]; Geschwister-Scholl-Platz 1, 80539 München (DE). **NANOTEMPER TECHNOLOGIES AG** [CH/CH]; Zugerstr. 74, CH-6349 Baar (CH).

(72) Inventors; and
(75) Inventors/Applicants *(for US only)*: **DUHR, Stefan** [DE/DE]; Fachnerstrasse 49, 80686 München (DE). **BAASKE, Philipp** [DE/DE]; Allacher Strasse 104, 80997 München (DE).

(74) Agent: **VOSSIUS & PARTNER**; Siebertstrasse 4, 81675 Munich (DE).

(81) Designated States *(unless otherwise indicated, for every kind of national protection available)*: AE, AG, AL, AM, AT, AU, AZ, BA, BB, BG, BH, BR, BW, BY, BZ, CA, CH, CN, CO, CR, CU, CZ, DE, DK, DM, DO, DZ, EC, EE, EG, ES, FI, GB, GD, GE, GH, GM, GT, HN, HR, HU, ID, IL, IN, IS, JP, KE, KG, KM, KN, KP, KR, KZ, LA, LC, LK, LR, LS, LT, LU, LY, MA, MD, ME, MG, MK, MN, MW, MX, MY, MZ, NA, NG, NI, NO, NZ, OM, PG, PH, PL, PT, RO, RS, RU, SC, SD, SE, SG, SK, SL, SM, SV, SY, TJ, TM, TN, TR, TT, TZ, UA, UG, US, UZ, VC, VN, ZA, ZM, ZW.

(84) Designated States *(unless otherwise indicated, for every kind of regional protection available)*: ARIPO (BW, GH, GM, KE, LS, MW, MZ, NA, SD, SL, SZ, TZ, UG, ZM, ZW), Eurasian (AM, AZ, BY, KG, KZ, MD, RU, TJ, TM), European (AT, BE, BG, CH, CY, CZ, DE, DK, EE, ES, FI, FR, GB, GR, HU, IE, IS, IT, LT, LU, LV, MC, MT, NL, PL, PT, RO, SE, SI, SK, TR), OAPI (BF, BJ, CF, CG, CI, CM, GA, GN, GQ, GW, ML, MR, NE, SN, TD, TG).

[Continued on next page]

(54) Title: FAST THERMO-OPTICAL PARTICLE CHARACTERISATION

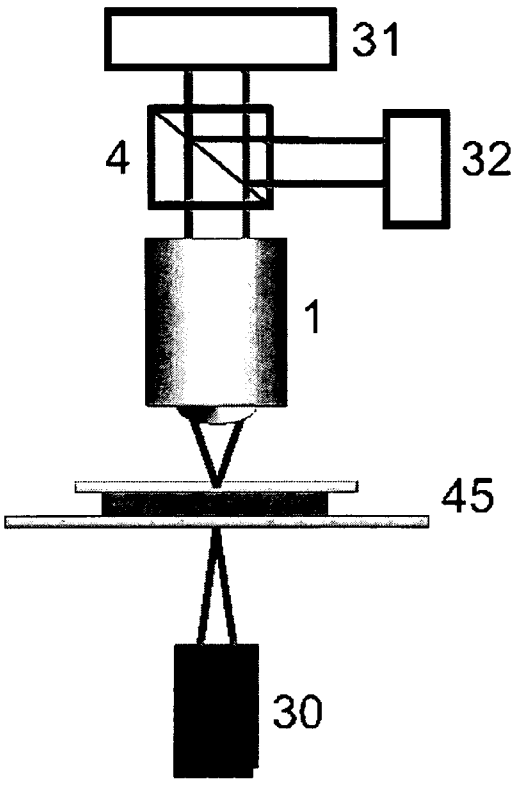

(57) Abstract: The present invention relates to a method and an apparatus for a fast thermo-optical characterisation of particles. In particular, the present invention relates to a method and a device to measure the stability of (bio)molecules, the interaction of molecules, in particular biomolecules, with, e.g. further (bio)molecules, particularly modified (bio)molecules, particles, beads, and/or the determination of the length/size (e.g. hydrodynamic radius) of individual (bio)molecules, particles, beads and/or the determination of length/size (e.g. hydrodynamic radius).

WO 2008/061706 A1

Claims

1. Method to measure thermo-optically characteristics of particles in a solution with the steps of:
   - providing a sample probe with marked particles in a solution;
   - exciting fluorescently said marked particles and firstly detecting fluorescence of said excited particles;
   - irradiating a laser light beam into the solution to obtain a spatial temperature distribution in the solution around the irradiated laser light beam;
   - detecting secondly a fluorescence of the particles in the solution at a predetermined time after irradiation of the laser into the solution has been started, and
   - characterizing the particles based on said two detections.

2. The method according claim 1, wherein the predetermined time is within the range of 1ms to 250ms

3. The method according to claim 1 or 2, wherein the detection time is in the range of 1ms to 50ms.

4. The method according to claim 1, 2 or 3, wherein the laser beam is defocused such that a temperature gradient within the temperature distribution is in the range of from 0.0 to 2K/µm, preferably from 0.0 to 5K/µm.

5. The method according to claim 4, wherein the laser beam is irradiated through an optical element into the solution.

6. The method according to claim 4, wherein the optical element is a single lens.

7. The method according to any of the preceding claims, further comprising the step of measuring the temperature distribution in said solution around the irradiated beam with a temperature sensitive dye.

8. The method according to claim 7, wherein the temperature distribution is determined based on detected fluorescence of the temperature sensitive dye, wherein the solution

comprising said temperature sensitive dye is heated by the irradiated laser beam and the fluorescence spatial fluorescence intensity is measured substantially perpendicular around the laser beam.

9. The method according to any of the claims 1 or 4 to 7, wherein the predetermined time is within the range of 0.5s to 250s.

10. The method according to claim 9, wherein in said predetermined time concentration change(s) within the spatial temperature distribution in the solution due to thermophoretic effects and such (an) concentration change(s) is(are) detected by a change of the distribution of fluorescence.

11. The method according to claim 9 or 10, wherein the laser beam is focused such that a temperature gradient within the temperature distribution is achieved in the range of from 0.001 to 10K/μm.

12. The method according to claim 9, 10 or 11, wherein said fluorescence is detected with a CCD camera.

13. The method according to claim 9, 10 or 11, wherein the brightness of said fluorescence is detected with a photodiode or a single pixel with the CCD in the centre of the laser beam.

14. The method according to any of the preceding claims, wherein the particles are biomolecules and/or nanoparticles and/or microbeads and/or combinations thereof.

15. The method according to any of the preceding claims, wherein the laser light is within the range of from 1200nm to 2000nm.

16. The method according to any of the preceding claims, wherein the laser is a high power laser within the range of from 0.1W to 10W, preferably from 4W to 6W.

17. The method according to any of the preceding claims, wherein the solution is an aqueous solution with an particle concentration within the range of from 1 atto Molar to 1M, preferably from 1 atto Molar to 100μMolar.

18. The method according to any of the preceding claims, wherein the solution is a saline solution with concentrations in the range of from 0 to 1M.

19. The method according to any of the preceding claims, wherein the spatial temperature distribution is between 0.1°C and 100°C.

20. The method according to claim 18, wherein said temperature gradient is created within 0.1μm to 500 μm in diameter around the laser beam.

21. The method according to any of the preceding claims, wherein the irradiation of the laser and the detection of the fluorescence is conducted from the same side with respect to the sample probe.

22. The method according to any of the preceding claims, wherein the solution is provided with a thickness in direction of the laser light beam from 1μm to 500μm.

23. The method according to any of the preceding claims, wherein the detection of the fluorescence is detected within a range of from 1nm to 500μm in direction of the laser beam.

24. The method according to any of the preceding claims, wherein the fluorescence is detected substantially perpendicular with respect to the laser light beam with a CCD camera.

25. The method according to claim 24, wherein the second fluorescence detection is spatial measurement of the fluorescence in dependence of the temperature distribution substantially perpendicular with respect to the laser light beam.

26. A method to thermo-optically trap particles, said method comprising the steps of

- providing a sample probe with preferably marked, particles;
- optionally detecting the marked particle; and
- trapping the, preferably marked, particle in accordance to the thermophoretic mobility of said particle.

27. A device for measuring thermo-optically characteristics of particles in a solution according to a method of any of claims 1 to 25 or for thermo-optically trapping particles in a solution according to claim 26.

28. A device for measuring thermo-optically characteristics of particles in a solution, in particular according to a method of any of claims 1 to 25 or for thermo-optically trapping particles in a solution according to claim 26, the device comprises:
- a receiving means for receiving marked particles within a solution;
- means for fluorescently exciting the marked particles;
- means for detecting the excited fluorescence in said solution; and
- a laser for irradiating a laser light beam into the solution to obtain a spatial temperature distribution in the solution around the irradiated laser light beam.

29. A device for measuring thermo-optically characteristics of particles in a solution or for thermo-optically trapping particles in a solution comprising:
a receiving means for receiving particles, preferably marked particles, within the solution;
means for exciting the particles, preferably the marked particles;
means for detecting the excitation of the particles, preferably the marked particles; and
means for obtaining a spatial temperature distribution in the solution.

30. The device according to claim 29, wherein the means for exciting is a means for optically, preferably fluorescently, exciting.

31. The device according to claim 29 or 30, wherein the means for obtaining a spatial temperature is means for irradiating light.

32. The device according to claim 27, wherein the means for fluorescently exciting the marked particles is a LED.

33. The device according to claim 27, 28 or 32 wherein the laser is a high power laser within the range of from 0.1W to 10W, preferably from 4W to 6W.

34. The device according to any of claims 27 to 33, wherein the laser and the means for detecting the excited fluorescence are arranged on the same side with respect to the receiving means.

35. The device according to any of claims 27 to 34, wherein the device further comprises an optic for magnifying the detected region.

36. The device according to any of claims 27 to 35, wherein the device further comprises an optic for focusing or defocusing the laser beam.

37. The device according claim 36, wherein the optic is a single lens.

38. The device according to any of claims 27 to 37, wherein the detecting means is a CCD camera.

39. The device according to any of claims 27 to 38, wherein the detecting means is a photo diode.

40. The method of any one of the claims 1 to 25 or the device of any of claims 27 to 39, wherein said particles to be measured is selected from the group consisting of (a) (bio)molecule(s), (nano)particles, (micro)beads, (an) organic substance(s), (an) inorganic substance(s) and/or combinations of these.

41. Use of the method of any one of claims 1 to 25 and 40 and the device of any one of claims 27 to 39 for detecting and/or measuring the characteristics of particles in solution.

42. The use of claim 41, wherein said characteristic is selected from the group of stability, length, size, conformation, charge, interaction, complex formation and chemical modification of particles.

43. The use of claim 41 or 42, wherein said particle is selected from the group consisting of (a) (bio)molecule(s), (nano)particles, (micro)beads, (an) organic substance(s), (an) inorganic substance(s) and/or combinations of these.

44. The method of claim 40 or the use of claim 43, wherein said (bio)molecule is selected from the group consisting of (a) protein(s), (a) peptide(s), (a) nucleic acid(s), (a) protein-nucleic acid fusion molecule(s), (a)PNA(s) and (a) locked DNA(s) (LNAs).

(12) INTERNATIONAL APPLICATION PUBLISHED UNDER THE PATENT COOPERATION TREATY (PCT)

(19) World Intellectual Property Organization
International Bureau

(43) International Publication Date
13 August 2009 (13.08.2009)

PCT

(10) International Publication Number
WO 2009/098079 A1

(51) International Patent Classification:
C12Q 1/68 (2006.01) *G01N 21/64* (2006.01)

(21) International Application Number:
PCT/EP2009/000847

(22) International Filing Date:
6 February 2009 (06.02.2009)

(25) Filing Language: English

(26) Publication Language: English

(30) Priority Data:
61/026,645 6 February 2008 (06.02.2008) US

(71) Applicant *(for all designated States except US)*: **LUDWIG-MAXIMILIANS-UNIVERSITÄT MÜNCHEN** [DE/DE]; Geschwister-Scholl-Platz 1, 80539 München (DE).

(72) Inventors; and

(75) Inventors/Applicants *(for US only)*: **DUHR, Stefan** [DE/DE]; Fachnerstrasse 49, 80686 München (DE). **BAASKE, Philipp** [DE/DE]; Gatterburgstr. 11, 890689 München (DE).

(74) Agent: **MEIER, Jürger**; Vossius & Partner, Siebertstrasse 4, 81675 Munich (DE).

(81) Designated States *(unless otherwise indicated, for every kind of national protection available)*: AE, AG, AL, AM, AO, AT, AU, AZ, BA, BB, BG, BH, BR, BW, BY, BZ, CA, CH, CN, CO, CR, CU, CZ, DE, DK, DM, DO, DZ, EC, EE, EG, ES, FI, GB, GD, GE, GH, GM, GT, HN, HR, HU, ID, IL, IN, IS, JP, KE, KG, KM, KN, KP, KR, KZ, LA, LC, LK, LR, LS, LT, LU, LY, MA, MD, ME, MG, MK, MN, MW, MX, MY, MZ, NA, NG, NI, NO, NZ, OM, PG, PH, PL, PT, RO, RS, RU, SC, SD, SE, SG, SK, SL, SM, ST, SV, SY, TJ, TM, TN, TR, TT, TZ, UA, UG, US, UZ, VC, VN, ZA, ZM, ZW.

(84) Designated States *(unless otherwise indicated, for every kind of regional protection available)*: ARIPO (BW, GH, GM, KE, LS, MW, MZ, NA, SD, SL, SZ, TZ, UG, ZM, ZW), Eurasian (AM, AZ, BY, KG, KZ, MD, RU, TJ, TM), European (AT, BE, BG, CH, CY, CZ, DE, DK, EE, ES, FI, FR, GB, GR, HR, HU, IE, IS, IT, LT, LU, LV, MC, MK, MT, NL, NO, PL, PT, RO, SE, SI, SK, TR), OAPI (BF, BJ, CF, CG, CI, CM, GA, GN, GQ, GW, ML, MR, NE, SN, TD, TG).

Published:

— *with international search report (Art. 21(3))*

— *with sequence listing part of description (Rule 5.2(a))*

(54) **Title**: THERMO-OPTICAL CHARACTERISATION OF NUCLEIC ACID MOLECULES

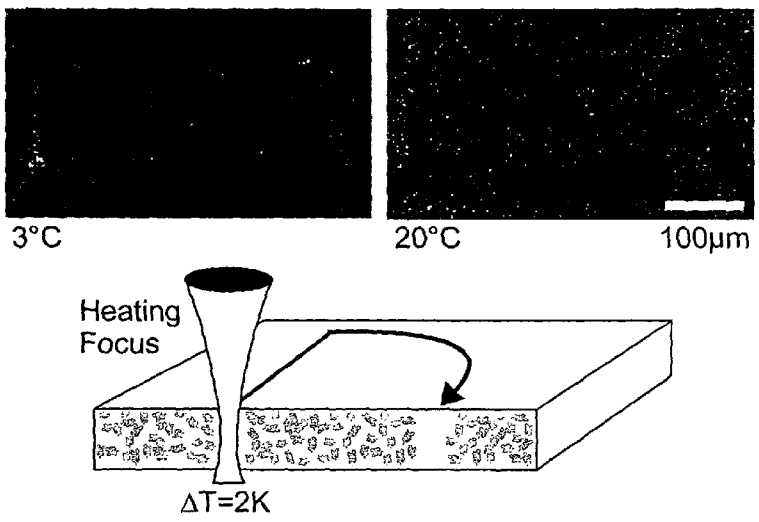

Fig. 7

(57) **Abstract**: The present invention pertains to a method and a device for the determination of thermo- optical properties, particularly the size or size distribution, of fluorescently labeled biomolecules or biomolecule complexes, particularly nucleic acids, in a reaction solution. The method comprises the steps of: (i) providing a reaction solution with fluorescently labeled biomolecules or biomolecule complexes; (ii) irradiating a laser light beam into the solution to obtain a spatial temperature distribution in the solution around the irradiated laser light beam; (iii) exciting fluorescently said fluorescently labeled biomolecules and detecting the fluorescence at two or more defined regions representing different mean temperatures in said spatial temperature distribution, wherein said detection of fluorescence is performed at least once at a predetermined time after the start of the laser irradiation; and (iv) determining the thermo-optical properties, particularly the size or size distribution, of the fluorescently labeled biomolecules or biomolecule complexes from the detected fluorescence intensity or fluorescence intensity distribution.

WO 2009/098079 A1

CLAIMS

1. A method for the thermo-optical determination of the size of fluorescently labeled nucleic acids in a reaction solution or the size distribution of fluorescently labeled nucleic acids in a reaction solution, comprising the steps of:
   - providing a reaction solution with fluorescently labeled nucleic acids;
   - irradiating a laser light beam into the solution to obtain a spatial temperature distribution in the solution around the irradiated laser light beam;
   - exciting fluorescently said fluorescently labeled nucleic acids and detecting the fluorescence at least at one position or at around one position in the solution or detecting the fluorescence distribution of said fluorescently excited nucleic acids, wherein said detection of fluorescence is performed at least once at a predetermined time after the start of the laser irradiation; and
   - determining the size or size distribution of the fluorescently labeled nucleic acids from the detected fluorescence intensity or fluorescence intensity distribution.

2. The method according to claim 1, wherein the fluorescence is detected at least at two positions or at around two positions in the solution.

3. The method according to claim 1 wherein additionally the detection of fluorescence is performed at least once before the start of the laser irradiation.

4. The method according to any one of the claims 1 to 3, wherein a second fluorescence detection is performed during laser irradiation or after the laser irradiation has been terminated.

5. The method according to any one of the claims 1 to 4, wherein said reaction solution is selected from the group of PCR reaction solution, nucleic acid restriction reaction solution and ligase chain reaction solution.

6. The method according to any one of the claims 1 to 5, wherein the fluorescently labeled nucleic acids are selected from the group of fluorescently labeled primers, fluorescently

labeled primer extension products, fluorescently labeled nucleic acid probes and fluorescently labeled PCR products.

7. The method according to any one of the claims 1 to 6, wherein the size of the fluorescently labeled nucleic acids is determined during or between PCR cycles or after PCR has been terminated.

8. The method according to claim 7, wherein the size of the fluorescently labeled nucleic acids is determined after or during the primer annealing phase, after or during the primer extension phase or after or during the denaturation phase.

9. The method according to claim 8, wherein for laser irradiation and fluorescence detection the reaction solution is cooled to a temperature of in the range of from about 0°C to 50°C.

10. The method according to any one of the claims 1 to 9, wherein the fluorescence distribution is a spatial fluorescence intensity distribution.

11. The method according to claim 10, wherein a spatial concentration distribution of said fluorescently labeled nucleic acids is determined from said spatial fluorescence intensity distribution.

12. The method according to any one of the claims 1 to 11, wherein the nucleic acids are fluorescently labeled by covalently attached dyes or are fluorescently labeled by non-covalently bound dyes.

13. The method according to any one of the claims 1 to 12, wherein said PCR reaction solution is a drop or droplet and/or is in a container selected from the group of capillary, multi-well plate, chamber, microfluidic chip and glass capillary chip.

14. The method according to claim 13, wherein the drop or droplet has a volume of from 1pl to 10µl.

15. The method according to any one of the claims 1 to 14, wherein said predetermined time after irradiation is from 5 s to 40 s.

16. The method according to any one of the claims 1 to 15, wherein the laser beam is focused such that a temperature gradient within the temperature distribution is achieved in the range of from 0.001 to 10K/µm.

17. The method according to any one of the claims 1 to 16, wherein said fluorescence is detected with a detector with spatial resolution or a detector without spatial resolution.

18. The method according to any one of the claims 1 to 16, wherein said fluorescence is detected with a detector with spatial resolution or with at least two detectors without spatial resolution.

19. The method according to claims 17 and 18, wherein said detector with spatial resolution is selected from the group of CCD camera, CMOS camera or line camera and said detector without spatial resolution is selected from the group of avalanche photodiode, photomultiplier tube and photodiode.

20. The method according to any of the claims 1 to 19, wherein the laser light is within the range of from 1200nm to 2000nm.

21. The method according to any one of the claims 1 to 20, wherein the laser is a high power laser within the range of from 0.1W to 10W, preferably from 4W to 6W.

22. The method according to any one of the claims 1 to 21, wherein the method is performed within a temperature range of from about 4°C to 100°C.

23. A device for thermo-optical determination of the size of fluorescently labeled nucleic acids in a reaction solution according to a method of any of claims 1 to 22.

24. A device for thermo-optical determination of the size or size distribution of fluorescently labeled nucleic acids in a reaction solution, in particular according to a method of any of claims 1 to 22, comprising:
    - a receiving means for receiving a reaction solution with fluorescently labeled nucleic acids;
    - a laser for irradiating a laser light beam into the solution to obtain a spatial temperature distribution in the solution around the irradiated laser light beam,
    - means for fluorescently exciting the labeled nucleic acids; and
    - means for detecting fluorescence and/or fluorescence distribution of the fluorescently excited nucleic acids; and wherein

    the device is adapted to perform at least two fluorescence detections at at least two predetermined points of time.

25. The device according to claims 23 or 24, further comprising a determination unit for determining the change in size of said nucleic acids based on the at least two fluorescence and/or fluorescence distribution detections.

26. The device according to any one of the claims 23 to 25, wherein the device is further adapted to fluorescently excite the fluorescently labeled nucleic acids and to detect a fluorescence and/or a fluorescence distribution of said fluorescently excited nucleic acids at least once before start of the laser irradiation and/or at least once at a predetermined point of time after start of the laser irradiation, preferably when the laser is still irradiating.

27. The device according to any one of claims 23 to 26, wherein the device is further adapted to fluorescently excite the fluorescently labeled nucleic acids and to detect a fluorescence and/or a fluorescence distribution of said fluorescently excited nucleic acids continuously or intermittendly at one or more predetermined or predeterminable points of time.

28. The device according to any one of claims 23 to 27, wherein the reaction solution is selected from the group or PCR reaction solution, nucleic acid restriction reaction solution and ligase chain reaction solution.

29. The device according to any one of claims 23 to 28, further comprising a temperature control element for heating and/or cooling the reaction solution to a desired, preferably constant, temperature and/or for performing a reaction such as a PCR reaction, preferably within a range of about 4°C to 100°C.

30. The device according to any one of claims 23 to 29, wherein the receiving means is adapted for receiving or is a container, a chamber, a capillary, a multi-well plate, a microfluidic chip, a glass capillary chip and/or or a means adapted for receiving a drop, a droplet, or a sealed droplet.

31. The device according to claim 30, wherein the receiving means is adapted to receive a drop or droplet having a volume of from about 0.001µl to 10µl.

32. The device according to any one of claims 23 to 31, wherein the device is adapted to cycle the whole PCR reaction solution through different temperatures needed to amplify DNA.

33. The device according to claim to 32, wherein the device is adapted to measure thermo-optical properties in each cycle of a PCR reaction.

34. The device according to any one of claims 23 to 33, wherein the means for fluorescently exciting the labeled nucleic acids is a Laser, Fibre Laser, Diode-Laser, LED, HXP, Halogen, LED-Array and/or HBO.

35. The device according to any one of claims 23 to 34, wherein the laser is a high power laser within the range of from 0.1W to 10W, preferably from 4W to 6W.

36. The device according to any one of claims 23 to 35, wherein the laser beam is focused such that a temperature gradient within the temperature distribution is achieved in the range of from 0.001 to 10K/µm.

37. The device according to any one of claims 23 to 36, wherein the laser light is within the range of from 1200nm to 2000nm.

38. The device according to any one of claims 23 to 37, wherein the laser and the means for detecting the excited fluorescence are arranged on the same side with respect to the receiving means.

39. The device according to any of claims 23 to 38, wherein the device further comprises an optic for magnifying the detected region.

40. The device according to any of claims 23 to 39, wherein the device further comprises an optic for focusing or defocusing the laser beam.

41. The device according to claim 40, wherein the optic is a single lens.

42. The device according to any of claims 23 to 41, wherein the detecting means comprises a detector with spatial resolution such as a CCD camera, a CMOS camera , and/or a line camera and/or a detector without spatial resolution such as an avalanche photodiode, a photomultiplier tube and/or a photodiode.

43. The device according to any of claims 23 to 42, wherein the means for detecting fluorescence and/or fluorescence distribution of the fluorescently excited nucleic acids is adapted to detect the fluorescence at least at two positions or at around two positions in the solution.

44. The device according to any of claims 23 to 43, wherein the means for detecting fluorescence and/or fluorescence distribution of the fluorescently excited nucleic acids comprises a detector with spatial resolution or at least two detectors without spatial resolution for detecting said fluorescence.

45. Use of the method according to any one of the claims 1 to 22 or use of the device according to any one of the claims 23 to 44 for the detection and/or quantification of

fluorescently labeled nucleic acids in real-time PCR; quantitive real-time PCR, nested PCR, reverse transcription PCR or in multiplex PCR or for the determination of the size of fluorescently labeled nucleic acids in real-time PCR; quantitive real-time PCR, nested PCR, reverse transcription PCR or in multiplex PCR.

46. Use according to claim 45 for detecting and/or monitoring nucleic acid elongation in PCR.

47. Use according to claim 45 for simultaneously detecting, quantifying and/or identifying two or more fluorescently labeled nucleic acids of different size.

METHOD AND DEVICE FOR PARTICLE ANALYSIS USING THERMOPHORESIS

The present invention relates to a method, device and its use for thermo-optical characterisation of particles. In particular, the present invention relates to a method and an apparatus for measuring the surface properties of small particles (e.g., submicron to μm scale) with thermophoresis. The present invention also relates to a method and apparatus for analyzing the physical and chemical properties of small particles and/or changes in these properties. More particularly, the invention uses thermophoresis in a created spatial temperature gradient combined with optical detection. Moreover, the present invention relates to a method and a device to measure characteristics, preferably size and surface properties, of molecules, like biomolecules, the interaction of molecules, particularly biomolecules with, e.g. further (bio)molecules, particularly modified biomolecules, particles, e.g. nanoparticles/ions or microparticles, beads, e.g. microbeads and/or the determination of the length/size (e.g. hydrodynamic radius) of individual molecules, particularly of biomolecules, of particles (e.g. nanoparticles, microparticles), or of beads (e.g. microbeads) as well as the determination of e.g. length or size (e.g. hydrodynamic radius) of (bio)molecules or particles. Also combinations these characteristics may be determined with the means, uses and methods of this invention. It is of note that the present invention is, however, not limited to the measurement/characterization of biomolecules. Therefore, also the characteristics of other compounds/particles can be measured and determined by the means and methods disclosed herein, for example kinetic events and interactions of molecules may be determined and/or measured. Accordingly, also chemical reactions (like inorganic or organic reactions) may be measured by the methods and under use of the devices of the present invention. It is also envisaged to determine complex formations and/or their dissociation. The method of the present invention applies to polar (e.g. water, ethanol, acetonitril-), non-polar (organic) solvents (e.g. hexane, toluene), emulsions (e.g. milk), foams and the like.

SUMMARY OF THE INVENTION

The present invention allows using all the advantages of a thermophoretic measurement of particles, particles' properties and/or changes in particle properties and circumvents the disadvantages such as the high costs of the setup known from the art and limitations on the liquids which can be heated.

The method of the present invention particularly allows thermo-optical measurements of parameters/characteristics such as size and surface properties , charge, conformation of a molecule, shape of a molecule, chemical groups on the surface, inter/intramolecular

interactions, conformation of molecule, small molecule/ion binding to molecules and interaction between biomolecules or biomolecules and particles/nanocrystals/microbeads with a simple, efficient, robust and reliable method/apparatus. In particular, the present invention allows an automated measurement with an improved through-put within improved time spans.

Also the present invention circumvents the need that laser radiation has to be absorbed by the solvent, an obstacle limiting the use of IR heating lasers to aqueous solutions. The present invention may be used with different polar and non-polar solvents, preferably a great variety of matter in the liquid phase may be used, e.g. molten materials (e.g. polymer melts) or Liquid Crystals (e.g. in the nematic phase). Also mixtures of all mentioned and other liquids and solvents may be used with the present invention.

In the context of this invention, in particular the claims, it is noted that the terms "particle" or "particles" also relate to beads and/or microparticles, particularly microbeads, nanoparticles or molecules, particularly biomolecules, e.g. nucleic acids (such as DNA, RNA, LNA, PNA), proteins and other biopolymers as well as biological cells (e.g. bacterial or eukaryotic cells) or sub-cellular fragments, viral particles or viruses and cellular organelles and the like or inorganic compounds. In the context of the present invention, a nanoparticle is a microscopic particle with at least one dimension less than 100 nm and a microparticle/microbead is a microscopic particle/bead which has a characteristic dimension of less than 1 mm but normally more than 100 nm. The term "modified particle" or "modified bead" relates in particular to beads or particles which comprise or are linked to molecules, preferably biomolecules. This also comprises coating of such beads or particles with these molecules or biomolecules.

Although the particles mentioned above are mainly biomolecules the invention is not limited to an application of biomolecules but allows also measuring.

The present invention provides means and methods for the thermo-optical measurements and/or thermo-optical characterization of particles or molecules, in particular biomolecules, by the measurements and/or the detection of differences in the thermo-optical properties. Their thermo-optical properties mainly originate from differences in thermophoretic mobility DT (e.g. the velocity of particles/molecules in a temperature gradient). In particular, the detected signal is dependent on the thermophoretic mobility $c/c_0 = \exp[-(D_T/D)(T - T_0)]$, with the diffusion coefficient D, concentration c and temperature T. A DT independent of the polymer length as expected from Duhr (2004; loc. cit.) and others (e.g. Chan et al., Journal of Solution Chemistry 32, 3 (2003); Schimpf et al., Macromolecules 20, 1561-1563 (1987)) would render the analytics of biopolymers like DNA

and proteins almost impossible since only changes in the diffusion constant would contribute to the thermo-optical properties, which are minute in most cases.

Thermo-optical characterization in accordance with this invention is based on the creation of temperature gradients at small length scales in a solution. The solution may be an aqueous solution but also a solution where the solvent is non-aqueous, for example non-polar (e.g. hexane). By doing so, the energetic states of the molecules in the solution are changed depending on the temperature and the properties of the molecule, i.e. the molecules experience a spatial potential originating from the spatial differences in temperature. This potential drives a directed motion of molecules along the temperature gradient, an effect called thermophoresis.

In other words, in this temperature profile particles move due to thermophoresis and establish a concentration profile. After a given time, depending on, i.a., the chamber dimensions and the particle's diffusion coefficient, the steady-state distribution is reached. The diffusion time is hereby very sensitive to the chambers dimension as it contributes quadratically while the diffusion coefficient contributes only linearly. When the temperature control system is switched off, the concentration gradient equilibrates and the particles diffuse back. The complete dynamics are preferably observed using microscopy techniques e.g. fluorescence microscopy.

With the present invention, thermophoresis is observed at times in a range from about 0.01 seconds to 30 minutes, preferably 0.01 seconds to 10 minutes, preferably 1 second to 5 minutes, preferably 60 second to 5 minutes

Thermophoresis is a method which is sensible to surface properties of molecules in a solution. It is not necessary to expose molecules to a different matrix (like in chromatography) or to interact with the molecules physically in any way (e.g. by direct contact or by adding substances). Only interactions within a temperature gradient are necessary. Heating and/or cooling elements are used for manipulation of matter by creating spatial temperature distribution and fluorescence is preferred to detect molecules.

The gist of thermo-optical or thermophoretic characterization based on thermophoresis as provided herein is that differences in thermophoretic mobility (i.e. the velocity of molecules in a temperature gradient) and hydrodynamic radius can be detected by analyzing the spatial distribution of concentration (i.e. by the spatial distribution of e.g. fluorescence) or the fluctuations of single particles trapped in the spatial temperature profile. This embodiment is of particular relevance for the herein described thermo-optical trap for trapping particles, molecules, beads, cellular components, vesicles, liposomes, cells and the like. While the

hydrodynamic radius is only related to the radius of a molecule, the thermophoretic mobility is sensitive to charge, surface properties (e.g. chemical groups on the surface), shape of a molecule (i.e. size of surface), conformation of a protein or interaction between biomolecules or biomolecules and particles/nanocrystals/microbeads. This means that if any of the mentioned properties are changed, the molecules will experience a different thermodynamical potential, resulting in differences in thermophoretic mobility (i.e. change in spatial concentration profile or fluctuation amplitude of trapped particles).

Thus, the present invention relates to thermally induced processes, e.g. temperature gradient induced directed motion of particles.

The approach according to the present invention differs from most state of the art analysis devices and methods where the generation of heat is an unwanted by-product. For dielectrophoresis the experimental results are corrected for temperature effects and it is tried to keep temperature effects negligible. (Ref: Ac electrokinetics: a review of forces in microelectrode structures A. Ramos et al 1998 J. Phys. D: Appl. Phys. 31 2338-2353). For the widespread analysis method of electrophoresis Joule heating is titled to “plague electro-driven separations” and leads to separation inefficiencies. (Ref: Joule heating and determination of temperature in capillary electrophoresis and capillary electrochromatography columns, Anurag S. Rathore, Journal of Chromatography A, Volume 1037, Issues 1-2, 28 May 2004, Pages 431-443).

Moreover the spatial localization of the temperature distribution is an unwanted effect for state of the art micro-heating elements. For example micro-hotplates for gas analysis devices use heat distribution plates to obtain a uniform temperature over the whole area. The methods presented in this invention allow taking advantage of the temperature inhomogeneities and using it for the characterisation of particles.

The thermo-optical characterization mentioned above provides the means for fast thermo-optical analysis of particles and/or molecules, in particular for the thermo-optical characterisation of biomolecules, like nucleic acid molecules (e.g. DNA, RNA, PNA) or proteins and peptideanalysis. This characterisation comprises, inter alia, size determination, length determination, determination of biophysical characteristics, like melting points or melting curves, complex formations, protein-protein interactions, protein or peptide folding/unfolding, of intra-molecular interactions, intermolecular interactions, the determination of interactions between particles or molecules, and the like. Prior art methods for detection and quantification of molecular interactions and characteristics, in particular biomolecular interactions and characteristics are very time consuming which means that the

time needed for an analysis is on in the order of 30 minutes up to hours. In accordance with the present invention, the method and device allow advantageous parallelization so that the overall measurement times can be significantly reduced. Depending on the actual embodiment, one measurement may typically take less than 600s, less than 300s, less than 200s, less than 100s or even less than 50s, which is clearly faster than the methods described in the prior art. The present invention can detect and quantify molecular interactions and characterisations, in particular biomolecular interactions and/or biochemical/biophysical properties within 1 second up to 10 minutes. The term interaction comprises interaction between biomolecules (e.g. protein, DNA, RNA, hyaluronic acids etc.) but also between (modified) (nano)particles/ions/(micro micro)beads and biomolecules. In this context, modified particles, molecules, biomolecules, nanoparticles, microparticles, beads or microbeads comprise fluorescently labelled particles, molecules, biomolecules, nanoparticles, microparticles, beads or microbeads. Fluorescently labelled particles, molecules, biomolecules, nanoparticles, microparticles, beads or microbeads may be e.g. particles, molecules, biomolecules, nanoparticles, microparticles, beads or microbeads, to which one or more fluorescent dyes have been attached, e.g. covalently attached. For example, the fluorescent dyes may be selected from the group of 6-carboxy-2',4,4',5',7,7'-hexachlorofluorescein (6-HEX SE; C20091, Invitrogen), 6-JOE SE or 6-TET SE. In other cases, the intrinsic fluorescence of e.g. particles, molecules, biomolecules may be exploited according to the invention, e.g. the fluorescence properties of tryptophan, tyrosine or phenylalanine in a protein may be exploited. The terms “marked” and “labelled” are used synonymously in the context of this invention. In the context of this invention, “marked particles” particularly refer to luminescently, e.g., fluorescently labelled molecules/particles or other molecules/particles which can be detected by fluorescence means, e.g. molecules/particles comprising an intrinsic fluorophor, molecules/particles comprising intercalating dyes or particles/molecules with fluorophores attached.

In short summary, the device and method according to the present invention make use of thermophoretic driven forces in order to separate, deplete and/or accumulate particles of interest in a solution. Since thermophoretic forces are based on a spatial temperature gradient, the present invention uses a temperature control system for generating or creating a sufficient temperature gradient. In particular, a temperature control system according to the present invention comprises one or a plurality of heating and/or cooling elements. In the following a non-limiting list of heating and/or cooling elements/devices, which may be used in order to create the desired temperature gradient, will be discussed in more detail. Desired temperature

gradients lie within the range from about 0.001 K/μm to 20K/μm, preferably from 0.001K/μm to 5K/μm, more preferably from 0.01K/μm to 1K/μm and more preferably is about 0.05K/μm.

Claims

1. Method to measure thermo-optical, preferably thermophoretic, characteristics of particles in a solution comprising the steps of:
    (a) providing a sample probe comprising marked particles in a solution;
    (b) providing a temperature control system for creating a temperature gradient within said sample probe by contact heating, electrical heating and/or cooling;
    (c) detecting the marked particles at a first time;
    (d) creating a temperature gradient within the sample probe by means of the temperature control system;
    (e) detecting the marked particles in the sample probe at a, preferably predetermined, second time and/or at a predetermined location within the temperature gradient, and
    (f) characterizing the particles based on said two detections.

2. Method according to claim 1, wherein the method comprises the step of performing a third detection at a, preferably predetermined, third time.

3. Method according to claim 1, 2, wherein the second time and/or third time is while and/or after heating, particularly in order to measure back diffusion

4. Method according to claim 1, 2 or 3, wherein the first, second and/or third times are predetermined times, preferably depending on absolute time, the completion or conduction of further method steps, and/or relative time between the two times.

5. Method according to any one of the preceding claims, further comprising the step of exciting luminescence, preferably fluorescence, of said marked particles wherein the detection steps comprise detecting luminescence, preferably fluorescence, of said excited particles.

6. Method according to any one of the preceding claims, wherein the temperature control system controls the temperature by using one or more of a wire, a Peltier element, a plate, a conductive path, means for creating a high frequency electric field in the

sample probe, an indium-tin-oxide (ITO) element and/or means with a radiation absorbing surface.

7. Method according to any one of the preceding claims, wherein detection is performed by use of one or more of epifluorescence (EPI) microscope, Total internal reflection fluorescence (TIRF) microscope, confocal microscope, CCD, APD, PMT, and/or a microscope.

8. Method according to any one of the preceding claims, wherein the temperature gradient lies in the range from about 0 K/µm to 20K/µm, preferably from 0.001K/µm to 5K/µm, more preferably from 0.01K/µm to 1K/µm and more preferably is about 0.05K/µm.

9. Method according to any one of the preceding claims, wherein the temperature increase in the sample probe lies in the range from about 0°C to 100°C, preferably from 2°C to 50°C and more preferably from 5°C to 20°C.

10. Method according to any one of the preceding claims, wherein the sample probe volume lies in the range from about 1pl to 100µl, preferably from 0.1 µl to 30 µl and also preferably from 0.5 µl to 5 µl

11. Method according to any one of the preceding claims, wherein the time span between the first time and the second time lies in the range from about 1µs to 60min, preferably about 0.01 sec to 20 min, preferably about 1 sec to 10 min preferably 60sec to 5 min.

12. Method according to any one of the preceding claims, wherein the predetermined location within the temperature gradient is at the surface, the bottom, the side of the measurement chamber or the sample probe and/or at a predetermined distance from heating means or at a place of specific temperature, preferably close to the heating means or near a surface in a region of high temperature gradients.

13. Method according to any one of the preceding claims, wherein a plurality of sample probes are measured subsequently and/or in parallel.

14. A device for measuring thermo-optical, preferably thermophoretic, characteristics of particles in a solution, in particular according to a method of any one of claims 1 to 14, the device comprises:

- a measurement chamber for receiving a sample probe containing marked particles in a solution;
- means for detecting the marked particles in the sample probe;
- a temperature control system for creating a temperature gradient within said sample probe by contact heating and/or cooling, and
- a control means adapted for controlling said detection means to detect fluorescence of said excited particles at a first time and for controlling said detection means and temperature control system to detect fluorescence of the marked particles in the sample probe at a second time and/or at a predetermined location within a temperature gradient created by the temperature control system.

15. Device according to claim 14, wherein the control means is adapted to control the first and/or second times to be predetermined times, preferably depending on absolute time, the completion or conduction of further method steps and/or relative time between the two times.

16. Device according to claim 14 or 15, wherein further comprising means for exciting luminescence, preferably fluorescence, of said marked particles wherein the detection means is adapted to detect luminescence, preferably fluorescence, of said excited particles.

17. Device according to claim 14, 15 or 16, wherein the temperature control system comprises one or more of each or more of the following heating and/or cooling means: a wire, a Peltier element, a plate, a conductive path, means for creating a high frequency electric field, an indium-tin-oxide (ITO) element and/or means with a radiation absorbing surface for controlling the temperature.

18. Device according to any one of claims 14 to 17, wherein detection means comprises one or more of epifluorescence (EPI) microscope, total internal reflection fluorescence (TIRF) microscope, confocal microscope, CCD, APD, PMT, and/or a microscope.

19. Device according to any one of claims 14 to 18, wherein the device comprises means for characterizing the particles based on said two detections.

20. Device according to any one of claims 14 to 19, wherein the temperature control system is adapted to create a temperature gradient lying in the range from about 0K to 20K, preferably from 0.001K/µm to 5K/µm, more preferably from 0.01K to 1K/µm and more preferably is about 0.05K.

21. Device according to any one of claims 14 to 20, wherein the temperature control system is adapted to create a temperature rise in the sample probe lying in the range from about 0°C to 100°C, preferably from 2°C to 50°C and more preferably from 5°C to 20°C.

22. Device according to any one of claims 14 to 21, wherein the device is adapted to receive a sample probe having a volume lying in the range from about 1pl to 100µl, preferably from 0.1 µl to 30 µl and also preferably from 0.5 µl to 5 µl.

23. Device according to any one of claims 14 to 22, wherein control means is adapted to control the time span between the first time and the second time to lie in the range from about 1µs to 60min, preferably about 0.01 sec to 20min, preferably about 1 sec to 10 min, preferably 60sec to 5 min.

24. Device according to any one of claims 14 to 23, wherein the detection means is adapted to conduct the detection at the surface, the bottom, the side of the measurement chamber or the sample probe and/or at a predetermined distance from heating means or at a place of specific temperature, preferably close to the heating means or near a surface in a region of high temperature gradients.

25. Device according to any one of claims 14 to 24, adapted to measure a plurality of sample probes subsequently and/or in parallel.

26. Device according to any one of claims 14 to 25, wherein the device comprises substrate containing a measurement chamber for receiving the sample probe.

27. Device according to any one of claims 14 to 26, wherein the measurement chamber and/or the sample probe is covered by a cover lid.

28. Device according to claim 27, wherein the cover lid comprises one or more filling holes and/or pin holes.

29. Device according to any one of claims 14 to 27, wherein the measurement chamber is defined as a recess in the substrate.

30. Device according to any one of claims 14 to 29, comprising filling holes for filling the measurement chamber.

31. Device according to any one of claims 14 to 30, wherein one or more of the heating and/or cooling means of the temperature control system extend into and/or through the measurement chamber and/or the sample probe.

32. Device according to any one of claims 14 to 31, wherein one or more of the heating and/or cooling means of the temperature control system contacts the measurement chamber and/or the sample probe.

33. Device according to any one of claims 14 to 32, wherein one or more of the heating and/or cooling means are electrically isolated vis-à-vis the measurement chamber and/or the sample probe, preferably by an electrical isolation coating and/or an electrical isolation layer.

34. Device according to any one of claims 14 to 33, wherein the measurement chamber and/or the sample probe is covered by a cover lid and wherein the cover lid is a heating and/or cooling element, preferably an ITO element.

35. Device according to any one of claims 14 to 34, wherein the measurement chamber is defined by a structured surface and/or the sample probe is a positioned on a surface as a droplet, and where the heating and/or cooling element is defined by/on/in the substrate on which the droplet is placed.

36. Device according to any one of claims 14 to 35, or method according to any one of claims 1 to 13, wherein the temperature of the measurement chamber and/or the sample probe can be / is controlled in a way that biochemical reactions such as PCR can be carried out.

37. Method to measure thermo-optical, particularly thermophoretic, characteristics of particles in a solution by using a device according to any one of claims 14 to 36.

38. Use of any of the methods according to claim 1 to 13 or 36 or any of the devices according to claim 14 to 36 for the characterization of thermo-optical, particularly thermophoretic properties of particles in solution.

39. Use of any of the methods according to claim 1 to 13 or 36 or any of the devices according to claim 14 to 36 for the determination of surface properties of particles in solution.

40 Use of any of the methods according to claim 1 to 13 or 36 or any of the devices according to claim 14 to 36 for the separation of particles in solution according to the thermophoretic properties of said particles.

41 Use of any of the methods according to claim 1 to 13 or 36 or any of the devices according to claim 14 to 36 for the characterization of interactions of biomolecules in solution.